DESIGN AND DEVELOPMENT OF Pt-BASED TRIMETALLIC WGS CATALYSTS

by

Özgü Özer

B.S., Chemical Engineering, Istanbul Technical University, 2013

Submitted to the Institute for Graduate Studies in
Science and Engineering in partial fulfillment of
the requirements for the degree of
Master of Science

Graduate Program in Chemical Engineering

Boğaziçi University

2016

to my family

ACKNOWLEDGEMENTS

First of all, I would like to express my truthful gratitude to my thesis supervisor Prof. Ahmet Erhan Aksoylu for his guidance, encouragement and trust in me. It was really a privilege to work with him during my thesis. I learned a lot from his wisdom and experiences in catalysis and reaction engineering. I am very grateful to Prof. Aksoylu for his real support in every condition.

Very special thanks to Burcu Selen Çağlayan for her help and guidance throughout my work. She did not hesitate to spent time for me. I also would like to thank her for her expertise and efforts in XPS and Raman Spectroscopy analyses.

I would like to express my sincere appreciation for the members of my thesis committee, Prof. Ramazan Yıldırım and Assoc. Prof. Hasan Bedir, for devoting their valuable time to read and comment on my thesis.

Heartfelt thanks are for my friends Göksu Acar, Çisem Yurtsever, Merve Gamze Yıldız, Kardelen Kaya and Bahar Kesim for their everlasting help, encouragement and the joyful memories we shared. Their intimate friendship was the most valuable gain of my master years. Deepest thanks to Furkan Karasoy for his encouragement, understanding and continuous support on any matter all these years.

I would like to thank Elif Erdinç and Coşar Doğa Demirhan for their help in the experimental systems without any hesitation and also for their friendship. Thanks are for Melek Selcen Başar, Merve Eropak and Ali Uzun, who guided me whenever I needed their help. I was very lucky to work with the CATREL team and thus I would like to thank all team members for their support.

Cordial thanks are for Bilgi Dedeoğlu for his technical assistance and also Melike Gürbüz, Başak Ünen, Belgin Balkan and Yakup Bal for their friendly attitude. I would also like to thank Bilge Gedik Uluocak and Erkan Karabekmez for their significant efforts in

SEM and XRD analyses conducted at Boğaziçi University Advanced Technologies Research and Development Center.

Finally, I would like to express my dearest thanks to my beloved family for their patience, encouragement and continuous support throughout my whole life. Their endless love and trust in me motivated me all the time. Especially, thanks to the best sister ever, Özgün Özer for always being there for me.

Financial support for this study provided by TÜBİTAK through project 214M170 is gratefully acknowledged.

ABSTRACT

DESIGN AND DEVELOPMENT OF Pt-BASED TRIMETALLIC WGS CATALYSTS

The aim of this study is to design and develop Pt-based catalysts having high WGS performance with suppressed methanation activity in HTS-LTS transition temperature region. In this context, a series of trimetallic Pt-Re-V/CeO_2 catalysts and a reference bimetallic Pt-Re/CeO_2 were prepared, characterized, and tested for their WGS performance. Pt- and Re-loadings of the catalysts were kept fixed as 1 wt.%, while V-loading levels were chosen as 0, 0.5, 1, and 3 wt.%. Performance tests were conducted at 300, 350 and 400 °C for two ideal and two real feed compositions with fixed GHSV as 120,000 ml g_{cat}^{-1} h^{-1}. In the tests, effects of V loading and reaction conditions (H_2O/CO ratio and temperature) on the WGS activity, selectivity and stability of the Pt-Re-V/CeO_2 catalysts were investigated. Results indicated that all catalysts used in this study showed plausible WGS performance, ie. high CO conversion levels and positive net H_2 production values with no methanation activity, and between those 1Pt-1Re-0.5V/CeO_2 and 1Pt-1Re-1V/CeO_2 catalysts have superior performance, ie. high activity and selectivity with performance stability, indicating their quite high potential to be used in a practical fuel processor. The freshly reduced and spent forms of the catalyst samples were characterized by SEM-EDX, XPS, XRD and Raman spectroscopy. SEM-EDX results showed that large Pt particle size may have a positive effect on high catalytic activity of the V-promoted catalysts compared to that of V-free sample. XPS analysis revealed that Ce^{3+} content, thus the extent of the electron transfer between the support and the metal sites, decreased during reaction as a consequence of high WGS activity. XRD results indicated there might be an interaction between V and CeO_2 leading to changes in CeO_2 crystallite size. Combined evaluation of XPS and Raman spectroscopy results revealed that VO_2 and $CeVO_4$ formations and polyvanadate surface species were present in the catalyst. No bulk V_2O_5 crystals were observed in any samples, inferring that the vanadium was highly dispersed at the surface. Coke formation was not observed on any spent samples.

ÖZET

Pt-BAZLI ÜÇ METALLİ WGS KATALİZÖRLERİNİN TASARIMI VE GELİŞTİRİLMESİ

Bu çalışmanın amacı HTS-LTS sıcaklık geçiş bölgesinde ikincil metanasyon aktivitesini baskılayan yüksek su-gaz değişimi reaksiyonu (WGS) performansı gösterecek Pt-bazlı katalizörler tasarlamak ve geliştirmektir. Bu kapsamda üç metalli Pt-Re-V/CeO_2 katalizörleri ve baz teşkil etmesi amacıyla çift metalli Pt-Re/CeO_2 katalizörü hazırlanarak karakterizasyonları yapılmış ve WGS performansları test edilmiştir. Katalizörlerin Pt ve Re yüklemeleri kütlece %1 olarak sabit tutulurken, V yüklemeleri kütlece %0, %0.5, %1 ve %3 olarak seçilmiştir. Performans testleri iki ideal ve iki gerçekçi besleme kompozisyonuyla 300, 350 ve 400 °C sıcaklıklarında ve besleme hızının katalizör miktarına oranı 120,000 ml g_{cat}^{-1} h^{-1} olarak sabit tutularak yürütülmüştür. Testlerde V yüklemesinin ve reaksiyon koşullarının (H_2O/CO oranı ve sıcaklık) Pt-Re-V/CeO_2 katalizörlerinin WGS aktivitesi, seçimliliği ve stabilitesi üzerindeki etkileri incelenmiştir. Test sonuçlarından, bu çalışmada kullanılan tüm katalizörlerin yüksek CO dönüşümü ve pozitif net H_2 üretimi ile makul WGS performansları gösterdiği ve en yüksek performansa sahip oldukları belirlenen 1Pt-1Re-0.5V/CeO_2 ve 1Pt-1Re-1V/CeO_2'nin yakıt işlemcisinde kullanılma potansiyaline sahip oldukları görülmüştür. Taze indirgenmiş ve kullanılmış katalizörler SEM-EDX, XPS, XRD ve Raman spektroskopisi ile analiz edilmiştir. SEM-EDX analizi ile V-yüklü katalizörlerin daha büyük Pt parçacık boyutunun, yüksek katalitik aktivite açısından pozitif etkisi olabileceği sonucuna varılmıştır. XPS analizinde, reaksiyon esnasında Ce^{3+} içeriğinin, dolayısıyla destek materyalinden aktif metal sitelere elektron transferinin, yüksek WGS aktivitesine bağlı olarak azaldığı görülmüştür. XRD sonuçları, olası V ve CeO_2 etkileşiminin CeO_2 kristal boyutunu değiştirdiğini işaret etmektedir. XPS ve Raman spektroskopisi sonuçları beraber incelendiğinde, katalizör üzerinde VO_2, $CeVO_4$ ve polivanadat yüzey oluşumları görülmüştür. Örneklerde büyük V_2O_5 kristallerine rastlanmaması, vanadyumun yüzeyde oldukça iyi dağıldığını göstermektedir. Hiçbir kullanılmış katalizör örneğinde kok oluşumu görülmemiştir.

TABLE OF CONTENTS

LIST OF FIGURES

LIST OF TABLES

LIST OF SYMBOLS

a	Lattice constant
K	Shape factor
K_{eq}	Equilibrium constant
m_{cat}	Catalyst weight
n	Molar flow rate
$n_{i,in}$	Molar flow rate of species i in the feed stream
$n_{i,out}$	Molar flow rate of species i in the product stream
P	Pressure
R	Universal gas constant
T	Temperature
V_{gas}	Volumetric flow rate of the gas
wt	Weight
β	Line broadening at half the maximum intensity
ΔH°_{298}	Standard enthalpy of reaction
λ	X-ray wavelength
θ	Bragg angle
τ	Mean size of the crystallites

LIST OF ACRONYMS/ABBREVIATIONS

ATR	Autothermal Reforming
BSE	Back Scattering Electron
DI	Deionized
DSS	Daily Start-Up and Shut-Down
EDX	Energy Dispersive X-Ray
FC	Fuel Cell
FP	Fuel Processor
FTIR	Fourier Transform Infrared Spectroscopy
GC	Gas Chromatograph
GHSV	Gas Hourly Space Velocity
HPLC	High Performance Liquid Chromatography
HSA	High Surface Area
HTS	High Temperature Shift
LSA	Low Surface Area
LTS	Low Temperature Shift
MFC	Mass Flow Controller
OD	Outer Diameter
OSC	Oxygen Storage Capacity
PEMFC	Proton Exchange Membrane Fuel Cell
PGM	Platinum Group Metal
POX	Partial Oxidation
PROX	Preferential Oxidation
RWGS	Reverse Water Gas Shift
SE	Secondary Electron
SEM	Scanning Electron Microscopy
SR	Steam Reforming
TCD	Thermal Conductivity Detector
TOF	Turn-over Frequency
TOS	Time-on-stream

WGS	Water-Gas Shift
XP	X-Ray Photoelectron
XPS	X-Ray Photoelectron Spectroscopy
XRD	X-Ray Diffraction

1. INTRODUCTION

More than 80% of the global energy demand is supplied by fossil fuels, i.e. oil, natural gas and coal. However, as burning of fossil fuels for heat and energy generation results in emission of greenhouse gases, their use causes environmental problems including air pollution, climate change and global warming. Hydrogen as an energy carrier has been proposed as one of the most attractive and clean fuel to overcome these environmental issues (Gradisher *et al*., 2015; Sharma *et al*., 2015). Hydrogen can be produced by catalytic reforming of hydrocarbons, and through the use of renewable technologies like electrolysis of water and biomass. Since the renewable technologies are not economically feasible yet, hydrogen production from hydrocarbons is a viable option (LeValley *et al*., 2014).

Water gas shift (WGS) is a reversible and mildly exothermic reaction, which converts carbon monoxide and steam to carbon dioxide and hydrogen. It is an important step in many industrial processes including production of ammonia, methanol, hydrogen and hydrocarbons. Each process requires WGS catalysts with different characteristics imposed by different operation conditions (Ratnasamy *et al*., 2009). WGS has an essential role in producing high purity hydrogen from hydrocarbons; it increases the hydrogen content of the reformer outlet while decreasing CO, which is the unwanted side product of the reformer (Sharma *et al*., 2015).

Fuel cells, which generate electricity from hydrogen, received extensive attention recently, mainly due to the environmental problems related with fossil fuel combustion. Among them, proton exchange membrane fuel cells (PEMFCs) are considered as the most suitable technology for small scale stationary applications, like residential and small scale business uses, due to their high power density, low operation temperature, mechanical robustness and fast start-up properties (Fiorot *et al*., 2007).

Since non-pressurized H_2 storage has technological barriers yet to be overcome and there is no well-proliferated H_2 distribution network; the viable option for guaranteeing wide use of PEMFC in distributed energy production is the use of FP-PEMFC systems; there FP (fuel processor) produces hydrogen on site from hydrocarbons having well-

established distribution networks and/or are easy-to-store (Çağlayan *et al*., 2009). Hydrogen, the only fuel for PEMFC, is the main product of hydrocarbon reforming, but the side product of the reaction is 1-10 vol.% CO. As CO poisons the Pt electrode of the PEMFC, it must be removed from the hydrogen stream. Therefore FPs, which have serial WGS and PROX reactors following the reformer, are utilized to reduce the CO concentration in the H_2-rich product stream down to at most 40 ppm. In the reformer of an FP, hydrocarbons are converted to a mixture including H_2, CO, CO_2 and H_2O; the following WGS unit consumes CO while increasing H_2 concentration, and lastly in PROX, CO is decreased to ppm levels, guaranteeing stable operation of the PEMFC (Çağlayan *et al*., 2009; Nishimura *et al*., 2010).

As WGS is a mildly exothermic and reversible reaction, equilibrium conversion decreases with the increase in the temperature, while the reaction is fast at high temperatures. To overcome these thermodynamic and kinetic limitations, WGS reaction in the industrial applications is commonly performed in a series of two adiabatic reactors; high temperature shift (HTS) and low temperature shift (LTS). HTS is mainly conducted over Fe_2O_3/Cr_2O_3 oxide catalysts at 350-500 °C and reduces the CO concentration to around 3%, while LTS is conducted over $Cu/ZnO/Al_2O_3$ catalysts at 180-240 °C for reducing the CO concentration down to about 0.5-1% (Ratnasamy *et al*., 2009).

The required properties and performance characteristics of WGS catalysts suitable for FP operation are totally different from those of the conventional Fe_2O_3/Cr_2O_3 oxide or $Cu/ZnO/Al_2O_3$ catalysts. The conventional catalysts cannot be used in FPs, as they are pyrophoric, need long pre-conditioning and have narrow range of operation temperature. In addition, they do not have enough mechanical stability during daily start-up/shut-down (DSS) operations, and they deactivate on exposure to air or water. Moreover, the two step (HTS and LTS) WGS reactors are not appropriate for small scale hydrogen production applications, as they constitute the bulkiest part of the whole fuel processor. Consequently, there has been a great research interest in the development of active, non-pyrophoric, poison resistant and robust Platinum-group metal (PGM) based WGS catalysts supported on reducible metal oxides (Li *et al*., 2011; Colussi *et al*., 2014). Recently, Pt and Au based WGS catalysts have been reported promising for small scale applications. Instead of conventional two stage WGS reactors; a single-stage WGS reactor operating at medium

temperatures, ie. in 250-350 °C range, utilizing active and stable catalysts capable of frequent start-up/shut-down is desirable (Zhu *et al*., 2011).

The aim of the proposed work is to design and develop Pt-based, CeO_2 supported trimetallic Pt-Re-V catalysts having high activity, selectivity and stability with suppressed methanation under ideal and real (i.e. feed having CO, H_2O, CO_2, H_2) feed conditions in HTS-LTS transition temperature region, allowing the use of a single WGS reactor in a fuel processor. Re was used as a second metal for modifying the electronic structure of Pt, analogous to previously observed for Au-Re system by other members of our research group, and V was used as a promoter in order to benefit from reducibility of V-O-Ce bond formed. In this context, Pt-Re-V/CeO_2 catalysts with different V loadings were developed and tested for their activity and selectivity in WGS reaction for ideal and real feeds.

In the present study, catalyst composition, temperature and H_2O/CO ratio in both types of the feeds were used as the experimental parameters. Activity, selectivity, and stability of the catalysts were considered as the performance criteria. The structural properties of the catalyst samples were characterized by SEM-EDX, XRD, XPS and Raman spectroscopy.

Chapter 2 contains a detailed literature survey on fuel processor-fuel cell systems, water-gas shift reaction and the catalysts used in this reaction. Chapter 3 involves the details of the experimental work carried out. The results obtained in the reaction and characterization tests are presented and discussed in Chapter 4. Finally, the conclusions of the current study and recommendations for the future work are presented in Chapter 5.

2. LITERATURE SURVEY

2.1. Fuel Processor-Fuel Cell Technology

Due to the environmental problems related with fossil fuel combustion causing climate change, fuel cell technologies have received extensive interest in recent years, owing to their high efficiencies and low emissions. Fuel cells (FCs), which are classified according to the type of electrolytes employed, are electrochemical devices that convert the chemical energy of H_2 or H_2-rich fuels directly into electricity. Among the various fuel cells, proton exchange membrane fuel cells (PEMFCs) are considered as the most suitable technology for small scale and stationary applications, due to their high power density, mechanical robustness, low operation temperature and fast start-up properties (Fiorot *et al*., 2007).

Reforming of hydrocarbons to produce hydrogen generates 10-15 vol.% CO as the side product. As CO poisons and deactivates the Pt electrode of the PEMFC, it must be removed from the system. Therefore fuel processors must be envisaged to decrease the CO concentration in the fuel stream to trace levels.

Since non-pressurized H_2 storage has technological barriers yet to be overcome and there is no well-proliferated H_2 distribution network, the best option is to use combined 'fuel processor-PEM fuel cell' systems for small scale stationary PEMFC applications; there hydrogen having required purity for PEMFC use, i.e. PEM-grade H_2, is produced on-site by fuel processors from hydrocarbons having well-established distribution networks and/or are easy-to-store. A fuel processor (FP) includes three serial catalytic units, which are reformer, WGS and preferential oxidation (PROX), respectively (Çağlayan *et al*., 2009).

The reformer, first reactor of a FP, converts hydrocarbon fuels and steam into a mixture including H_2, CO, CO_2 and H_2O. Among a variety of reforming options, steam reforming (SR) is the most widely employed process to produce synthesis gas with high H_2/CO ratio. In the reformer, a variety of gaseous (methane, propane, etc.) or liquid

(gasoline, diesel, etc.) fuels can be utilized (Shekhawat *et al.*, 2011). Among these, reforming of gaseous fuels is currently the main source for hydrogen production. Besides, the vast majority of today's hydrogen is produced via steam reforming of methane (CH_4). The SR of methane reaction uses methane and steam to produce H_2 and CO (LeValley *et al*., 2014):

$$CH_4 + H_2O \leftrightarrow CO + 3H_2 \qquad \Delta H^{\circ}_{298} = 206.2\ \mathrm{kJ/mol} \tag{2.1}$$

Steam reforming is highly endothermic and therefore the reaction proceeds very poorly at low temperatures, indicating the requirement of high energy input and high reaction temperatures (above 700 °C). The most widely studied SR catalysts are Ni-based, since they are cheap and fairly active. However, the use of Ni-based catalysts for SR has disadvantages as Ni-based catalysts are prone to sulfur poisoning, carbon formation and sintering during operation.

An alternative reforming option overcoming high external energy supply need is to combine SR with partial oxidation (POX); the combined reaction is known as 'autothermal reforming (ATR)'. As an example, Rh- and Pt-based catalysts are commonly used for POX reaction, which utilizes oxygen to convert methane into H_2 and CO: (LeValley *et al.*, 2014):

$$CH_4 + \tfrac{1}{2}O_2 \leftrightarrow CO + 2H_2 \qquad \Delta H^{\circ}_{298} = -35.6\ \mathrm{kJ/mol} \tag{2.2}$$

The autothermal reforming option includes endothermic reforming along with exothermic oxidation reaction, thus providing a thermal balance. However the SR reaction results in higher H_2 yields compared to ATR (Kalmula *et al*., 2014).

In an FP of an FP-PEMFC system, the reformer effluent stream enters the following unit, WGS, in which carbon monoxide and steam react to form carbon dioxide and hydrogen:

$$CO + H_2O \leftrightarrow CO_2 + H_2 \qquad \Delta H^{\circ}_{298} = -41.2\ \mathrm{kJ/mol} \tag{2.3}$$

WGS is a critical step for a fuel processor (FP) producing CO-free H_2, as it reduces CO levels in the reformate gas stream down to 0.5-1% while maximizing H_2 yield. In order to achieve high rate with high conversion, industrial WGS reaction is typically performed in two serial reactors, namely high temperature shift (HTS) and low temperature shift (LTS). HTS is conducted over Fe_2O_3/Cr_2O_3 catalysts at 350-500 °C, while LTS is carried out over $Cu/ZnO/Al_2O_3$ catalysts at 180-240 °C (Ratnasamy *et al*., 2009).

The last catalytic reactor of an FP is the PROX unit, which provides further elimination of the remaining CO in the reformate steam to CO_2 before H_2-rich product is sent to the FC. Since CO is toxic to the Pt electrode of PEMFC, it is decreased to ppm levels in PROX reactor in order to guarantee the stable operation of the PEMFC. The following reaction occurs in the PROX system (Mishra and Prasad, 2011):

$$CO + \tfrac{1}{2}O_2 \rightarrow CO_2 \qquad \Delta H^{\circ}_{298} = -283.6\ \text{kJ/mol} \tag{2.4}$$

An efficient PROX catalyst should be selective, ie. it should suppress possible hydrogen oxidation (Equation 2.5), while eliminating CO under the presence of H_2, CO_2, water vapor and CH_4.

$$H_2 + \tfrac{1}{2}O_2 \leftrightarrow H_2O \qquad \Delta H^{\circ}_{298} = -243.5\ \text{kJ/mol} \tag{2.5}$$

Taking into account the energy efficiency of combined 'FP-PEMFC' systems, the PROX unit is best operated between 100˚C and 130˚C. Supported catalysts based on noble metals, especially Pt are reported to be promising for PROX reaction (Çağlayan *et al*., 2011).

2.2. Water-Gas Shift Reaction

Water gas shift (WGS) reaction, first reported in 1888, is a reversible, moderately exothermic and equilibrium-limited reaction, in which carbon monoxide and water react to form carbon dioxide and hydrogen:

$$CO + H_2O \leftrightarrow CO_2 + H_2 \qquad \Delta H^{\circ}_{298} = -41.2\ \text{kJ/mol} \tag{2.3}$$

The thermodynamic equilibrium constant (K_{eq}) of the WGS reaction can be calculated as a function of absolute temperature (T) from the simple empirical equation derived by Moe (Iulianelli *et al*., 2015):

$$K_{eq} = [\exp(4577.8/T) - 4.33] \quad (2.6)$$

WGS is an important step for a fuel processor (FP) producing CO-free H_2, as it increases H_2 and decreases CO in the reformate gas stream. There has been a renewed interest worldwide on WGS reaction, owing to its potential use in the fuel processor of the combined 'fuel processor-PEM fuel cell' systems, as the Pt electrode of PEMFC is poisoned by CO (Lenite *et al*., 2011).

In order to overcome thermodynamic and kinetic limitations, WGS reaction in industry is carried out in two serial stages: a high temperature shift (HTS) and a low temperature shift (LTS) reactors, which operate at 350-500 °C and 180-240 °C respectively. Conventional HTS catalysts are Fe_2O_3/Cr_2O_3 oxide, while $Cu/ZnO/Al_2O_3$ catalysts are used for LTS. However, they are not suitable for FPs due to their drawbacks related to thermodynamic limitations, i.e. low achievable conversion at high temperatures; due to their pyrophoric nature, their need for lengthy pre-conditioning and slow WGS kinetics over them at low temperatures. They also do not meet the activity and stability requirements for on site PEM fuel cells. Therefore active, selective, stable, water-tolerant, non-pyrophoric and poison resistant platinum-group metal (PGM) based WGS catalyst formulations over metal oxide supports are of great research interest (Çağlayan *et al*., 2011). Additionally, the catalyst should enable the use of a single reactor operating at mid-temperature as single stage WGS unit is preferred for small scale applications, instead of two shift stages, aiming to reduce the FP size (Pradhan *et al*., 2009).

The WGS catalyst must inhibit the methanation reaction given in the Equation 2.7, as it consumes H_2, thus lowering selectivity towards H_2:

$$CO + 3H_2 \leftrightarrow CH_4 + H_2O \qquad \Delta H^{\circ}_{298} = -206.2\ \text{kJ/mol} \quad (2.7)$$

Unlike conventional catalysts used in steady-state WGS processes, catalysts used for small scale stationary FP-PEMFC applications are operated under daily shut-down and start-up (DSS) conditions. The shut-down and start-up conditions involve cooling down the reactor bed with condensing steam, followed by rapid heating to restart the WGS reaction under varying loads. However, WGS catalysts used in the industry are affected negatively during such DSS operations (Ilinich *et al*., 2007).

2.2.1. Conventional Fe- and Cu-based Catalysts for WGS Reaction

Many studies have been reported about the commercial Fe-based HTS and Cu-based LTS catalysts for WGS reaction, investigating different reaction parameters and operation conditions.

HTS is the first step of the WGS unit and conducted over Fe_2O_3/Cr_2O_3 oxide catalysts in the temperature range of 350-500 °C. Iron-chromium (ferrochrome, Fe/Cr) oxide was first patented as a WGS catalyst by Bosch and Wild in 1914 and is still utilized for HTS due to their reasonable activity, low cost and long lifetime in many applications (Lee *et al*., 2013). Studies on HTS catalysts have mainly focused on the preparation methods and developing Cr-free Fe based HTS catalysts.

Marano *et al.* (2009) studied the high temperature WGS performance of Fe-Cr based catalysts synthesized by co-precipitation and oxi-precipitation methods, and compared their activity with a commercial Fe-Cr based catalyst. They concluded that the oxi-precipitation method was more suitable to prepare highly active Fe-Cr based WGS catalysts, and exhibited similar CO conversion with the commercial catalyst. They mentioned that the active phase (Fe_3O_4) is obtained directly when the catalyst is synthesized by oxidation-precipitation method, whereas the catalysts prepared by co-precipitation (Fe_2O_3 phase) needed a reduction step for being active in WGS reaction.

Meshkani *et al.* (2014) focused on developing Fe_3O_4 catalysts by a facile direct pyrolysis method for HTS-WGS reaction and investigated the effects of chromium and copper addition on catalytic activity. For the experiments, pure Fe oxide, Fe-Cr mixed oxide, Fe-Cu mixed oxide, and Fe-Cr-Cu mixed oxide catalysts were prepared by pyrolysis

route. They found out that the pyrolysis method yields the formation of the active Fe_3O_4 phase. It was concluded that Fe-Cr-Cu catalysts showed the highest conversion and a stable performance, indicating the positive effect of Cr and Cu addition on pure Fe oxide.

The development of Cr-free iron based HTS catalysts was also studied previously, as Cr is highly toxic. Liu *et al.* investigated the activity and stability of Cr-free iron catalysts promoted by Al_2O_3 and CeO_2 for HTS. Their study indicated that WGS activity and stability of the developed Cr-free iron catalyst was comparable to those of the commercial Fe-Cr WGS catalysts. It was proposed that the catalyst studied had the redox regenerative mechanism for the WGS reaction (Liu *et al.*, 2005).

Natesakhawat *et al.* (2006) investigated the potential textural promoters for Cr replacement and structural promoters for increasing the WGS activity of Fe-based WGS catalysts. In the studies, Cr-free iron based HTS catalysts were prepared by adding both aluminum and copper via different preparation methods. The results obtained showed that aluminum is a promising alternative for Cr replacement in HTS catalysts, and copper promotes the catalytic activity in Fe-based catalysts. However, the promotional effect of Cu was found strongly dependent on the preparation method.

Ba-promoted Cr-free Fe_2O_3-Al_2O_3-NiO catalysts was studied for their WGS activity for HTS by Meshkani *et al*. (2015). The catalysts used in the study were prepared by coprecipitation method. It was observed that Ba-promoted Cr-free Fe_2O_3-Al_2O_3-NiO catalyst exhibited high surface area and mesoporous structure with higher CO conversion than those of Fe_2O_3-Al_2O_3-NiO and commercial Fe_2O_3-Cr_2O_3-CuO catalysts. They also reported that Ba addition suppressed the CO methanation.

The second step of the WGS unit is LTS and it is conducted mainly over Cu/ZnO/Al_2O_3 catalysts at 180-240 °C. There are many studies on Cu-based catalysts investigating the effect of support and Cu loading on WGS activity and performance specs of the catalysts in shut-down/start-up operations, etc.

Guo *et al.* (2009) studied the effect of the calcination temperature on the WGS activity and stability of the Cu/ZnO/Al_2O_3 catalyst in shut-down/start-up operation. They

observed continuous deactivation of the catalyst in the cyclic operation, and proposed the blocking or deterioration of the active sites by the formation of $Zn_6Al_2(OH)_{16}CO_3 \cdot 4H_2O$ species as the reason of deactivation. It was concluded that calcination temperature affects the formation and extent of interfacial sites between Cu crystallites, and the oxide have a significant role in WGS performance and stability.

The effect of Cu loading on Cu/ZnO catalysts for WGS performance was investigated by Liu *et al.* (2012). In their experiments, catalysts with different Cu loadings, varying between 5-44 wt.%, were used both in steady state and transient (shut-down/start-up) operation modes. Their study indicated that Cu loading can be reduced to 25 wt.% in a steady state WGS reaction. In addition, they proposed that the Cu loading could be reduced further to 15 wt.% for transient/cyclic operation mode, and that low Cu-loaded catalysts are suitable for cyclic operation.

The catalytic WGS activity of Cu/ZnO was compared with that of $Cu/ZnO/Al_2O_3$ in shut-down/start-up cycles by Guo *et al.* (2009). Based on their results, they concluded that Cu/ZnO catalyst reached comparable activity to that of $Cu/ZnO/Al_2O_3$ and it achieved superior stability in the cyclic operation as well. It was suggested that the main reason of $Cu/ZnO/Al_2O_3$ deactivation is the presence of alumina, as it forms carbonate species blocking the active Cu-ZnO interface sites.

Li *et al.* (2011) studied the catalytic WGS performance of CuO/CeO_2 catalysts prepared by precipitation method by using different precipitation agents. They found out the best catalytic activity and stability was achieved when $NH_3.H_2O$ was used as the precipitant. They concluded that high and stable activity is related to less surface 'carbonate-like' species, higher Cu dispersion and better interaction between CuO and CeO_2. It was also mentioned that surface 'carbonate-like' species are disadvantageous for the WGS activity of CuO/CeO_2 catalysts.

Cu-based catalysts supported on CeO_2, CeO_2-ZrO_2, CeO_2-TiO_2 were investigated for their WGS activity by Pradhan *et al.* (2009). They conducted their study by changing gas hourly space velocity and adding CO_2 to the feed stream to compare the performance of the catalysts properly. In the end, CuO-CeO_2-ZrO_2 and CuO-CeO_2 showed improved

performance than $CuO-CeO_2-TiO_2$, and the activity order is: $CuO-CeO_2-ZrO_2$>$CuO-CeO_2$>$CuO-CeO_2-TiO_2$. Consequently, the changes in WGS activities were attributed to the difference in interaction between CuO phase and different supports.

Jeong *et al.* (2014) also studied the effect of different supports on the WGS performance of Cu-based catalysts recently. The supports used were CeO_2, ZrO_2, MgO and Al_2O_3. CO conversions reached over the catalysts in the tests conducted between 200-400 °C showed that Cu/ZrO_2 has the highest conversion at 200 °C, while Cu/CeO_2 is the most active system between 320-400 °C. The group also investigated the effect of precipitation method through comparative performance analysis of co-precipitated and impregnated Cu/CeO_2 catalysts. It was concluded that both catalysts are 100% selective to CO_2, but co-precipitated Cu/CeO_2 exhibits the highest activity and stability in WGS, owing to its easier reducibility and high surface area.

Although these Fe-based HTS and Cu-based LTS catalysts are widely used in the industry, they are not appropriate for mobile applications, as specific reduction procedures and safety precautions on air are necessary, due to their pyrophoricity. Therefore, non-pyrophoric, active and stable catalysts, which are robust to daily start-up/shut-down operations, are need to be developed for small scale applications, like fuel processors. Accordingly, a single stage WGS is desirable and Platinum-group metal (PGM) based catalysts supported on reducible oxides have received a great interest lately (Castaño *et al*., 2014).

2.2.2. Platinum-Group Metal (PGM) Catalysts for WGS Reaction

Platinum group metal (PGM) catalysts have been developed in order to overcome the performance limitations of conventional WGS catalysts, and to achieve higher catalytic activity and stability at moderate temperatures while suppressing methanation. Recent studies have been focused on new WGS catalysts based on precious metals, including Ru, Ro, Pd, Os, Ir, Au and Pt supported on oxides. Pt was found to be the most promising metal for the WGS reaction compared to other precious metals (Rebrov *et al*., 2011; Gökaliler *et al*., 2013).

Despite the extended number of the studies reported on the use and performance analysis of the PGM catalysts, it is still hard to compare their WGS performance as different authors prepared their catalysts by various methods via using various precursors, and they performed the tests under different reaction conditions and feed compositions (Ratnasamy *et al*., 2009).

Through the precious metal-based catalysts, most of the studies were conducted on Pt and Au based catalysts, which were found as leading candidates to be used in small scale fuel processors. The studies on Au-based WGS catalysts revealed that, Au supported on metal oxides show high catalytic WGS activity, especially at low temperatures, and have the potential to be used in practical WGS applications, owing to their advantages like lower price compared to other noble metals (Pt, Rh).

Lenite *et al.* (2011) studied the WGS activity of Au-supported catalysts on Al_2O_3 and CeO_2 under the flow of both ideal (CO, H_2O) and realistic (CO, H_2O, H_2, CO_2) reformate feeds. In their studies, Au/Al_2O_3 catalyst was observed to exhibit poor catalytic activity (less than 30%), indicating the unsuitability of using Al_2O_3 support. Conversely, Au/CeO_2 catalyst showed higher activity: with the ideal feed, the activity approached to equilibrium when the pH of the precursor is optimized. Nonetheless, very low CO conversion was obtained over Au/CeO_2 catalyst, when the realistic reformer outlet was used as the feed.

The deactivation behavior of Au/CeO_2 in WGS was investigated by Liu *et al.* (2013) under both steady-state and shut-down/start-up conditions for a realistic reformer outlet as the feed. Deactivation was detected in both conditions at the studied temperature, 250 °C. In steady-state operation, the reason behind deactivation was suggested as the reduction during reaction by H_2 and CO, resulting in weak Au-CeO_2 interaction, which is crucial for WGS activity. On the other hand, in shut-down/start-up operations, the deactivation was attributed to the deposition of the carbonate species, originating from CO_2 and H_2O. It was indicated that by calcining the catalyst, carbonate species can be removed, and 90% of the original activity was reached over the reactivated sample. They proposed the possibility of preventing Au/CeO_2 deactivation by adding satisfactory amount of CO to the realistic feed in order to enhance the oxidizing potential of the atmosphere.

The effect of mixed oxide support type on WGS activity of Au catalysts was also investigated. Vindigni *et al.* (2012) compared the catalytic activity of gold catalysts supported on pure CeO_2 and ZrO_2-CeO_2. Different amounts of ZrO_2 addition were used and it was deduced that ZrO_2 addition to CeO_2 resulted in the highest WGS activity and stability. Furthermore, it was observed that the catalytic performance is directly proportional with the amount of ZrO_2.

Some authors studied the influence of adding second active metal to gold catalysts and observed enhanced WGS activity. Çağlayan *et al.* (2011) explored the effect of Re addition on Au/CeO_2 catalyst for ideal feed. Different preparation methods were used in the experiments, and the best result was obtained with precipitation of gold on impregnated Re/CeO_2. They concluded that Re addition increases the WGS activity of Au/CeO_2, and the highest WGS activity was obtained over 1%Au-0.5%Re/CeO_2 catalyst.

Yu *et al.* (2010) investigated the WGS activities of bimetallic Au-M/CeO_2 (M= Cu, Ni, Ag, Pd and Pt) catalysts. The WGS activity order of those catalysts was found as: Au-Pt/CeO_2>Au-Ni/CeO_2>Au/CeO_2>Au-Cu/CeO_2>Au-Ag/CeO_2>Au-Pd/CeO_2. Au-Pt/CeO_2 catalyst exhibits the highest activity with 78% CO conversion at 250 °C. The effect of Pt in Au–Pt/CeO_2 catalyst was found to be the production of partly oxidized gold species. Moreover, it was observed that presence of both Au and Pt is beneficial for creation of oxygen vacancies and Ce^{3+} species.

WGS activities of Au and Pt-based catalysts supported on ceria modified materials were compared by Castaño *et al*. (2014) for both ideal and realistic feed mixtures. Ceria or mixed CeFe oxide supports were concluded to be beneficial for WGS activity for both Au and Pt-based systems, whereas Au-based systems were found to be affected more by the electronic properties of the support. According to their results, Au-based catalysts show higher activity at low temperatures (180 °C), while the opposite is true for Pt-based catalysts. Moreover, Pt-based catalysts are able to resist changes in feed stream composition, have higher TOF values, and attain the equilibrium conversion at temperatures around 250 °C.

2.3. Pt-based Catalysts in WGS Reaction

Pt-based catalysts have received more interest recently, owing to their superior WGS activity and stability. It was demonstrated that for Pt-based WGS catalysts, the use of reducible oxide support is crucial. Therefore, in the studies CeO_2, Al_2O_3, TiO_2, ZrO_2 and their mixed oxides have been used as the supports for Pt-based catalysts.

2.3.1. Pt-based Mono and Multi-Metallic WGS Catalysts

Çağlayan *et al.* (2009) focused on the WGS activity of bimetallic Pt-Ni/Al_2O_3 catalysts, and investigated the effects of Ni content and H_2O/CO feed ratio on the catalytic performance. Reaction tests were conducted in the temperature range of 200-450 °C by using a feed consisting of CO and H_2O. By increasing Ni content and H_2O/CO ratio, equilibrium conversions were approached at lower temperatures. It was stated that Pt-Ni/Al_2O_3 catalysts exhibit high activity and stability for WGS under ideal conditions.

Wang *et al*. (2014) compared the WGS performance of Pt-Ni bimetallic catalysts supported on γ-Al_2O_3, SiO_2, TiO_2, CeO_2 and ZrO_2 (both high surface area (HAS) and low surface area (LSA)). The WGS activity order of the Pt-Ni bimetallic catalysts was found as: CeO_2>HSA-ZrO_2>TiO_2>γ-Al_2O_3>SiO_2>LSA-ZrO_2. In addition, when CO uptake values were considered, similar activity order was observed, except that Pt-Ni/TiO_2 reaches the activity level of Pt-Ni/CeO_2. Selectivity towards CH_4 was also studied, and it was found that Pt-Ni/TiO_2 and Pt-Ni/HAS-ZrO_2 catalysts have very low selectivity to undesired CH_4. In conclusion, CeO_2, TiO_2 and HSA-ZrO_2 are claimed to be promising supports for the bimetallic Pt-Ni WGS catalyst.

Zhu *et al*. (2011) studied the effect of Na addition on the structural properties of Pt/TiO_2 and consequently on its WGS activity. In the experiments, different Na loadings in 0-10 wt.% range were used, while Pt loading was fixed at 1 wt.%. It was observed that the activity is greatly affected by the amount of Na loading. It was concluded that 3-4 wt.% Na addition significantly increases the catalytic performance of 1% Pt/TiO_2. Moreover, it was stated that the strong interaction between the metal and the promoter provides highly active sites for WGS and prevents Pt sintering.

The pyrophoricity and stability of Cu and Pt-based WGS catalysts was comparatively studied by Kam *et al.* (2010) under shut-down/start-up operations. The resistance of Pt-catalysts to chlorine and sulfur poisoning was also investigated. During the experiments, Cu/ZnO- based catalysts were experienced high temperature rises during start-up and shut-down operations and suffered from pyrophoricity, while no pyrophoricity was observed for Pt-based catalysts. Moreover, Pt/TiO_2 and Pt/ZrO_2 catalysts went through sintering during steady-state operation. Cu/ZnO catalyst exhibited significant activity lost during DSS operations.

This section involved the WGS studies with Pt-based catalysts on different supports, excluding CeO_2. However, among the Pt-based WGS systems, the studies were mostly performed on CeO_2 or CeO_2-based mixed oxides supports. Some of those studies are reported as separate sections; in Section 2.3.2, CeO_2-supported Pt-based catalysts are the focus of interest, while in Section 2.3.3, the studies on Re and V promotion are overviewed.

2.3.2. Ceria Supported Pt-based WGS Catalysts

CeO_2 catalysts are extensively used in the purification of H_2 and exhaust gases in automative catalytic converters. This interest is mainly due to the ability of CeO_2 to easily form and eliminate oxygen vacancy defects, leading to high oxygen storage capacity (OSC). Most of the studies mentioned CeO_2 as the primary contributor in the WGS performance, as it enhances the activity of the -mainly- noble metal based catalysts (Esch *et al.*, 2005; Campbell and Peden, 2005; Gradisher *et al.*, 2015).

Oxygen vacancies are reported to be the most reactive sites on metal oxide surfaces and known as defects. A surface oxygen vacancy is created when an adsorbate is oxidized at the surface, and it is very important for the binding of catalytically active species to ceria (Campbell and Peden, 2005). In ceria, the excess electrons left behind after the removal of neutral oxygen are stated to localize on empty f states. Consequently, Ce^{4+} ions are reduced to Ce^{3+} ions and this reduction greatly improves the reactivity of the CeO_2 substrates (Esch *et al.*, 2005).

Gonzalez *et al.* (2010) compared the WGS activities of Pt catalysts supported on cerium-modified TiO_2, pure CeO_2 and TiO_2. Among the catalysts studied, best activity and stability was observed over Pt supported on cerium-modified TiO_2. When Ce-TiO_2 catalyst was characterized, it was revealed that cerium was highly dispersed on the support with a close interaction with Ti atoms. In addition, the interaction between Pt and Ce facilitated the reducibility of Ce at low temperatures, while preventing Ti from over-reduction at high temperatures. This modification in the reducibility of the support was proposed to be the reason of high WGS activity and stability of Pt based Ce-TiO_2 catalyst.

WGS reaction was studied on Pt/CeO_2, Pt/ZrO_2 and Pt/$Ce_xZr_{1-x}O_2$ catalysts by Vignatti et al. (2011). Their results showed that Pt supported on $Ce_xZr_{1-x}O_2$ mixed oxides with $x \geq 0.5$ have higher WGS activities than Pt supported on single oxides. The reason behind that was proposed as addition of Zr to ceria increased its surface area and reducibility, leading to higher concentration of surface OH groups formed on these catalysts. On the other hand, the lower catalytic activity exhibited by Pt/ZrO_2 and Pt/$Ce_xZr_{1-x}O_2$ samples was associated with the higher stability of formate species generated on those samples.

Kalamaras *et al.* (2011) investigated the effect of Pt particle size on WGS kinetics over Pt/CeO_2 catalysts. The particle size of the Pt catalysts changed between 1.3 and 8 nm and the WGS reaction was conducted at 300 °C. Considering the mechanistic and kinetic study carried out, it was suggested that the WGS reaction on Pt/CeO_2 occurs mostly via the 'redox' mechanism, and to a lesser extent via 'the associative formate with -OH group regeneration' mechanism. The change in the particle size slightly affected the TOF (s^{-1}) of WGS, whereas the specific rate of reaction was significantly increased with the increase of the particle size.

2.3.3. Rhenium and/or Vanadium Promoted Pt-based WGS Catalysts

Bimetallic Pt-Re/Al_2O_3 catalysts have been largely used in the naphtha reforming process since 1960's and showed higher stability than monometallic Pt/Al_2O_3 catalysts. Many researchers have investigated the Pt-Re catalysts in order to explain the positive effect of Re (Azzam *et al.*, 2013).

Iida *et al.* (2006) performed a study focusing on the improved WGS activity resulted from the Re addition to Pt/TiO_2 and Pt/ZrO_2 catalysts. It was found out that Re has quite different roles on those catalysts. For the $Pt\text{-}Re/TiO_2$ catalyst, stronger interaction was observed between Pt and Re compared to that for ZrO_2 supported catalyst, and Re state was stable. The group reported that adding Re increased the dispersion of Pt on TiO_2, which was stated as the reason of the superior WGS activity of $Pt\text{-}Re/TiO_2$ catalyst. For the $Pt\text{-}Re/ZrO_2$, the interaction between Re and ZrO_2 was stronger and the redox reaction of Re was led to changes of oxidation states between Re^{4+}-Re^{7+}, contributing to high catalytic activity of $Pt\text{-}Re/ZrO_2$, although it had lower Pt dispersion.

Azzam *et al.* (2007) investigated Pt-Re catalysts on different supports, including CeO_2, ZrO_2, TiO_2, $Ce_xZr_{1-x}O_2$, $Ti_xZr_{1-x}O$ and $Ti_xCe_{1-x}O_2$. It was observed that the addition of Re increased both the WGS activity and stability of the catalysts studied. Best catalytic activity was obtained over $Pt\text{-}Re/TiO_2$, where Re prevented Pt sintering observed in Pt/TiO_2. Pt/CeO_2 catalysts suffered from deactivation caused by the formation of stable carbonate species on CeO_2 support. Using mixed oxides did not improve the activity but increased the red-ox properties of the supports. It was proposed that under the reaction conditions some part of Re is present in oxidized form (ReO_x), probably leading to an improvement in the catalyst activity.

Same group also conducted a kinetic study to understand the role of Re in $Pt\text{-}Re/TiO_2$ for WGS, and to determine the reaction sequences in the presence of Re. Characterization results showed that Re addition has no effect on the surface area of TiO_2 and on Pt dispersion. In the kinetic part of the study, it was suggested that ReO_x sites on catalyst surface provides an additional redox route for WGS reaction, in which ReO_x is reduced by CO forming CO_2 and then reoxidized with H_2O generating H_2. Therefore, the possible WGS reaction routes were found out to be the associative formate route with redox generation as well as two classical redox routes involving both TiO_2 and ReO_x, between which the first one was proposed to be the dominant pathway (Azzam *et al.*, 2008).

A further study of Azzam *et al.* (2013) focused on the interaction between Re and Pt in $Pt\text{-}Re/TiO_2$ catalysts, and on the role of Pt-Re interaction in improved WGS activity. For

the study, Pt-Re/TiO_2 catalysts were prepared by different methods and impregnation sequences. The results showed that the best preparation strategy for WGS activity and stability is the sequential impregnation of Re prior to Pt without intermediate drying and calcination. As an early study reported that Re has higher affinity for chlorine than oxygen, it was suggested in this study that high performance is obtained when Re reacts with the chlorine coming from the deposited $PtCl_6^{2-}$ on TiO_2, indicating the effect of the Pt precursor used. The effect of the Pt:Re ratio on WGS activity was also investigated. The optimum activity and stability was obtained at a Pt:Re molar ratio of unity. In FTIR study, addition of water was found having more influence on Pt-Re catalyst than on Pt catalyst. By adding H_2O, CO peaks on Re disappeared, proposing that Re was oxidized and thus CO adsorption was prevented. From the TPR results, it was suggested that the presence of Re caused lower PtO_x reduction temperatures. The group concluded that the improved WGS performance of Pt-Re/TiO_2, compared to that of Pt/TiO_2 catalyst, is not related with the interaction between Pt and Re. The ability of ReO_x to provide an additional route through redox mechanism to activate water is the only reason of the high activity and stability for WGS.

There are only few papers in the literature regarding the use of vanadium in WGS catalytic systems. However, vanadium oxide has widely been studied in oxidation reactions and is known to present high oxygen mobility when it is partially reduced. This is a direct consequence of the structural defect generation ability of vanadium, which makes it beneficial for the WGS reaction (Duarte de Farias *et al.*, 2008).

The effect of adding vanadia to Pt/ZrO_2 catalyst for improving WGS performance was investigated by Nguyen-Thanh *et al*. (2008). In the experiments, monoclinic ZrO_2 (m-ZrO_2) support was used, and V loadings, measured as weight percent (wt.%) of V_2O_5, was changed between 1-13 wt.%. The results revealed that WGS activity increased with the addition of vanadia compared to the vanadia-free Pt/ZrO_2 catalysts regardless of the amount of vanadia. The best catalyst contained 3 wt.% of vanadia, when the monovanadate is the predominant species. The promoting effect of monovanadate was proposed to be a result of enhanced reducibility provided through formation of V–O–Zr bonds.

Silva *et al.* (2008) studied the effect of V addition to WGS activity and stability of Pt/CeO_2 catalyst. In the study, $Pt/V\text{-}CeO_2$ catalyst was prepared by wet impregnation of V on CeO_2 support, following by incipient-to-wetness impregnation of Pt. The reaction was conducted between 200-350 °C under the flow of exact reformate composition. At the end of the experiments, it was concluded that the $Pt/V\text{-}CeO_2$ is more active than Pt/CeO_2 in the wide range of temperature studied, reaching a maximum value at 325 °C. $Pt/V\text{-}CeO_2$ catalyst also exhibited better stability compared to that of Pt/CeO_2, which started to deactivate after 10 h. It was suggested that the higher WGS activity of $Pt/V\text{-}CeO_2$ catalyst is related to the redox properties of V_2O_5 phase.

Duarte de Farias *et al.* (2008) focused on describing the vanadium structures generated on Pt/CeO_2 catalyst and their role in improving the WGS reaction. They prepared the catalysts through using the procedure mentioned by Silva *et al.*, 2008, and changed the V loading, as wt.% of V_2O_5, between 1 and 18 wt.%. They used several spectroscopic techniques to investigate the possible species involved. In the characterization part of their study, BET surface area results suggested that addition of V decreases the surface area. In the XRD analysis, peaks for CeO_2 were observed for almost all samples. However, the catalysts with high V loading also showed the reflections of V_2O_5 and $CeVO_4$ phases. The formation of those crystalline phases were further used to explain the BET surface area behaviors of the samples. V^{5+}-O-Ce^{3+} sites were developed due to the ability of surface vanadia to remove oxygen from CeO_2, which is the most easily reducible oxide present on the catalyst surface.

XPS analysis revealed that the distribution of V oxidation states became wider, consisting of V^{5+}, V^0, V^{2+} and V^{3+}states, with the increase in V loading. Conversely, for low V loadings ($Pt/1VCeO_2$ catalyst with 1 wt.% V_2O5), narrower distribution of oxidation states, mainly V^{5+},and the formation of dispersed VO_x species were observed rather than isolated or polymeric formations. Besides, XPS results showed that the distribution of Pt oxidation states was directly affected by the presence of vanadium.

The WGS reaction was carried out at different temperatures in the range of 200-350 °C under the flow of a typical ethanol reformer. It was concluded that the addition of V to Pt/CeO_2 catalyst leads to an improvement in WGS activity, regardless of the V amount.

Through the different catalysts studied, Pt/6VCeO_2 (containing ~3 wt.% of V) exhibited the highest activity over the whole temperature range investigated. V loadings lower and higher than this value resulted in less activity.

V addition increased the catalytic activity up to a vanadium surface density of 6V atoms/nm^2, which is below monolayer coverage. In this concentration, mono and polyvanadates species were formed, as confirmed by XRD and DRIFTS analyses. They concluded that the improvement in WGS kinetics is related with the V-O-Ce bonds, while the V-O-V bonds have no effect at all (Duarte de Farias *et al*, 2008).

3. EXPERIMENTAL WORK

3.1. Materials

3.1.1. Chemicals

The chemicals used for catalyst preparation are listed in Table 3.1. All chemicals used are research grade.

Table 3.1. Chemicals used in catalyst preparation.

Chemicals	**Formula**	**Source**	**Molecular Weight (g/mol)**
Ammonium carbonate	$CH_6N_2O_2{\cdot}CH_5NO_3$	Merck	157.13
Ammonium meta-vanadate	NH_4VO_3	Riedel-de Haën	116.98
Ammonium perrhenate	NH_4ReO_4	Sigma-Aldrich	268.24
Cerium (III) nitrate hexahydrate	$Ce(NO_3)_3{\cdot}6H_2O$	Sigma-Aldrich	434.23
Oxalic acid dihydrate	$C_2H_2O_4{\cdot}2H_2O$	Alfa Aesar	126.07
Sodium carbonate	Na_2CO_3	Merck	105.99
Tetraammineplatinum(II) nitrate	$Pt(NH_3)_4(NO_3)_2$	Aldrich	387.22

3.1.2. Gases and Liquids

The specifications and applications of the liquid and gases used in this study are presented in Table 3.2. and Table 3.3, respectively. All of the gases used in this research were supplied by the Linde Group, Gebze, Turkey.

Table 3.2. Specification and application of the liquid used.

Liquid	Specification	Application
Water	Deionized (DI)	Aqueous solutions, Reactant

Table 3.3. Specifications and applications of the gases used.

Gas	Formula	Specification	Application
Argon	Ar	99.995%	Inert, Reducing agent, GC carrier gas
Carbon dioxide	CO_2	99.995%	Reactant, GC calibration
Carbon monoxide	CO	99.999%	Reactant, GC calibration
Dry air	N_2O_2 mixture	99.998%	GC 6-way pneumatic valve
Hydrogen	H_2	99.995%	Reactant, Reducing agent, GC calibration
Methane	CH_4	99.995%	GC calibration

3.2. Experimental Systems

There are four main types of experimental systems used in this study:

(i) Catalyst Preparation Systems: This group involves the set-ups used for support preparation and for incipient-to-wetness impregnation steps of catalyst preparation.

(ii) Catalyst Characterization Systems: These systems are used to characterize the structural properties of the catalyst samples prepared and analyze the changes occur during the reaction.

(iii) Catalytic Reaction System: This system consists of a feed section including mass flow controllers, HPLC pump and a mixing zone; a reaction section composed of a continuous flow microreactor in a temperature controlled oven. This catalytic reaction system is used for determining the catalytic activity, selectivity and stability.

(iv) Product Analysis System: The quantitative analysis of the reactant and product streams is carried out by a gas chromatograph that is connected on-line to the microreactor flow system.

3.2.1. Catalyst Preparation Systems

The system used for preparing catalysts by incipient-to-wetness impregnation technique (Figure 3.1.) consists of a Retsch UR1 ultrasonic mixer, a vacuum pump, a Büchner flask and a MasterFlex computerized-drive peristaltic pump. Support preparation system by precipitation method is shown in Figure 3.2. and contains a Julabo water bath, a 500 ml beaker, a Heidolph impeller and a Mettler Toledo pH-meter.

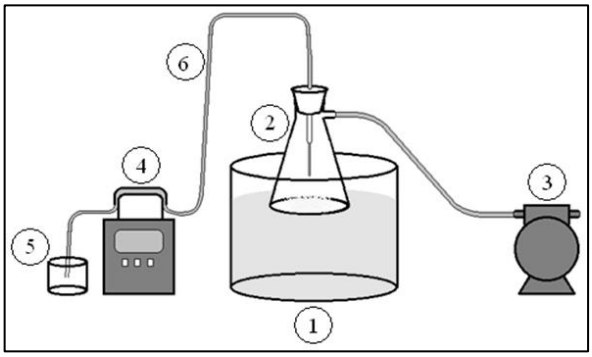

Figure 3.1. Schematic diagram of the impregnation system
(1. Ultrasonic mixer, 2. Büchner flask, 3. Vacuum pump, 4. Peristaltic pump, 5. Precursor solution, 6. Silicone tubing).

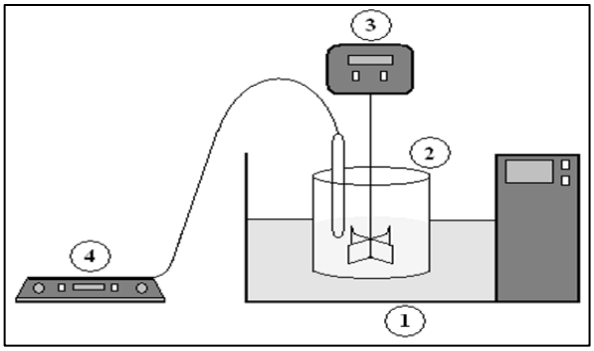

Figure 3.2. Schematic diagram of the precipitation system
(1. Water bath, 2. Beaker, 3. Impeller, 4. pH-meter).

3.2.2. Catalyst Characterization Systems

3.2.2.1. Scanning Electron Microscopy and Energy Dispersive X-Ray (SEM-EDX). SEM and SEM-EDX (Energy Dispersive X-Ray) micrographs of freshly reduced catalyst samples were used to obtain information on their microstructure and metal dispersion, and to observe morphological differences. The tests were conducted in a Philips XL 30 ESEM-FEG system, having a maximum resolution of 2 nm. The experiments were performed at the Advanced Technologies Research and Development Center of Boğaziçi University.

3.2.2.2. X-Ray Photoelectron Spectroscopy (XPS). The extent of electronic interaction between metal components of the freshly reduced catalyst samples was identified through determining the amounts of metallic phases by X-ray photoelectron spectroscopy (XPS). The XPS characterization was made by a Thermo Scientific K-Alpha X-ray Photoeleectron Spectrometer. The spectra were referenced to C1s line. The peak intensities were estimated by calculating the integral of each peak, after substracting of the S-shaped Shirley-type background and fitting the curve to a combination of Lorentzian/Gaussian lines. The tests were performed at the Advanced Technologies Research and Development Center of Boğaziçi University.

3.2.2.3. X-Ray Diffraction (XRD). The crystalline phases of the catalysts samples and their particle sizes were identified by using a Rigaku D/MAX-Ultima+/PC X-ray diffraction equipment having an X-ray generator with Cu target and scan speed of 2°/min. The analyses were performed at the Advanced Technologies Research and Development Center of Boğaziçi University.

3.2.2.4. Raman Spectroscopy. The extents of V–O–Ce bond formation on the freshly reduced catalysts and possible coke formations on spent catalysts after reaction were investigated with Raman spectroscopy by using a Renishaw inVia Raman microscope with a 514 nm-20 mW Ar^+ laser, with ~2mW intensity, 10 s acquisition time and a total of 10 accumulation per spectrum. The analyses were performed at the Advanced Technologies Research and Development Center of Boğaziçi University.

3.2.3. Catalytic Reaction System for WGS Reaction

The catalytic reaction system (Figure 3.3) used in this study was designed and constructed in the Catalysis and Reaction Engineering Laboratory of Chemical Engineering Department, Boğaziçi University and involves three main sections: feed, reaction and product analysis.

The stystem used was originally designed for sequential OSR-WGS reactions with two consecutive reactors. Morever there are two gas chromatographs (GC) connected to the system to analyze different gases involved in those two reactions. However this study focused on the WGS performance of Pt-Re-V catalysts and therefore only the first reactor and GC, which are circumscribed on Figure 3.3, were used in the experiments.

The feed section was composed of mass flow control systems, an HPLC pump, 1/4'', 1/8'' and 1/16'' stainless steel tubes, valves and fittings for feeding liquid water and gaseous species, i.e. hydrogen, argon, carbon dioxide and carbon monoxide. Gaseous reactants were supplied by pressurized cylinders passing through gas flow regulators at the pressure of 2.5 bar. The flow rates of the gasses were controlled by Brooks Instrument mass flow controllers and the set values were adjusted by the Brooks Instrument 0154 series control box. On-off valves were placed in front of the mass flow controllers to protect them from possible back-pressure fluctuations. Each gas was fed from an independent line, in order to calculate the flow of individual species and adjust desired feed composition. The flow direction of feed gases could be diverted to the bypass line before entering the reactor by using a three way valve to let the feed mixture come to an equilibrium state.

The liquid water was introduced into the reaction system at constant flow rates by using a Jasco PU-2089 Plus quaternary gradient pump. To feed water in the gaseous state, 1/16" stainless steel tubing, through which water was allowed to flow and the whole reactant mixing zone were kept about at 140±5 °C by using a Cole-Parmer heating tape covered with ceramic wool insulation, a 16-gauge wire K type sheathed thermocouple and Shimaden SR91 temperature controller.

The reactants, metered and mixed in the feed section, were allowed to flow through the reaction section. This section was composed of a 47 cm × 20 cm × 20 cm furnace with 3.4 cm OD, whose temperature was controlled by a Shimaden FP23 programmable temperature controller connected to a K-type sheathed thermocouple. A down-flow, 56 cm long ¼" OD stainless steel tubular microreactor was placed inside the furnace. Silane treated glass wool was placed in the center of the reactor to stabilize the catalyst bed. In order to prevent heat loss and provide a stable temperature profile, ceramic glass wool insulations were placed in top and bottom ends of the reactor furnace. Since the product stream contains steam, which is harmful for GC columns, a cold trap consisting of two condensers connected in series was placed inside an ice-water bath at the reactor exit to condense water before the GC inlet. The line between reactor exit and cold trap was also heated to prevent the condensation of steam along the line.

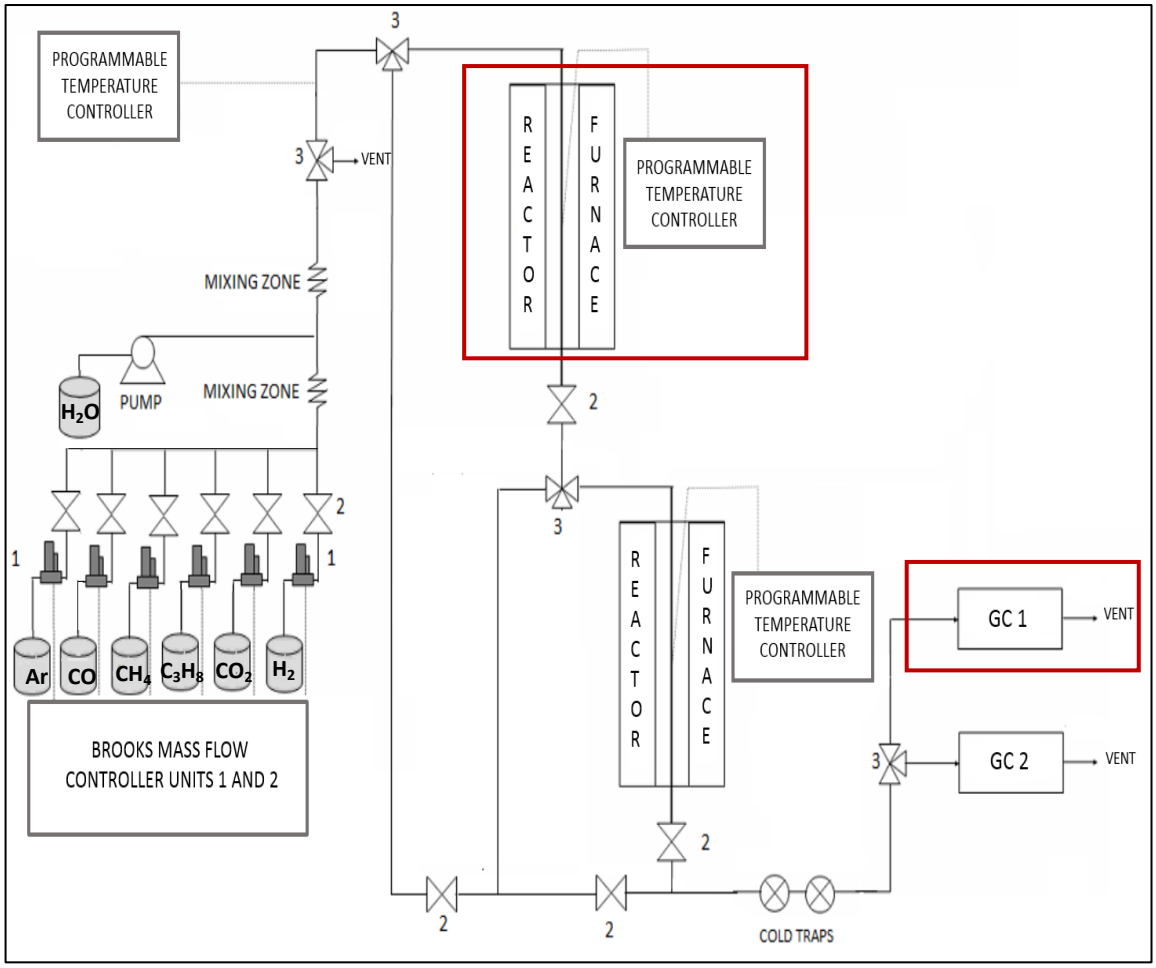

Figure 3.3. Schematic representation of the WGS reaction system (Gökaliler, 2012). (1) Mass flow controller, (2) On-off valve, (3) Three-way valve.

3.2.4. Product Analysis System for WGS reaction

An Agilent Technologies 6850 gas chromatograph (GC) equipped with Hayesep D column, and a Thermal Conductivity Detector (TCD) was used to analyze feed and dry product streams. Time-on-stream (TOS) data were used for reporting the catalyst performance. Analysis conditions of the GC are given in Table 3.4 below.

Table 3.4. Reactant and product gas analysis conditions.

GC Specifications	**Agilent Technologies 6850**
Detector type	TCD
Column temperature, °C	40
Inlet temperature, °C	100
Detector temperature, °C	150
Carrier gas	Argon
Carrier gas flow rate, ml/min	15
Column packing material	Hayesep D
Column tubing material	Stainless steel
Column length & ID	3m x 3 mm
Sample loop	1 ml

Prior to the experiments, the gas chromatograph was calibrated by feeding known volumes of gases under the conditions given in Table 3.4 and calculating the peak areas. By using this method, volume versus peak area curves were obtained for each gas and the corresponding calibration factors were determined by linear regression (Çağlayan, 2011).

3.3. Catalyst Preparation and Pretreatment

Ceria support was prepared by homogeneous precipitation of cerium (III) nitrate hexahydrate with sodium carbonate. Briefly, aqueous Na_2CO_3 solutionwas slowly added to the cerium-precursor containing solution, which was kept at 60 °C and stirred at 200 rpm in a water bath. Addition of sodium carbonate solution continued until the pH value

reached to 8. The resulting suspension was left mixing for an hour in the water bath at 60°C under controlled temperature and pH. Afterwards, it was filtered by using Watman filter paper under vacuum, and washed with deionized water several times. It was then dried overnight at 110 °C and finally calcined in a muffle furnace at 400 °C for 4 h (Çağlayan, 2011).

V addition to CeO_2 support was conducted via incipient to wetness impregnation technique by using aqueous solution of ammonium meta-vanadate and oxalic acid dihydrate. CeO_2 support was placed in a Büchner flask and mixed ultrasonically for 25 minutes under vacuum. The precursor solution containing the mixture of ammounium meta-vanadate and oxalic acid with 1:1.5 molar ratio was then impregnated on the support by using a peristaltic pump at a rate of 0.5 ml/min. Afterwards, the resulting slurry formed was left under vacuum and ultrasonic mixing for 1.5 h, then dried overnight at 110 °C and later on calcined at 400 °C for 2 h in a muffle furnace.

Re addition to V impregrated CeO_2 support was conducted via incipient to wetness impregnation technique by using aqueous solution of ammonium perrhenate. The V impregrated CeO_2 support was placed in a Büchner flask and mixed ultrasonically for 25 minutes under vacuum. The precursor solution was then impregnated on the support by usinga peristaltic pump at a rate of 0.5 ml/min. Afterwards, the resulting slurry formed was left under vacuum and ultrasonic mixing for 1.5 h, then dried overnight at 110 °C and later on calcined at 400 °C for 2 h in a muffle furnace.

Finally, Pt addition to V and Re impregnated CeO_2 support was conducted via incipient to wetness impregnation technique by using aqueous solution of $Pt(NH_3)_4(NO_3)_2$. The V and Re impregrated CeO_2 support was placed in a Büchner flask and mixed ultrasonically for 25 minutes under vacuum. The precursor solution was then impregnated on the support by usinga peristaltic pump at a rate of 0.5 ml/min. Afterwards, the resulting slurry formed was left under vacuum and ultrasonic mixing for 1.5 h, then dried overnight at 110 °C and later on calcined at 400 °C for 4 h in a muffle furnace.

All catalysts tested in this study were prepared in the sequence explained above (sequential impregnation). Table 3.5 represents the Pt, Re and V loadings of the catalysts

studied on CeO_2 supports. The Pt and Re loadings were kept fixed as 1 wt.% for all samples, while V loadings were changed. Prior to the reaction tests, the catalyst samples (75 mg) were reduced *in situ* under 15% H_2/Ar flow at 375 °C for 2 h at a flow rate of 100 ml/min. The temperature of the furnace was increased at a rate of 8.75 °C/min.

Table 3.5. List of Pt-Re-V/CeO_2 catalysts.

Catalyst Name	**Pt wt.%**	**Re wt.%**	**V wt.%**
1Pt-1Re-3V/CeO_2	1	1	3
1Pt-1Re-1V/CeO_2	1	1	1
1Pt-1Re-0.5V/CeO_2	1	1	0.5
1Pt-1Re/CeO_2	1	1	0

3.4. WGS Reaction Tests

The WGS performance of Pt-Re-V/CeO_2 catalysts given in Table 3.5 was investigated at 300, 350 and 400 °C for two ideal and two real feed compositions. The feed compositions are given in Tables 3.6 and 3.7 for ideal and real cases, respectively. The experiments were performed using 75 mg freshly reduced catalyst with 120,000 ml $g_{cat}^{-1}h^{-1}$ GHSV for 6 hour TOS.

Table 3.6. Ideal feed compositions used in this study.

Feed	**H_2O/CO**	**CO%**	**H_2O%**	**Ar%**
Ideal #1	5.0	3.0	15.0	82.0
Ideal #2	2.0	3.0	6.0	91.0

Table 3.7. Real feed compositions used in this study.

Feed	**H_2O/CO**	**CO%**	**H_2O%**	**H_2%**	**CO_2%**	**Ar%**
Real #1	6.7	4.9	32.7	30.0	10.4	22.0
Real #2	16.2	2.1	34.1	23.7	12.3	27.8

TOS starts when the reactant gases and catalyst bed firstly contact with each other. Initial product analysis was conducted 30 minutes after the first contact. Then at the end of every hour the product was analyzed, totally for 6 hours. On the other hand, feed analyses were performed after the product analyses. In the end, seven product analyses and three feed analyses were carried out during each reaction test.

In this work, the effects of V loading, steam/carbon monoxide ratio (H_2O/CO) and temperature on the WGS activity and stability of the Pt-Re-V/CeO_2 cataysts were studied. Performed experiments are listed in Table 3.8 below.

Table 3.8. Summary of the performed experiments.

Experiment #	**Catalyst**	**Feed**	**Temperature (°C)**
1	1Pt-1Re-3V/CeO_2	Ideal #1	300
2	1Pt-1Re-3V/CeO_2	Ideal #1	350
3	1Pt-1Re-3V/CeO_2	Ideal #1	400
4	1Pt-1Re-3V/CeO_2	Ideal #2	300
5	1Pt-1Re-3V/CeO_2	Ideal #2	350
6	1Pt-1Re-3V/CeO_2	Ideal #2	400
7	1Pt-1Re-3V/CeO_2	Real #1	300
8	1Pt-1Re-3V/CeO_2	Real #1	350
9	1Pt-1Re-3V/CeO_2	Real #1	400
10	1Pt-1Re-3V/CeO_2	Real #2	300
11	1Pt-1Re-3V/CeO_2	Real #2	350
12	1Pt-1Re-3V/CeO_2	Real #2	400
13	1Pt-1Re-1V/CeO_2	Ideal #1	300
14	1Pt-1Re-1V/CeO_2	Ideal #1	350
15	1Pt-1Re-1V/CeO_2	Ideal #1	400
16	1Pt-1Re-1V/CeO_2	Ideal #2	300
17	1Pt-1Re-1V/CeO_2	Ideal #2	350
18	1Pt-1Re-1V/CeO_2	Ideal #2	400
19	1Pt-1Re-1V/CeO_2	Real #1	300

Table 3.8. Summary of the performed experiments (cont.).

Experiment #	Catalyst	Feed	Temperature (°C)
20	1Pt-1Re-1V/CeO_2	Real #1	350
21	1Pt-1Re-1V/CeO_2	Real #1	400
22	1Pt-1Re-1V/CeO_2	Real #2	300
23	1Pt-1Re-1V/CeO_2	Real #2	350
24	1Pt-1Re-1V/CeO_2	Real #2	400
25	1Pt-1Re-0.5V/CeO_2	Ideal #1	300
26	1Pt-1Re-0.5V/CeO_2	Ideal #1	350
27	1Pt-1Re-0.5V/CeO_2	Ideal #1	400
28	1Pt-1Re-0.5V/CeO_2	Ideal #2	300
29	1Pt-1Re-0.5V/CeO_2	Ideal #2	350
30	1Pt-1Re-0.5V/CeO_2	Ideal #2	400
31	1Pt-1Re-0.5V/CeO_2	Real #1	300
32	1Pt-1Re-0.5V/CeO_2	Real #1	350
33	1Pt-1Re-0.5V/CeO_2	Real #1	400
34	1Pt-1Re-0.5V/CeO_2	Real #2	300
35	1Pt-1Re-0.5V/CeO_2	Real #2	350
36	1Pt-1Re-0.5V/CeO_2	Real #2	400
37	1Pt-1Re/CeO_2	Ideal #1	300
38	1Pt-1Re/CeO_2	Ideal #1	350
39	1Pt-1Re/CeO_2	Ideal #1	400
40	1Pt-1Re/CeO_2	Ideal #2	300
41	1Pt-1Re/CeO_2	Ideal #2	350
42	1Pt-1Re/CeO_2	Ideal #2	400
43	1Pt-1Re/CeO_2	Real #1	300
44	1Pt-1Re/CeO_2	Real #1	350
45	1Pt-1Re/CeO_2	Real #1	400
46	1Pt-1Re/CeO_2	Real #2	300
47	1Pt-1Re/CeO_2	Real #2	350
48	1Pt-1Re/CeO_2	Real #2	400

Before proceeding with the experiments, the catalyst bed was heated to the reaction temperature and trapped with Ar gas after reduction. Meanwhile, the reactants with specific compositions were bypassed and mixed for 1.5 hour to obtain a steady state gas composition.

4. RESULTS AND DISCUSSIONS

The results of this study are presented and discussed in two sections. In the first section, the results of the WGS performance tests are reported. In the performance tests, the effects of V loading, reaction temperature and feed composition on the WGS performance of Pt-Re-V/CeO_2 catalysts were investigated.

Second section includes the results of the characterization analyses. Characterization analyses were carried out to investigate physical and chemical properties of the catalyst samples. This section involves the SEM-EDX, XPS, XRD, and Raman spectroscopy analyses for all trimetallic Pt-Re-V/CeO_2 and bimetallic Pt-Re/CeO_2 catalysts. Relation between WGS activity and microstructural/chemical properties of the catalysts was tried to be formed.

4.1. WGS Performance Tests

WGS activity and stability performance of the catalysts were investigated by using the experimental conditions listed in Table 3.8. Catalytic activity was reported as CO conversion for both ideal and real feeds, while for real feeds the amount of net H_2 produced was also reported. 2 h TOS data were used to compare the activities of the catalyst samples (Figures 4.1-4.6 and 4.9-4.10).

Blank tests were previously performed by Çağlayan in 2011 to ensure that the reactor, glass wool and CeO_2 support had no catalytic activity. The results indicated that both the system and the support were inactive under the reaction conditions (Çağlayan, 2011).

Calculation methods for CO conversion and the net H_2 production rate, as the percentage increase in molar flow rate of hydrogen in the product stream on the basis of molar flowrate of H_2 in the feed, are given in Equations 4.1 and 4.2, respectively:

$$\text{CO conversion (\%)} = \left[\frac{n_{CO,in} - n_{CO,out}}{n_{CO,in}}\right] 100 \quad (4.1)$$

$$\text{Net } H_2 \text{ production (\%)} = \left[\frac{n_{H_2,out} - n_{H_2,in}}{n_{H_2,in}}\right] 100 \quad (4.2)$$

where the molar flow rates in both feed (in) and product (out) streams are calculated by using Equation 4.3:

$$n_i \ (\mu mol\ s^{-1}) = \frac{P\ V_{i,gas}}{R\ T} \quad (4.3)$$

where P is the atmospheric pressure, which is the operating pressure of the WGS test rig, $V_{i,gas}$ is the volumetric flow rate of the gas, R is the universal gas constant, and T is the absolute temperature.

By using the molar flow rates of the species of interest in the feed and product streams, CO conversion rate and net gas (H_2, CO_2) production rates are calculated from Equations 4.4 and 4.5, respectively:

$$\text{CO conversion rate } (\mu mol\ g^{-1} s^{-1}) = \frac{n_{CO,in} - n_{CO,out}}{m_{cat}} \quad (4.4)$$

$$\text{Net gas production rate } (\mu mol\ g^{-1} s^{-1}) = \frac{n_{gas,out} - n_{gas,in}}{m_{cat}} \quad (4.5)$$

where m_{cat} is the catalyst weight used in the WGS performance tests, which is 75 mg.

Stability of the catalyst activity is measured and reported on the basis of the degree of activity loss and commonly reported as the percent loss of initial activity and calculated as in Equation 4.6:

$$\text{Activity loss (\%)} = \left[\frac{(\text{CO conversion})_{0.5\text{h}} - (\text{CO conversion})_{6\text{h}}}{(\text{CO conversion})_{0.5\text{h}}}\right] 100 \qquad (4.6)$$

TOS activity and stability data for all WGS performance tests are given in detail in Appendix A.

4.1.1. Ideal Feed Tests

The tests were conducted under atmospheric pressure and at three different temperatures, 300, 350, and 400 °C, for two ideal feed compositions presented in Table 3.6. Each test was conducted by using freshly reduced catalysts and continued for 6 h TOS. GHSV was kept fixed as 120,000 ml g_{cat}^{-1} h^{-1} for all tests.

The effect of temperature on catalytic activity of the trimetallic Pt-Re-V/CeO_2 and bimetallic Pt-Re/CeO_2 catalysts was studied first; the results are presented in Figure 4.1 for ideal feed #1 (H_2O/CO = 5) and in Figure 4.2 for ideal feed #2 (H_2O/CO = 2). The equilibrium CO conversions calculated by HSC-Chemistry Software are also shown in the figures. Those activity profiles clearly show that nearly all catalysts have high WGS activity with minor differences.

For ideal feed #1, 1Pt-1Re/CeO_2 and 1Pt-1Re-0.5V/CeO_2 catalysts showed similar activity trends and their activities increased by increasing reaction temperature. They almost had the same activity at 300 and 350 °C, while the activity of 1Pt-1Re-0.5V/CeO_2 was the highest at 400 ºC with ~94% CO conversion, almost reaching to 98.02% equilibrium conversion at that temperature. 1Pt-1Re-1V/CeO_2 showed approximately the same activity (~89% CO conversion) at all temperatures and it had the highest activity at 300 °C among all catalysts. The activity of 1Pt-1Re-3V/CeO_2 peaked at mid temperature and began to decrease slightly with further increase in temperature. At 350 °C, CO conversion reaching to 93% was achieved, which is fairly close to equilibrium conversion, 98.84%. As CO conversion values close to equilibrium conversions were obtained (Figure 4.1), the results indicated that even when the feed had high concentration of steam, reverse water gas shift (RWGS) was suppressed.

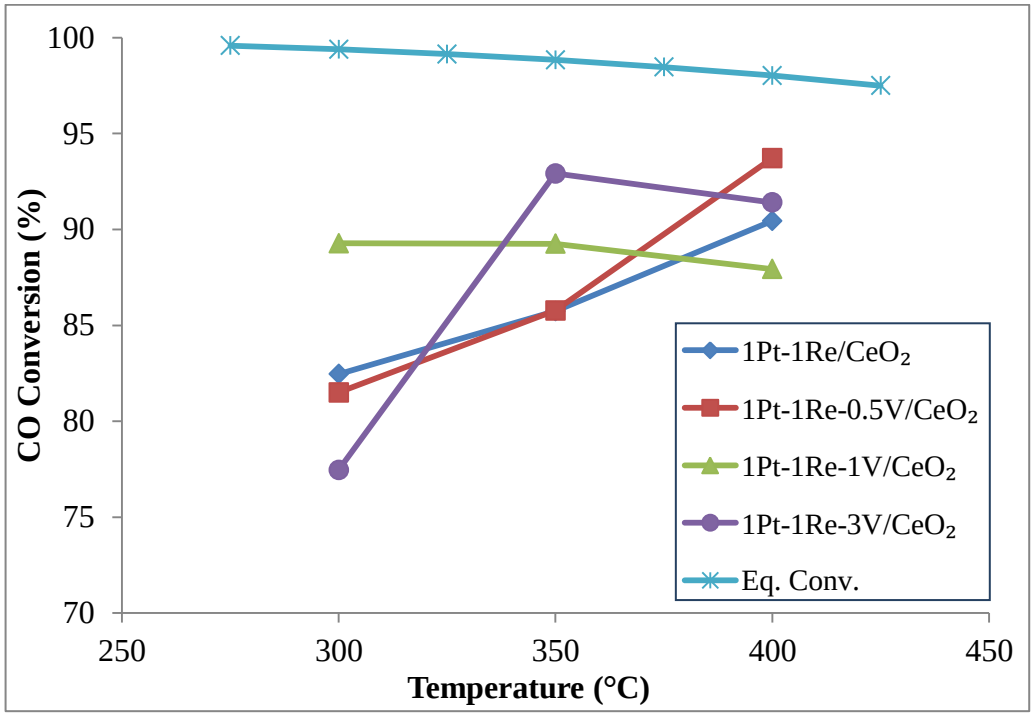

Figure 4.1. Temperature dependence of the catalytic activity for ideal feed #1 (3% CO, 15% H_2O, 82% Ar; H_2O/CO = 5).

Lowering the H_2O/CO ratio (Figure 4.2) led to decreased activity for all samples, especially at 300 °C. Under the ideal feed #2 conditions, the activity levels of the catalysts came close at all temperatures. The CO conversions of all catalysts, except 1Pt-1Re-1V/CeO_2, followed the same trend: They reached a peak at 350 °C and then declined at 400 ºC. On the other hand, CO conversion over 1Pt-1Re-1V/CeO_2 increased with temperature for the whole range, reaching to a maximum at 400 °C with a value of 82%. 1Pt-1Re-1V/CeO_2 also showed the highest activity at 300 °C with ~57% CO conversion. At 350 °C, the highest activity was observed for the 1Pt-1Re-0.5V/CeO_2 catalyst with 81% CO conversion.

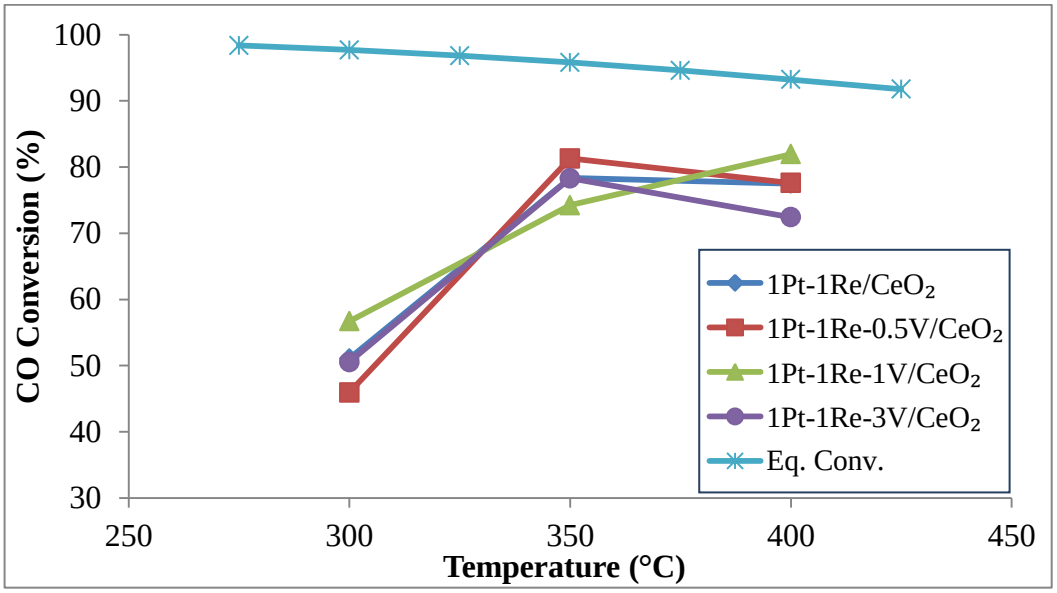

Figure 4.2. Temperature dependence of the catalytic activity for ideal feed #2 (3% CO, 6% H_2O, 91% Ar; H_2O/CO = 2).

The effect of H_2O/CO ratio on the catalytic activity of 1Pt-1Re-3V/CeO_2 catalyst is presented in Figure 4.3 for ideal feed #1 and #2. CO conversions increased when the temperature was increased from 300 to 350 ºC for both ideal feeds. The activity remained nearly constant at 350 and 400 °C for high H_2O/CO ratio feed, while little decrease was observed in CO conversion for low H_2O/CO ratio feed.

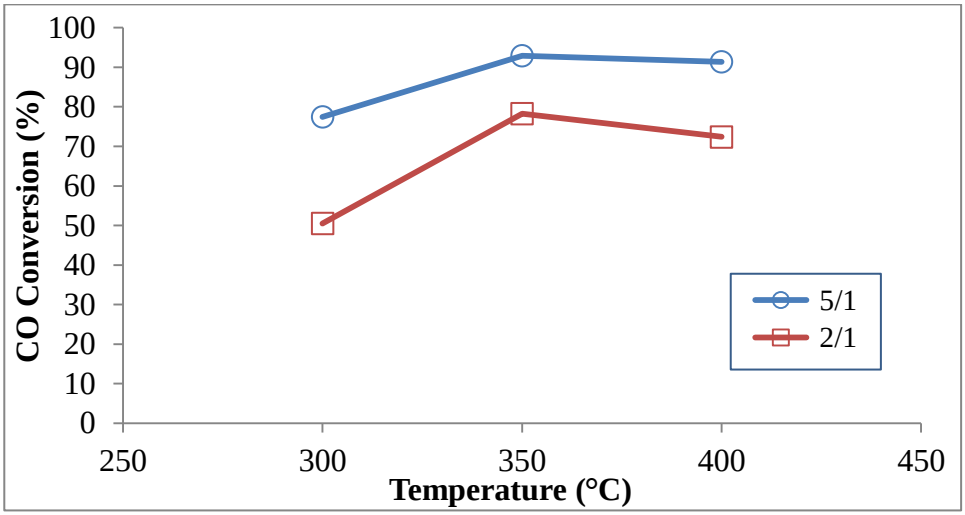

Figure 4.3. Effect of H_2O/CO feed ratio on the catalytic activity of 1Pt-1Re-3V/CeO_2.

Figure 4.4 shows the comparison of catalytic activities obtained with 1Pt-1Re-1V/CeO_2 using ideal feed #1 and #2. The activity was not influenced by changing temperature for feed containing high H_2O. On the other hand, under the low H_2O-content feed, there was an increase in activity with temperature, while percent increase in CO conversion from 300 °C to 350 °C was higher than that of the increase from 350 °C to 400 °C.

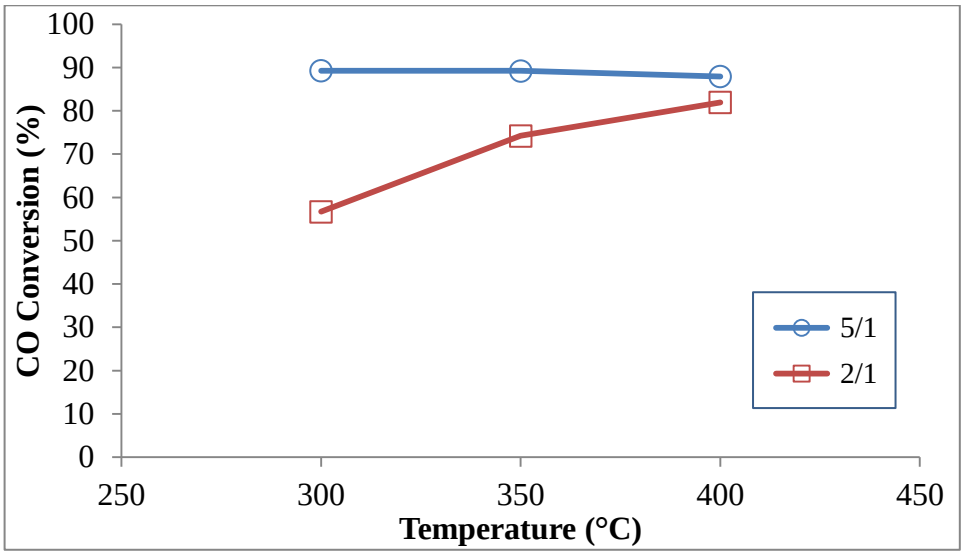

Figure 4.4. Effect of H_2O/CO feed ratio on the catalytic activity of 1Pt-1Re-1V/CeO_2.

The catalytic activity of 1Pt-1Re-0.5V/CeO_2 for two ideal feeds with different H_2O/CO ratios is compared in Figure 4.5. When H_2O/CO ratio was high, the activity increased slightly between 300 and 350 °C, followed by a sharp rise at 400 °C, leading to the highest activity achieved with this catalyst for both feeds. On the other hand, CO conversions obtained for low H_2O/CO ratio raised rapidly at 350 ºC, reaching nearly the conversion of high H_2O-content feed at that temperature. Increasing the temperature to 400 °C, on the other hand, caused a slight decrease in the activity. The reason of the decrease in activity might be the increase in the rate of RWGS activity at higher temperature when H_2O/CO feed ratio is low.

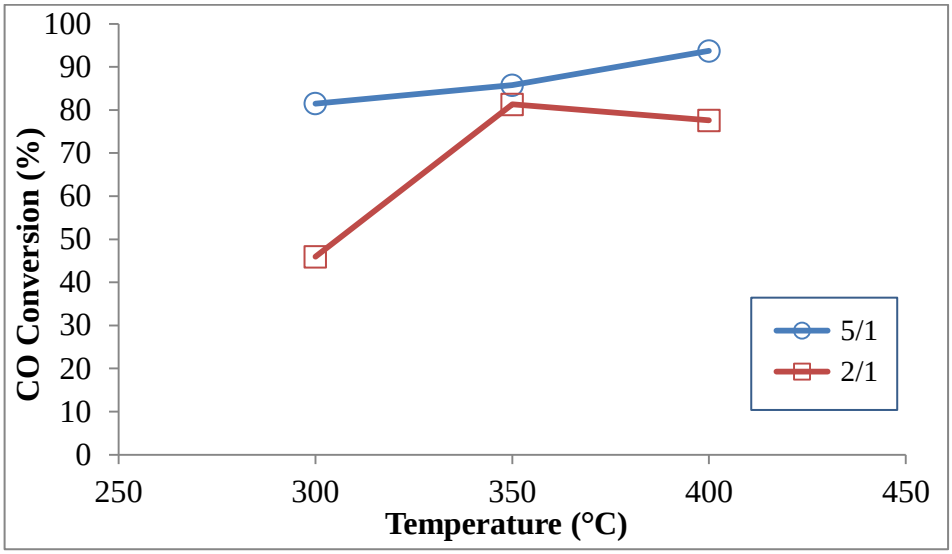

Figure 4.5. Effect of H_2O/CO feed ratio on the catalytic activity of 1Pt-1Re-0.5V/CeO_2.

A comparison of the activity over 1Pt-1Re/CeO_2 catalyst for ideal feeds #1 and #2 is given in Figure 4.6. The activity trends and CO conversions obtained for both feeds were almost the same as those observed over 1Pt-1Re-0.5V/CeO_2 (Figure 4.5).

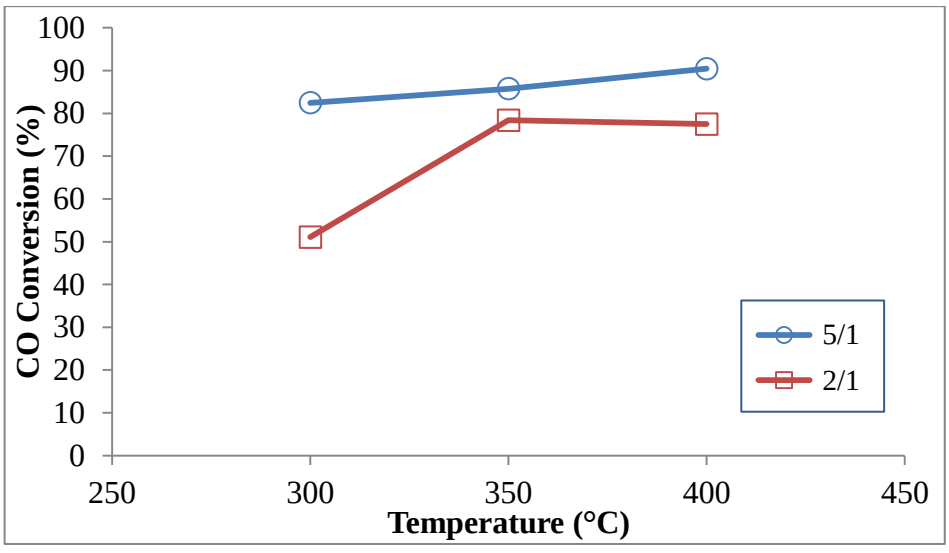

Figure 4.6. Effect of H_2O/CO feed ratio on the catalytic activity of 1Pt-1Re/CeO_2.

WGS time-on-stream (TOS) activities of all Pt-Re-V/CeO_2 catalysts and the unpromoted Pt-Re/CeO_2 at 350 °C under flow of ideal feed #1, having high H_2O/CO ratio were measured and the TOS activity trends are presented in Figure 4.7. Although there is

no dramatic activity difference between the catalysts, TOS CO conversion profiles suggest that adding 1 and 3 wt.% V increases the initial catalytic activity of Pt-Re system, whereas 0.5 wt.% V addition to Pt-Re seems not affecting the activity. In 6 h TOS tests, no considerable activity losses were detected at all for all the catalysts, indicating their good stability. Especially, 1Pt-1Re-0.5V/CeO_2 and 1Pt-1Re-1V/CeO_2 catalysts were very stable, with ca. 5% activity loss. The activity losses of 1Pt-1Re/CeO_2 and 1Pt-1Re-3V/CeO_2 were found as ca. 8% and 12%, respectively.

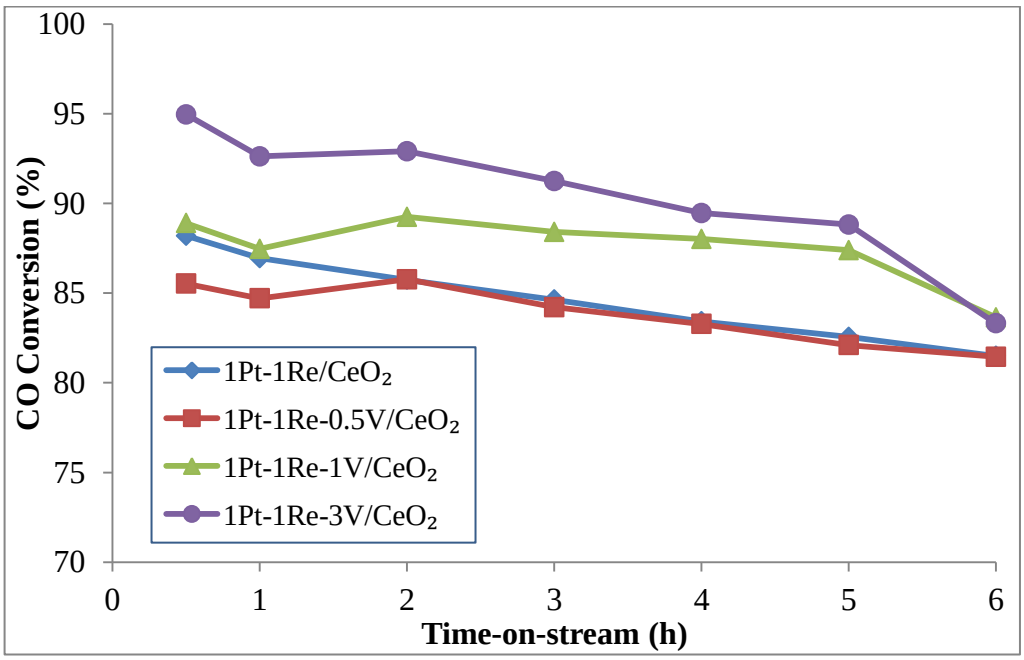

Figure 4.7. Effect of V-loading on the activity for ideal feed #1 at 350 ºC (3% CO, 15% H_2O, 82% Ar; H_2O/CO = 5).

In Figure 4.8 TOS activities of all Pt-Re-V/CeO_2 catalysts having V-loadings between 0-3% under the flow of ideal feed #1 at 400 °C are presented. 1Pt-1Re-0.5V/CeO_2 catalyst became almost totally stable when the temperature was increased to 400 °C and exhibited the highest activity for 6h TOS among all catalysts. The stabilities of 1Pt-1Re-3V/CeO_2 and 1Pt-1Re/CeO_2 catalysts did not change with increasing temperature, while higher activity loss was observed for 1Pt-1Re-1V/CeO_2 compared to the activity loss of this catalyst at 350 °C.

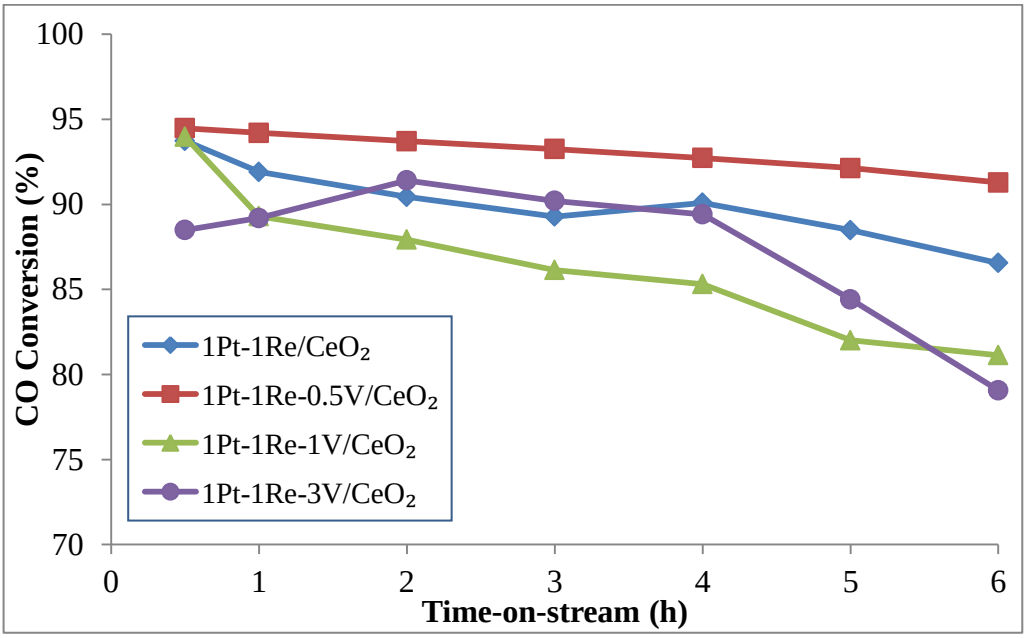

Figure 4.8. Effect of V-loading on the activity for ideal feed #1 at 400 ºC (3% CO, 15% H_2O, 82% Ar; H_2O/CO = 5).

TOS tests were performed for both ideal feeds over all catalysts at 300, 350 and 400 °C. In the tests, the changes in activity and selectivity profiles of the catalysts were observed. 1Pt-1Re-3V/CeO_2 catalyst experienced ca. 12% activity loss at 6 h TOS with both feeds at all temperatures, except the test conducted at 300 °C with H_2O/CO feed ratio of 5. At this condition, all catalysts were almost completely stable (not shown). 1Pt-1Re/CeO_2 was also very stable at the same temperature with low H_2O/CO ratio feed, while ca. 8% activity loss was observed under all other conditions studied. There seemed to be no correlation between reaction temperature and catalyst stability for 1Pt-1Re-1V/CeO_2, when the results obtained for both feeds were considered. In overall evaluation, one can conclude that all catalysts studied have very high stabilities under ideal feed conditions. However, 1Pt-1Re-0.5V/CeO_2 was found to be the most stable catalyst under all ideal WGS conditions, with only ca. 4-5% activity loss at 6 h TOS.

4.1.2. Real Feed Tests

The tests were conducted under atmospheric pressure and at 300, 350, and 400 °C for two real feed compositions, ie. low H_2O/CO and high H_2O/CO feeds, given in Table 3.7.

These real feeds were used to simulate the conditions of the typical reformer outlet of a conventional FP. Each test was performed over freshly reduced catalysts for 6 h TOS. During the tests, GHSV was kept fixed at 120,000 ml g_{cat}^{-1} h^{-1}.

During the performance tests, no methane formation was detected under any of the experimental conditions used, indicating that the Pt-Re-V and Pt-Re systems suppressed secondary methanation activity.

Figure 4.9(a) and 4.9(b) present the temperature dependence of the CO conversions and percentage increase in the H_2 molar flow in the WGS product stream led by net H_2 production over the catalysts, ie. net H_2 produced for real feed #1 (H_2O/CO= 6.7), respectively. Figure 4.9(a) also includes the equilibrium conversion for CO calculated by HSC-Chemistry Software. Similar to what was observed in ideal feed tests, there was no considerable difference between the catalytic activities of the catalysts studied. However this time, the activities and net H_2 productions at 300 °C were significantly lower compared to those at 350 and 400 °C.

The highest CO conversions obtained were at 350 °C over 1Pt-1Re-0.5V/CeO_2 and 1Pt-1Re-1V/CeO_2 catalysts reaching to ca. 62%. The results showed that there was a 10% net increase in H_2 molar flow in the product stream on the basis of molar flow of H_2, 30.2 μmol/s in the feed stream. These catalysts also exhibited similar and superior activities at 400 °C with 58% CO conversion levels along with 9% net H_2 production. At 300 °C, the highest CO conversion (36%) and additional H_2 production (6.5%) were observed over 1Pt-1Re-3V/CeO_2. By increasing temperature to 350 °C its activity increased to 55%, while the amount of net H_2 produced reached to 11%. Further increase in temperature decreased the activity slighlty to 47% but did not change the additional H_2 production at all. In the absence of vanadia, the activity at 300 °C was dropped to 23%, then increased to the conversion level of 1Pt-1Re-3V/CeO_2 at 350 °C. Besides, comparable net H_2 productions were obtained by 1Pt-1Re/CeO_2 at 300 and 400 °C. In general, CO conversion levels obtained were not significantly below the equilibrium conversions except the conversions measured at 300 °C.

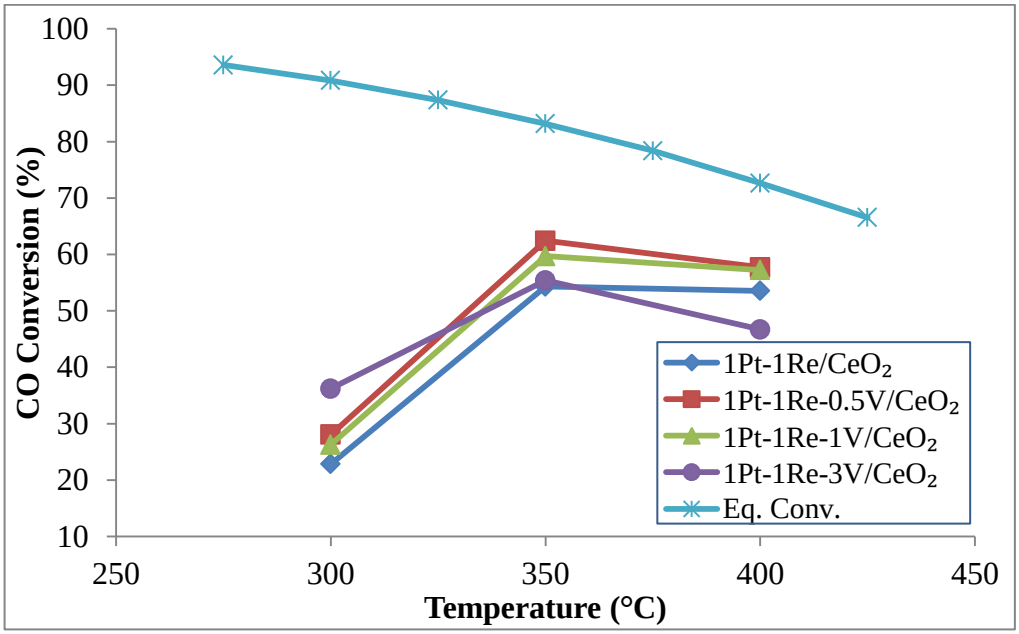

(a)

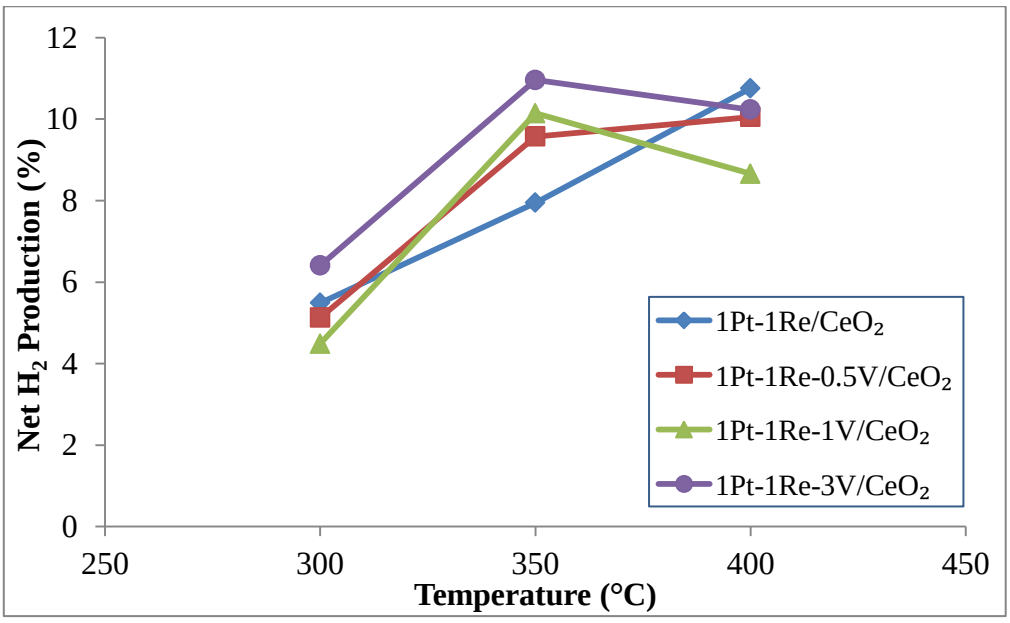

(b)

Figure 4.9. Temperature dependence of (a) catalytic activity and (b) net H_2 production for real feed #1 (4.9% CO, 32.7% H_2O, 30.0% H_2, 10.4% CO_2, 22.0% Ar; H_2O/CO = 6.7).

Figure 4.10(a) and 4.10(b) display the CO conversions and the rate of net H_2 produced in percentage for real feed #2 (H_2O/CO = 16.2), respectively. Figure 4.10(a) also involves the CO equilibrium conversion determined by HSC-Chemistry Software.

Increasing the H_2O content of the feed from H_2O/CO ratio of 6.7 to 16.2 resulted in higher activities at 300 °C and comparable activities at 350 °C, while lower CO conversions were obtained at 400 °C. On the other hand, the net H_2 production values decreased significantly when the feed stream was changed from #1 to #2. It should be noted that CO conversions obtained were close to the equilibrium conversion levels at 350 and 400 °C.

In the case of H_2O-rich real feed #2, all the catalysts except 1Pt-1Re-3V/CeO_2 showed similar activity-temperature trends as they had with real feed #1. The activiy and rate of net H_2 produced over 1Pt-1Re-3V/CeO_2 catalyst remained almost constant when the temperature was increased from 300 to 350 °C, then decreased slowly with a further increase in temperature to 400 °C. 1Pt-1Re-3V/CeO_2 had the highest activity (47% CO conversion) at 300 °C compared to those of the other catalysts, as in the case of real feed #1, while the lowest CO conversion levels were obtained over it at higher temperatures. Catalysts with 0, 0.5 and 1% V loadings exhibited similar CO conversions at all temperatures; the highest conversion, 59%, was reached over 1Pt-1Re-0.5V/CeO_2 at 350 °C. The net H_2 production rate was maximized to 7% at 350 °C for 1Pt-1Re-0.5V/CeO_2 and 1Pt-1Re/CeO_2 catalysts. By increasing temperature to 400 °C, the highest net H_2 production rate was yielded by 1Pt-1Re-0.5V/CeO_2 as 5.5%, followed by 1Pt-1Re/CeO_2 with 4.7%. Lower net H_2 production rate values were observed for 1Pt-1Re-1V/CeO_2 catalyst.

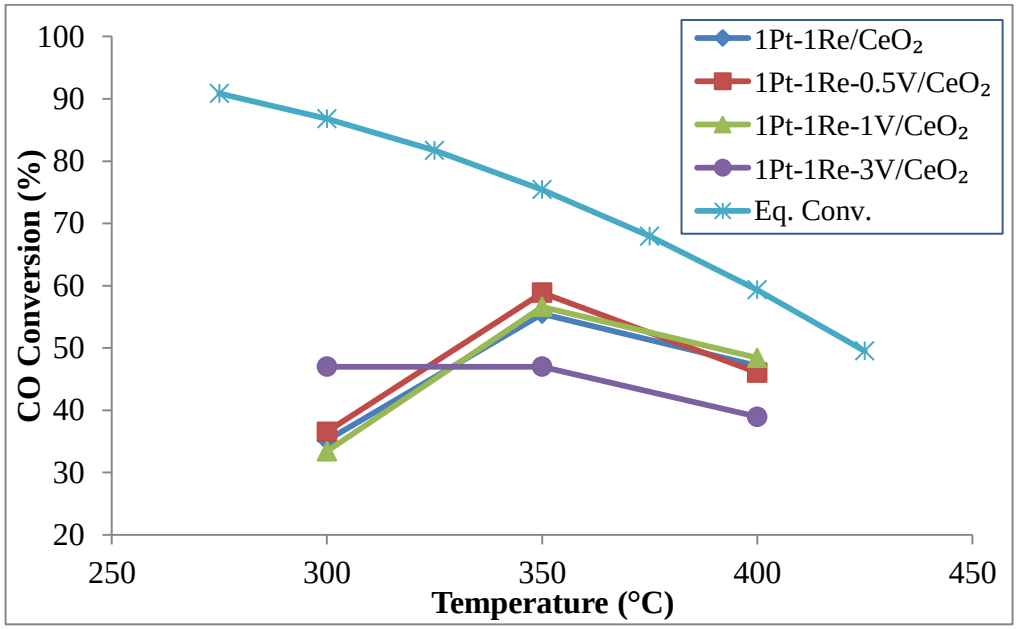

(a)

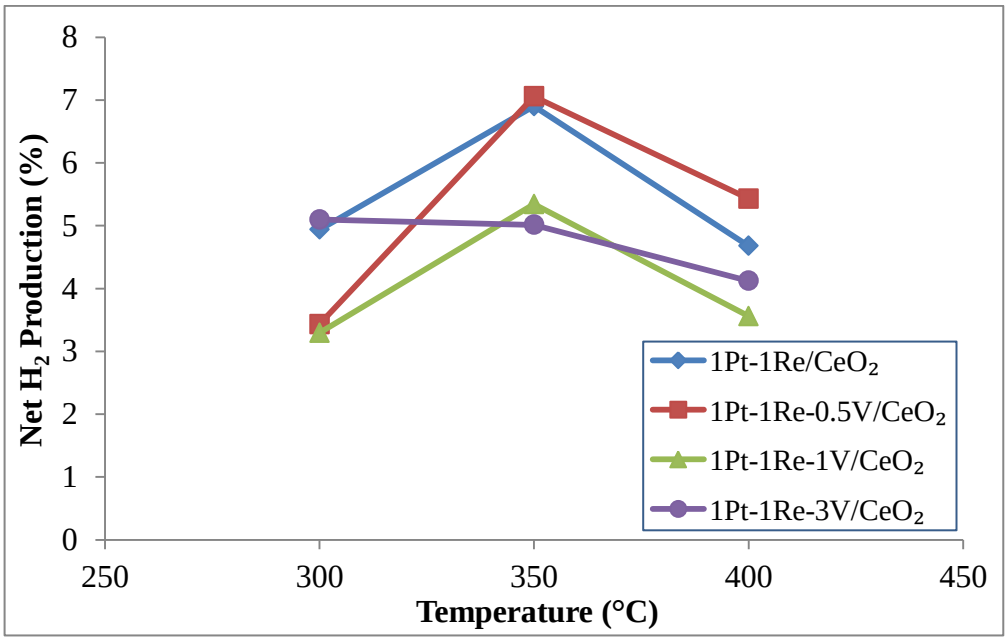

(b)

Figure 4.10. Temperature dependence of (a) catalytic activity and (b) net H_2 production for real feed # 2 (2.1% CO, 34.1% H_2O, 23.7% H_2, 12.3% CO_2, 27.8% Ar; H_2O/CO = 16.2).

Time-on-stream activity profiles of Pt-Re-V and Pt-Re catalysts under the flow of real feed #1 at 350 ºC are presented in Figure 4.11. Very similar and superior catalytic activities especially after 3h TOS, were obtained over 1Pt-1Re-0.5V/CeO_2 and 1Pt-1Re-1V/CeO_2, where the latter had the highest stability with only 6% activity loss during 6h TOS. 1Pt-1Re/CeO_2 catalyst showed comparable activity and stability with 1Pt-1Re-3V/CeO_2 catalyst; they experienced the highest activity losses, ca. 17%. Net H_2 production (not shown) of V-loaded catalysts were similar after 3h TOS and higher than that of V-free 1Pt-1Re/CeO_2.

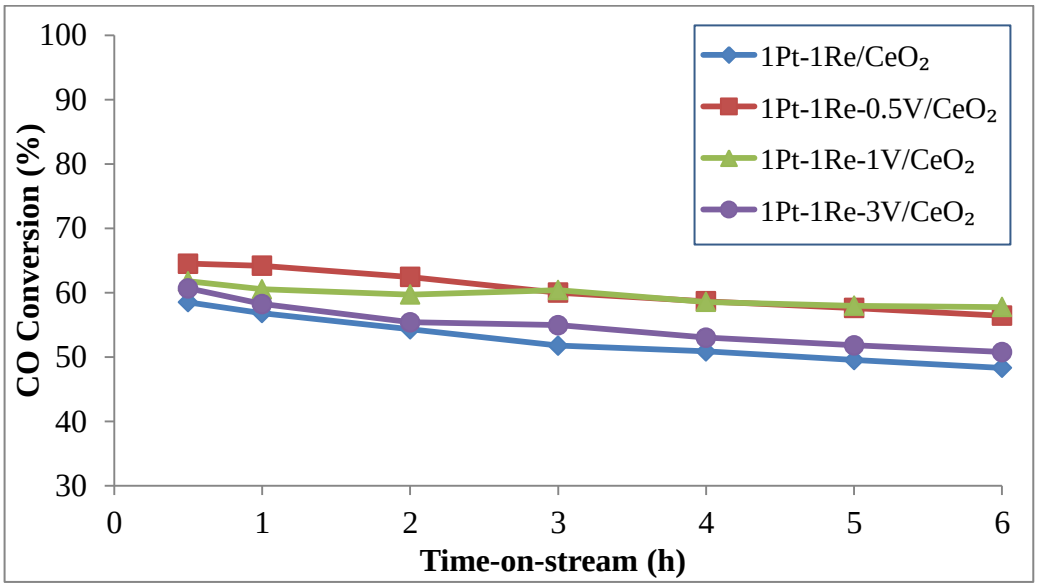

Figure 4.11. Effect of V-loading on the activity for real feed #1 at 350 °C (4.9% CO, 32.7% H_2O, 30.0% H_2, 10.4% CO_2, 22.0% Ar; H_2O/CO = 6.7).

Figure 4.12 displays the time-on-stream activity profiles of the all catalysts studied for real feed #1 at 400 °C. The catalytic activity and stability of 1Pt-1Re/CeO_2 increased with the increase in reaction temperature from 350 °C to 400 °C and approached to those of 1Pt-1Re-1V/CeO_2 and 1Pt-1Re-0.5V/CeO_2 catalysts. CO conversion values decreased for 1Pt-1Re-3V/CeO_2 catalyst, while its stability was unchanged. For 1Pt-1Re-0.5V/CeO_2, a decrease in activity loss from 13% to 7% was observed when temperature was increased from 350 to 400 °C. According to TOS activity results, 1Pt-1Re-0.5V is the most stable catalyst; the stability series is 1Pt-1Re-0.5V>1Pt-1Re-1V/CeO_2>1Pt-1Re. At 400 °C, the

lowest net H_2 production rate (not shown) was obtained over 1Pt-1Re-1V/CeO_2, whereas the difference is minor between all the catalysts.

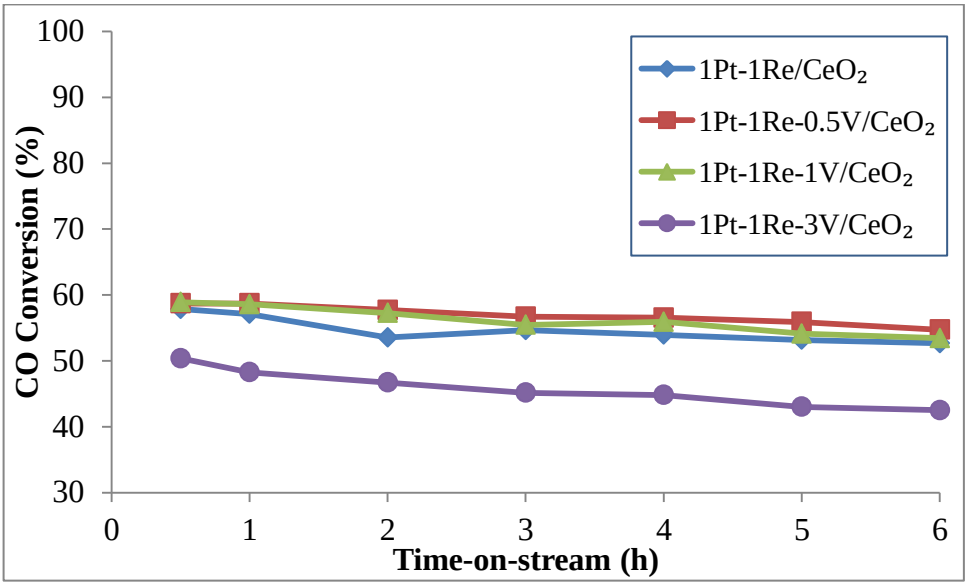

Figure 4.12. Effect of V-loading on the activity for real feed #1 at 400 °C (4.9% CO, 32.7% H_2O, 30.0% H_2, 10.4% CO_2, 22.0% Ar; H_2O/CO = 6.7).

TOS data were recorded for all real feed experiments over Pt-Re-V/CeO_2 catalysts having V loadings between 0-3 wt.%. An overall evaluation of the relation between H_2O/CO ratio of the feed and the stability observed during 6h TOS indicated that all catalysts showed higher stability when real feed #2, having high H_2O/CO ratio of 16.2, was used. For real feed #2, the activity loss values of the catalysts changed from 4 to 15% for the temperature range 300-400 °C. Although no solid correlation between reaction temperature and catalyst stability was observed over all catalysts for both real feeds, 0.5 wt.% and 1 wt.% V promoted samples were found to have superior stabilities with slight activity losses under all real feed conditions studied, as in the case of ideal feed experiments.

The performance results obtained for two real feeds showed that higher net H_2 production rate values were achieved by real feed #1 having low H_2O/CO ratio at the temperature levels studied. As the H_2O, CO_2 and H_2 amounts were similar for both real feeds, the main difference was their CO concentrations; real feed #1 had more than twice

the CO concentration of real feed #2. Consequently, as the WGS reaction rate depends on concentrations of CO, H_2O, CO_2 and H_2, the main reason behind the lower H_2 productions obtained for real feed #2 was the limitation in CO amount.

Selectivity is very important for a WGS catalyst: side reactions like methanation should be avoided in order to prevent hydrogen consumption. Despite having high CO conversion levels, a successful WGS catalyst should produce additional hydrogen under real feed conditions. No methane formation was detected during the catalytic reaction tests performed in this study, and positive net H_2 production rates were observed for all catalysts. Figure 4.13 and 4.14 clearly show the high selectivity of the Pt-Re-V/CeO_2 systems for real feed #1 and #2 having H_2O/CO ratio as 6.7 and 16.2, respectively. The rates measured at 6 h TOS are given in both figures.

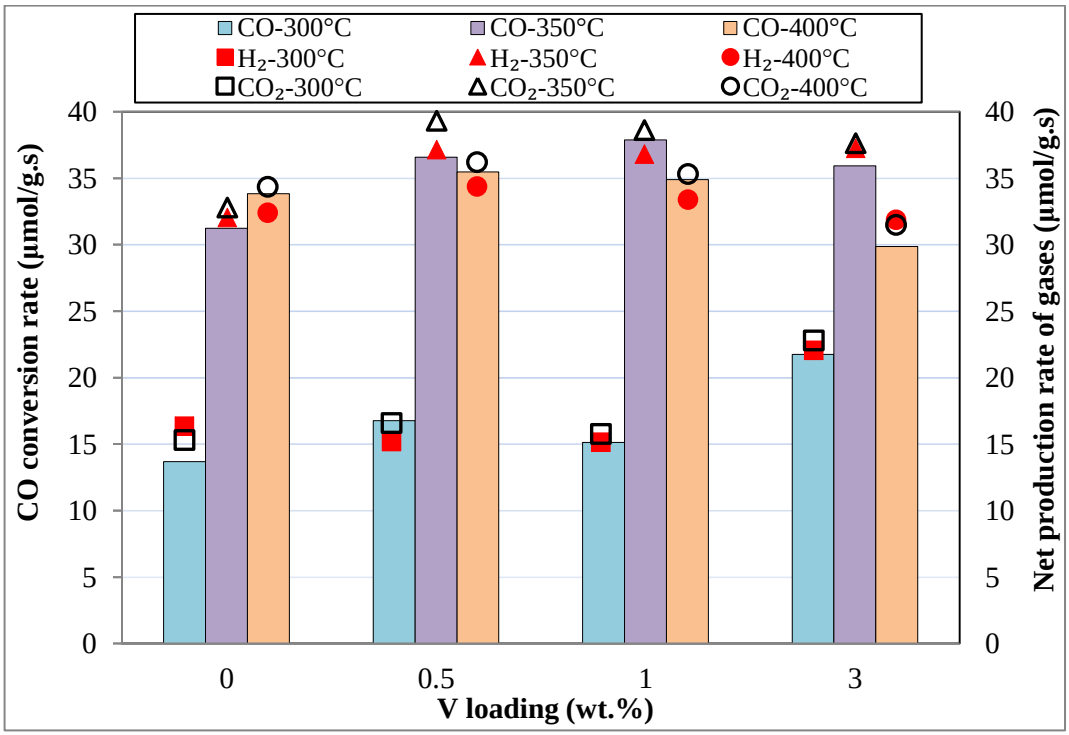

Figure 4.13. Effect of V-loading on the CO conversion and net H_2, CO_2 production rates for real feed #1 (H_2O/CO = 6.7) at the end of 6 h TOS.

The results obtained for both real feeds reveal that 1Pt-1Re-0.5V/CeO_2 and 1Pt-1Re-1V/CeO_2 catalysts have great potentials to be used in a FP with their high activity, stability and selectivity enabling the use of a single WGS unit operating at HTS-LTS transition temperature, instead of a two-stage WGS operation in separate HTS and LTS units.

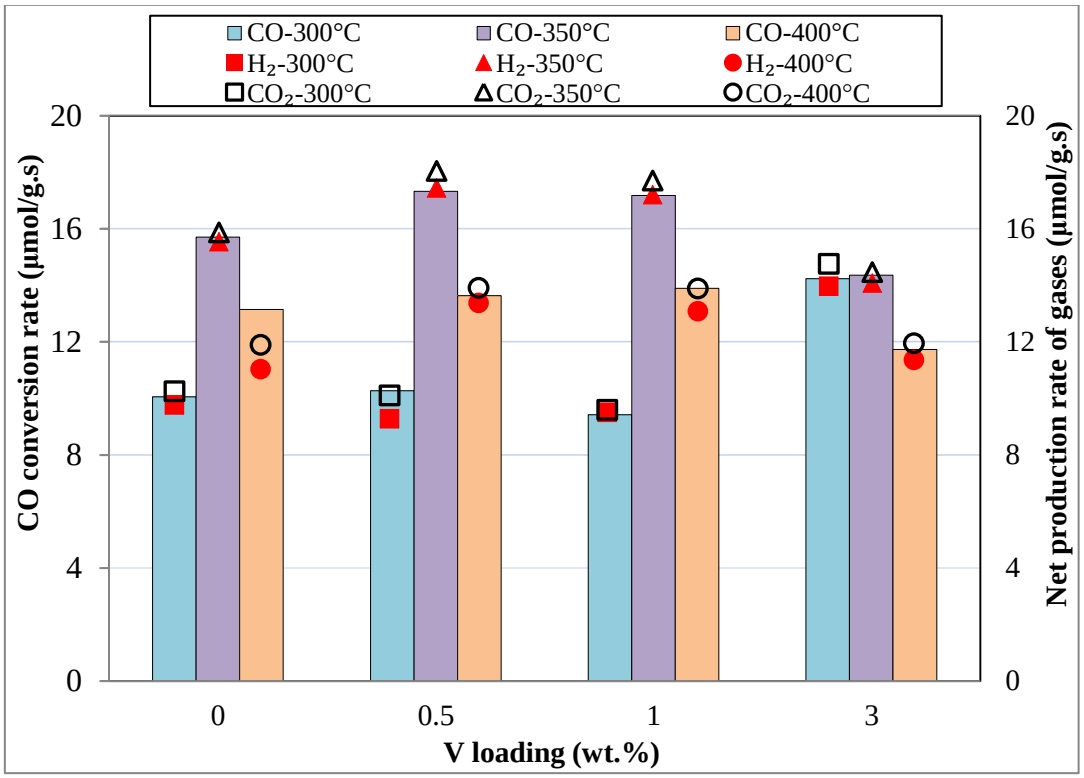

Figure 4.14. Effect of V-loading on the CO conversion and net H_2, CO_2 production rates for real feed #2 (H_2O/CO = 16.2) at the end of 6 h TOS.

4.2. Catalyst Characterization

4.2.1. SEM-EDX

Freshly reduced catalysts were characterized using scanning electron microscopy (SEM) with energy dispersive X-ray (EDX) to obtain information on their microstructural properties. Metal mapping analyses were also conducted in order to examine the metal dispersion and homogeneity of the prepared samples.

A very porous, blossom-like texture was observed in the SEM micrographs of all catalysts; the SEM micrographs of 1V and V-free catalysts at 100,000x magnification are given as examples in Figures 4.15(a) and 4.15(b), respectively. As can be seen from the images, the samples have similar microstructural characteristics and they have uniform metal dispersion on their surfaces, as were confirmed by EDX and mapping studies.

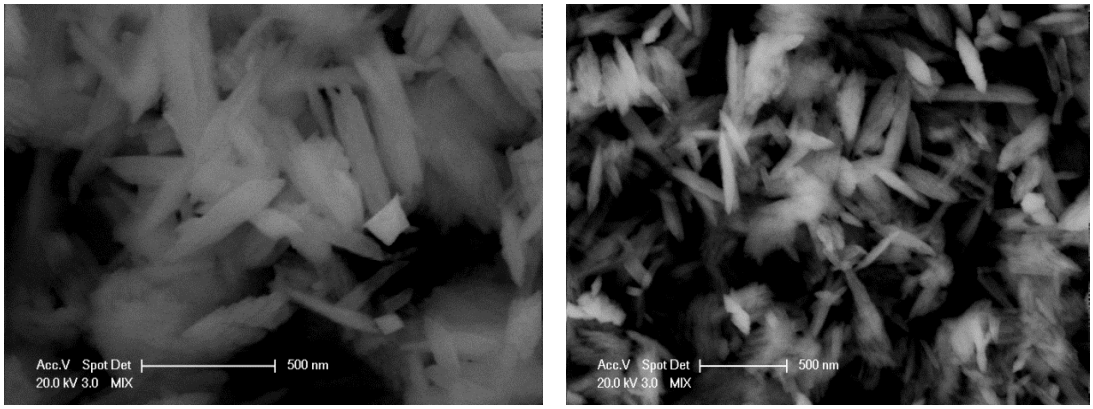

(a) (b)

Figure 4.15. SEM micrographs of freshly reduced catalysts (x100000) for (a) 1Pt-1Re-1V/CeO_2 and (b) 1Pt-1Re/CeO_2.

In order to provide a closer look at the morphology of the 1V sample, SEM images were also taken at 200,000x magnification from two different regions of the catalyst sample. Those images are given in Figures 4.16(a) and 4.16(b). As calculated from EDX analyses, the latter region (Fig. 4.16(b)) contains significantly higher Pt amount (2.03 wt.%) compared to that of the former region (Fig. 4.16(a)), which has 1.31 wt.% Pt. The

bright areas shown in Figure 4.16(b) are mainly composed of platinum particles. Those bright areas have approx. 62 nm diameter, corresponding to platinum average particle size. Distribution of bright areas around the entire catalyst was confirmed by SEM-EDX analyses performed for the other regions of the catalyst sample.

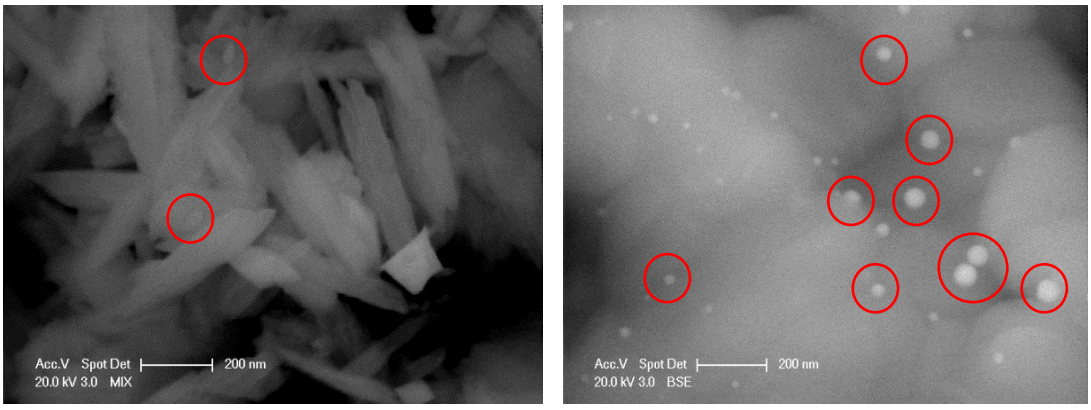

(a) (b)

Figure 4.16. SEM micrographs of freshly reduced 1Pt-1Re-1V/CeO_2 catalyst (x200000) from two different regions.

V atoms on the surface were not distinguishable to secondary electron (SE), since SE only shows the topographical differences. Moreover, K and L energy levels of V-atoms in EDX analysis overlapped with L and K energy levels of Ce- and O-atoms, respectively, resulting in the invisibility of V- atoms by EDX. However, Pt- and Re-atoms have larger atomic weights than V- or Ce-; thus, clusters of Pt and Re were observed in Figures 4.16(a) and 4.16(b), and their existence on the surface was also confirmed by EDX and mapping analysis.

Figure 4.17 shows the metal mapping of the region given in Fig. 4.16(b) for 1Pt-1Re-1V/CeO_2. The mappings of Pt and Re clearly indicate the uniform dispersion of metals on CeO_2 surface. Especially, the distinctive, highly populated big spots shown in Pt mapping prove the existence of Pt particles observed in Fig. 4.16(b). It should be noted that as metal mapping and EDX analysis use the same detectors, the mappings of V and Ce given in Figure 4.17 are not reliable and thus, are not taken into consideration.

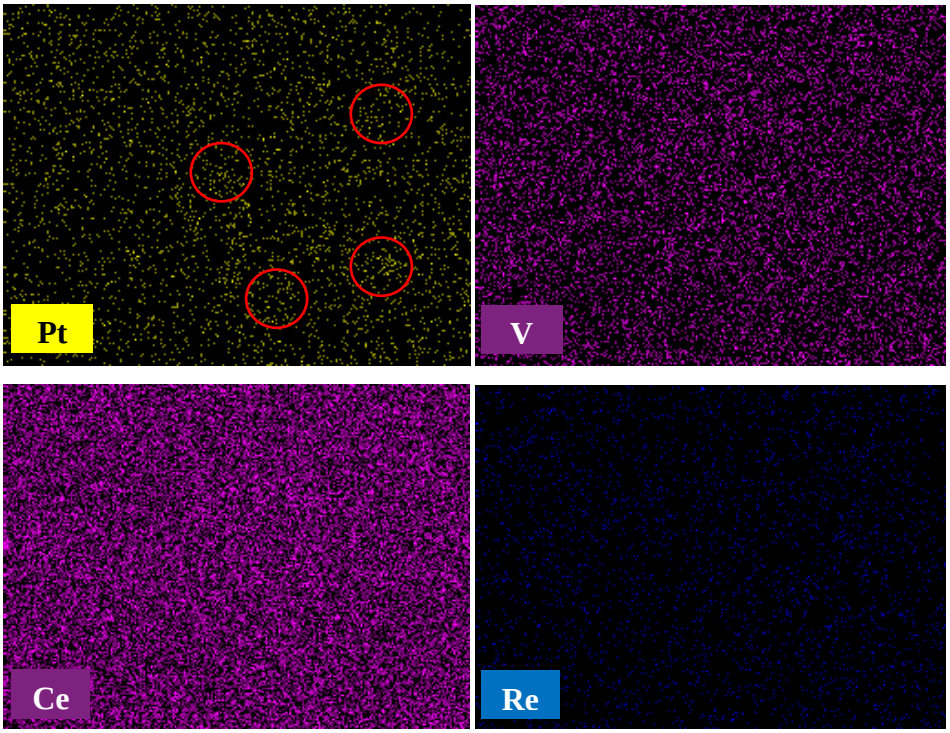

Figure 4.17. Mapping of freshly reduced 1Pt-1Re-1V/CeO_2 catalyst.

On the other hand, in the SEM images of the V-free sample at 200,000x magnification, bright areas of approx. 19 nm diameter assigned to Pt atoms were observed, as presented in Figure 4.18. Lower Pt particle size of Pt-Re catalyst compared to that of 1V promoted catalyst suggested that the addition of V atoms might have increased the average Pt particle size.

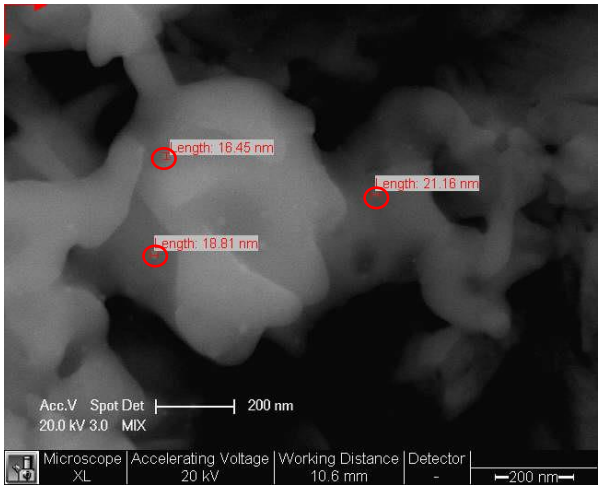

Figure 4.18. SEM micrograph of freshly reduced 1Pt-1Re/CeO_2 catalyst (x200000).

Performance test results showed that the WGS activity of 1V catalyst is higher than the V-free catalyst. Considering the SEM-EDX analysis, having larger Pt particle size may have a positive effect on high catalytic activity for the V-promoted sample. Similar result was observed by Kalamaras *et al*. and it was reported that the catalytic activity of Pt/CeO_2 increased with increasing Pt particle size (Kalamaras *et al*., 2011).

4.2.2. XPS

Oxidation states and elemental compositions of the metallic species present on the catalysts' surface were investigated by X-ray photoelectron spectroscopy (XPS). Due to the redox properties of CeO_x and VO_x, XPS is an important method to analyze the changes occurred on the surface of the spent catalyst. Characteristic oxidation states of Ce, V, O, Pt and Re atoms were observed in the XP spectra of the samples.

XP spectra of Ce 3d core level electrons of all freshly reduced catalysts are displayed in Figure 4.19. The spectra includes two principal energy spin-orbit states: $Ce3d_{3/2}$, represented by peaks labeled v, and Ce $3d_{5/2}$, labeled u. Ce atoms have two oxidation states, namely Ce^{3+} and Ce^{4+} in those spin-orbit states, respectively. The formation of WGS active OH groups is reported to occur on Ce^{3+} defect sites (Vignatti *et al*., 2011- Hwang *et al*., 2011). It is observed that the XP spectra for Ce 3d region of the catalyst samples used in this study were in accordance with the literature (Leppelt *et al*., 2006-Çağlayan and Aksoylu, 2011).

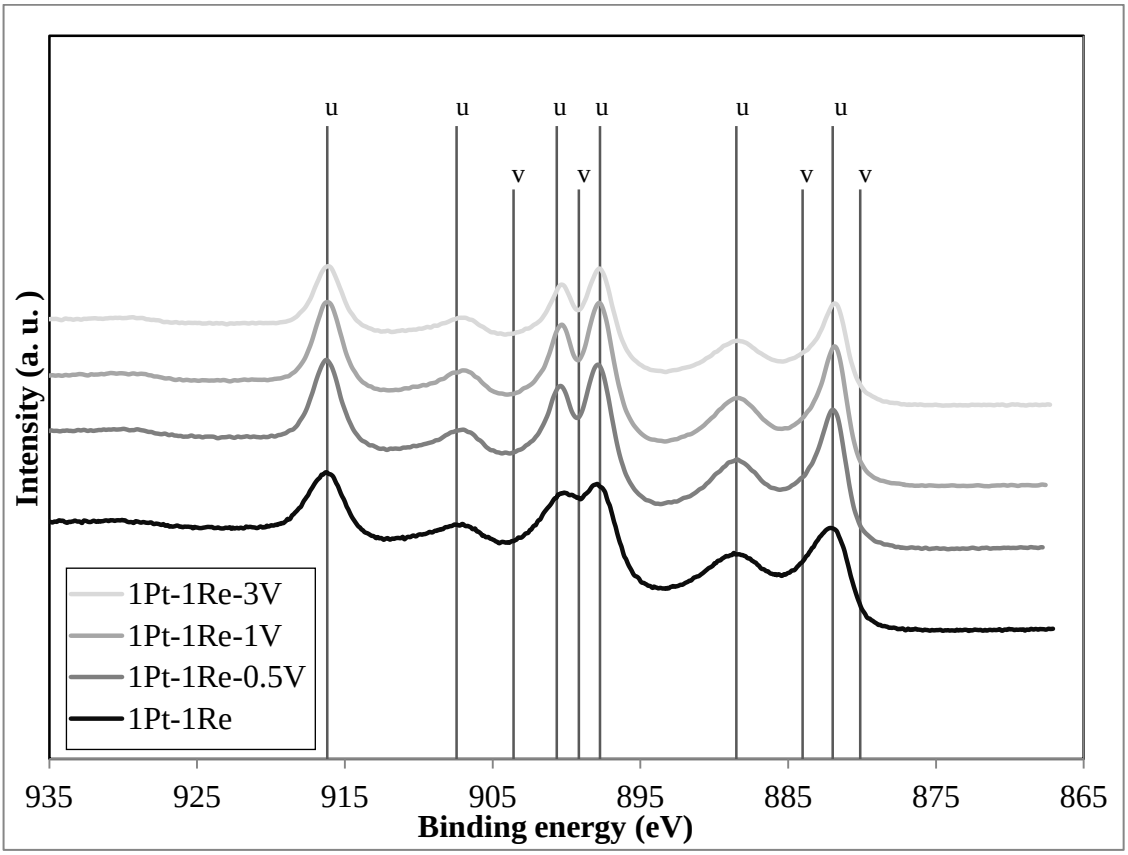

Figure 4.19. XP spectra showing the Ce 3d region of freshly reduced catalyst samples (v: Ce^{3+}, u: Ce^{4+}).

In order to understand the effect of V-addition in the oxidation states of Ce, XP spectra of Ce 3d regions of the freshly reduced and spent bimetallic Pt-Re and 0.5 wt.% and 1 wt.% V-promoted trimetallic samples are comparatively analyzed (Figure 4.20). The spent samples were used in WGS tests during 6h TOS at 350 °C with real feed #2, which has H_2O/CO ratio of 16.2. The resulting spectra indicate that the peaks corresponding to Ce^{3+} and Ce^{4+}'s are still observed in the spent catalyst samples, with lowered peak intensities.

Deconvolution of the peaks was done via using the Avantage software. Using the deconvolution results and calculated peak areas corresponding to Ce^{3+} and Ce^{4+} regions, relative amount of Ce^{3+} was estimated for both reduced and spent catalysts by using the following equation (Çağlayan and Aksoylu, 2011):

$$[Ce^{3+}] = I - Ce^{3+}/(I - Ce^{3+} + I - Ce^{4+}) \quad (4.7)$$

where I – Ce^{3+} and I – Ce^{4+} represent the sum of intensities of two doublets resulting from Ce_2O_3 and three doublets resulting from CeO_2, respectively.

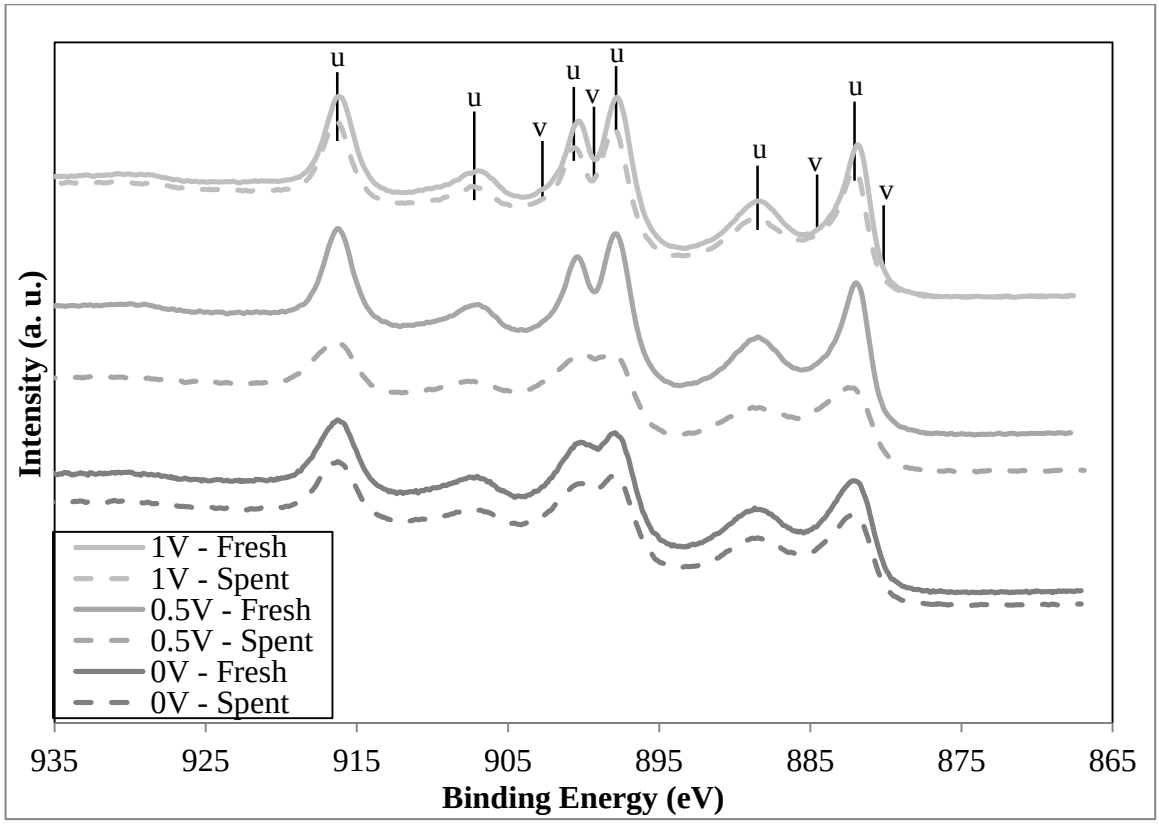

Figure 4.20. XP spectra showing the Ce 3d region of freshly reduced and spent (real feed #2, 350 °C) catalyst samples with different V loadings (v: Ce^{3+}, u: Ce^{4+}).

The Ce^{3+} contents of the catalyst samples with different V loadings are presented in Table 4.1. Ce^{3+} content found out to be slightly higher in the case of the catalysts with higher WGS activity, which are 1Pt-1Re-0.5V/CeO_2 and 1Pt-1Re-1V/CeO_2. This result is in accordance with the explanation that Ce^{3+} plays a crucial role in increasing electron transfer ability from the support to metallic sites, hence resulting in higher catalytic activity (Tabakova *et al*., 2003-Çağlayan and Aksoylu, 2011). As a result of the electron transfer during reaction, the amount of Ce^{3+} decreased for all catalysts, especially for Pt-1Re-0.5V/CeO_2. However, there seemed to be no correlation between WGS activity of the catalyst samples and their percentage Ce^{3+} loss.

Table 4.1. Effect of V-loading on Ce^{3+} contents (%) of the freshly reduced and spent (real feed #2, 350 °C) catalyst samples.

Catalyst	**Ce^{3+} (%)**	
	Freshly reduced	**Spent**
1Pt-1Re-1V/CeO_2	22.6	20.3
1Pt-1Re-0.5V/CeO_2	23.2	14.1
1Pt-1Re/CeO_2	19.8	13.0

In order to establish a close relation between the WGS activity of 1 wt.% V loaded sample and the change in its Ce^{3+} percentage during reaction, XP spectra of Ce 3d region (not shown) was also taken for spent 1V samples tested under real feed #1 having H_2O/CO ratio of 6.7, at the same temperature (350 °C). The reaction under low H_2O/CO feed ratio resulted in a lower Ce^{3+} percentage (19.4%) compared to that of the spent catalyst used with real feed #2. This result was not surprising according to the explanations above, since higher activity was achieved with real feed #1.

Figure 4.21 displays the effect of V loading on the XP spectra of V 2p region for freshly reduced and spent catalysts. The samples with vanadium showed a peak at 516.7 eV corresponding to V^{4+} oxidation state, which is in a good agreement with the previously reported binding energies of 516.5-517.1 eV for V^{4+} given in the literature (Suchorski *et al*., 2005-Duarte de Farias *et al*., 2008). V^{4+} ions were assigned to VO_2 compounds (Demeter *et al*., 2000-Silversmit *et al*., 2004). Junior *et al.* similarly observed the emergence of V^{4+} ions in their XPS analysis and reported the promotion effect of those ions on WGS activity (Junior *et. al*., 2005). On the other hand, Ballarini *et al*. claimed that V_2O_3 compound having V^{3+} oxidation state is the active phase in WGS at temperatures above 450 °C (Ballarini *et al*., 2006). As only a few groups studied the use of vanadium in WGS catalytic systems, the active vanadium structures still remain controversial.

Another peak around 523 eV, belonging to V^{5+} ions, was found in freshly reduced and spent catalysts. The binding energy of this peak is little higher than the literature values (Silversmit *et al*., 2004-Duarte de Farias *et al*., 2008). V^{5+} ions were attributed mainly to V_2O_5 compounds, which are reported to be inactive in WGS reaction mostly due

to the presence of V–O–V bonds. Increase in the surface presence of structures involving V-O-V bonds reported to lead gradual drop in the WGS rate (Ballarini *et al*., 2006-Duarte de Farias *et al*., 2008).

Several studies also reported the formation of $CeVO_4$ phase due to a solid-state reaction between surface V^{5+} species and CeO_2 on ceria-supported vanadium catalysts. The ability of $CeVO_4$ formation was attributed to surface vanadia species stabilizing Ce^{3+} sites on CeO_2 support resulting in V^{5+}–O–Ce^{3+} bonds, which are stated to be active for selective oxidation and WGS reactions (Martinez-Huerta *et al*., 2008-Duarte de Farias *et al*., 2008). However, transformation of $CeVO_4$ single crystals to a more bulk crystalline phase reportedly decreased the number of active V^{5+}–O–Ce^{3+} sites on the support at high temperatures (Martinez-Huerta *et al.*, 2008). Note that, XPS analysis did not precisely conclude whether V_2O_5 or $CeVO_4$ was present on the surface, since they both have V^{5+} ions.

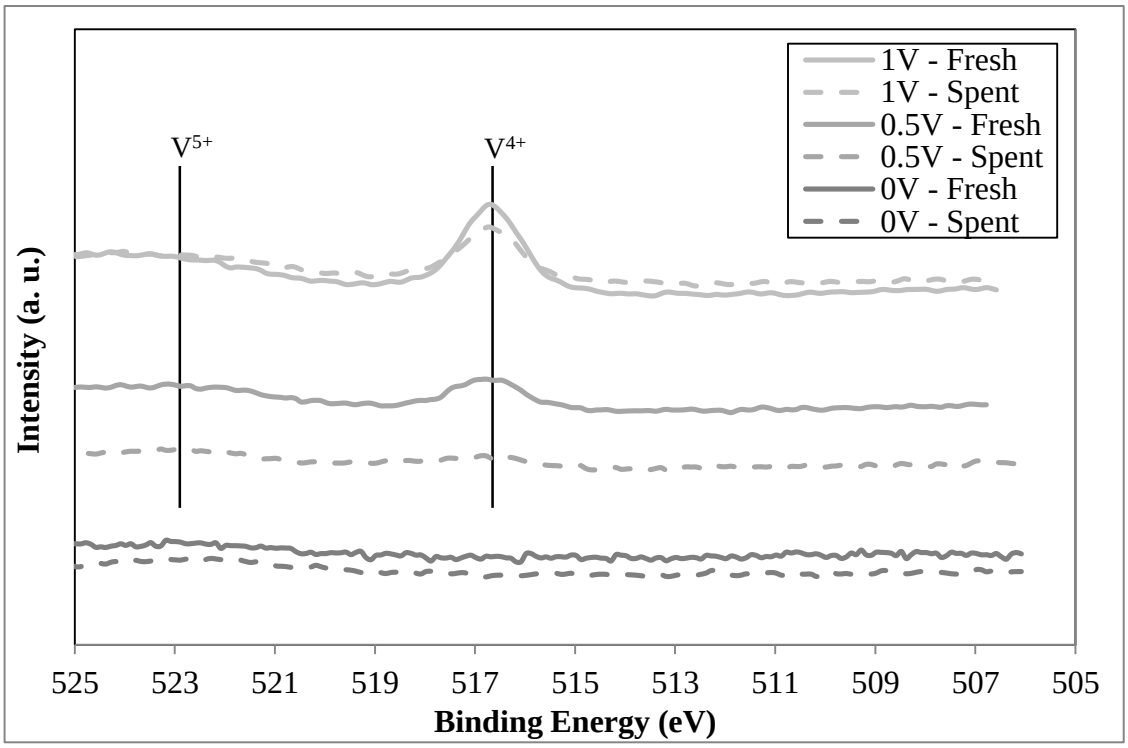

Figure 4.21. XP spectra showing the V 2p region of freshly reduced and spent (real feed #2, 350 °C) catalyst samples with different V loadings.

The O 1s spectra of freshly reduced and spent catalysts are given in Figure 4.22. Freshly reduced samples showed peaks at ca. 529, 531 and 533 eV, which correspond to oxygen in the ceria lattice, chemisorbed water and hydroxlys, and weakly adsorbed water only on the ceria in oxidized state, respectively (Çağlayan and Aksoylu, 2011). Comparably higher amounts of adsorbed water and hydroxyls were observed for freshly reduced 1Pt-1Re-0.5V/CeO_2 and 1Pt-1Re-1V/CeO_2 catalyst samples. After the water gas shift reaction, the intensity of 529 eV peaks decreased, while 531 eV peaks increased. The extents of the mentioned changes in both ways are more evident in 0.5V and 1V catalysts, compared to those measured for V-free sample. The decline of the oxygen in the ceria lattice indicates that CeO_2 plays an active role in the reaction, while the increment of hydroxyl groups after the reaction might point out to a reaction mechanism involving OH participation in rate determining step.

The decrease in 529 eV peak area and increase in 531 eV peak area were also observed in the O 1s spectra of the spent 1V sample (not shown) tested under real feed #1, at the same temperature (350 °C) supporting the role of ceria and hydroxyl groups in WGS.

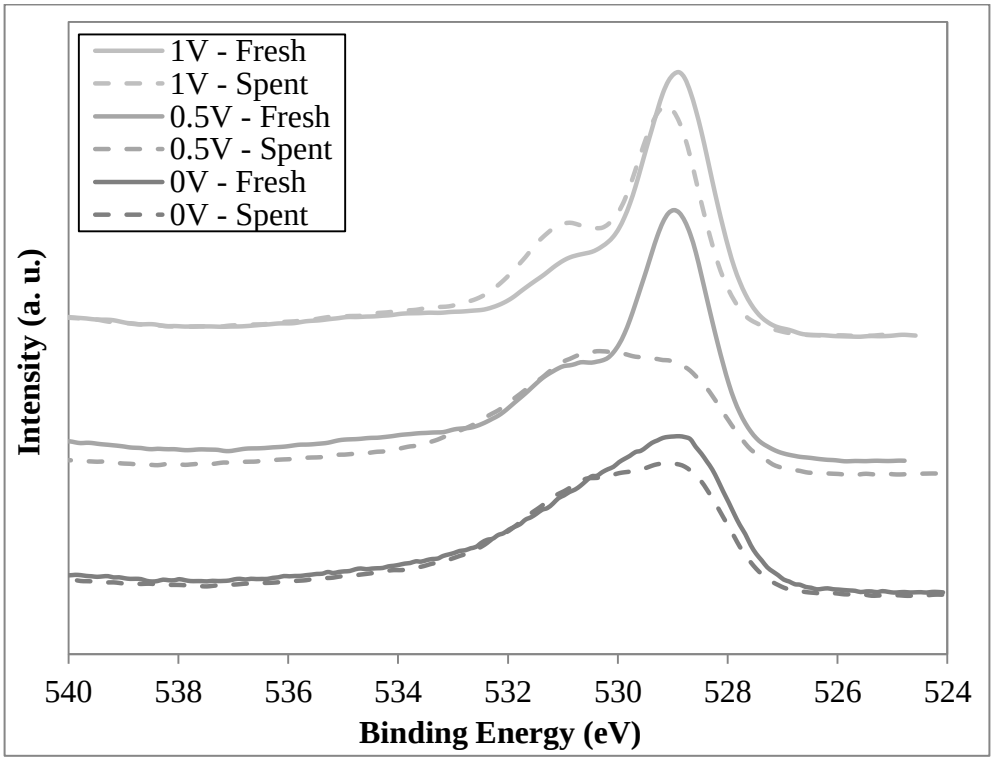

Figure 4.22. XP spectra showing the O 1s region of freshly reduced and spent (real feed #2, 350 °C) catalyst samples with different V loadings.

The Pt 4f region of the samples were also studied and shown in Figure 4.23. According to the literature, the Pt $4f_{7/2}$ peak at 71.0 eV and the Pt $4f_{5/2}$ peak at 74.2 eV are assigned to Pt^0; the peaks at 71.9 and 75.1 eV are assigned to Pt^{2+} and the peaks at 74.3 and 77.5 eV are assigned to Pt^{4+} species (Pierre *et al*., 2007-Yu *et al*., 2010). In all samples studied, the majority of Pt existed in +2 oxidation state. Pt^{2+} species are known to be active species for WGS reaction (Pierre *et al*., 2007- Roh *et al*., 2012). 1V sample also had negligible amount of Pt^{4+}. XP spectra of the spent samples revealed that Pt^{2+} species continue to dominate in 0.5V and 1V samples, which were more active and stable under the conditions studied. Those samples had negligible quantity of Pt^{4+}, which was reported to have no effect on the catalyst stability (Pierre *et al*., 2007). However, spent V-free sample showed significant amount of Pt^0, which was found out to be unnecessary for WGS activity. Moreover, it is stated that metallic platinum may cause the annealing of ceria oxygen vacancies, leading to the loss of CeO_2 surface area (Pierre *et al*., 2007).

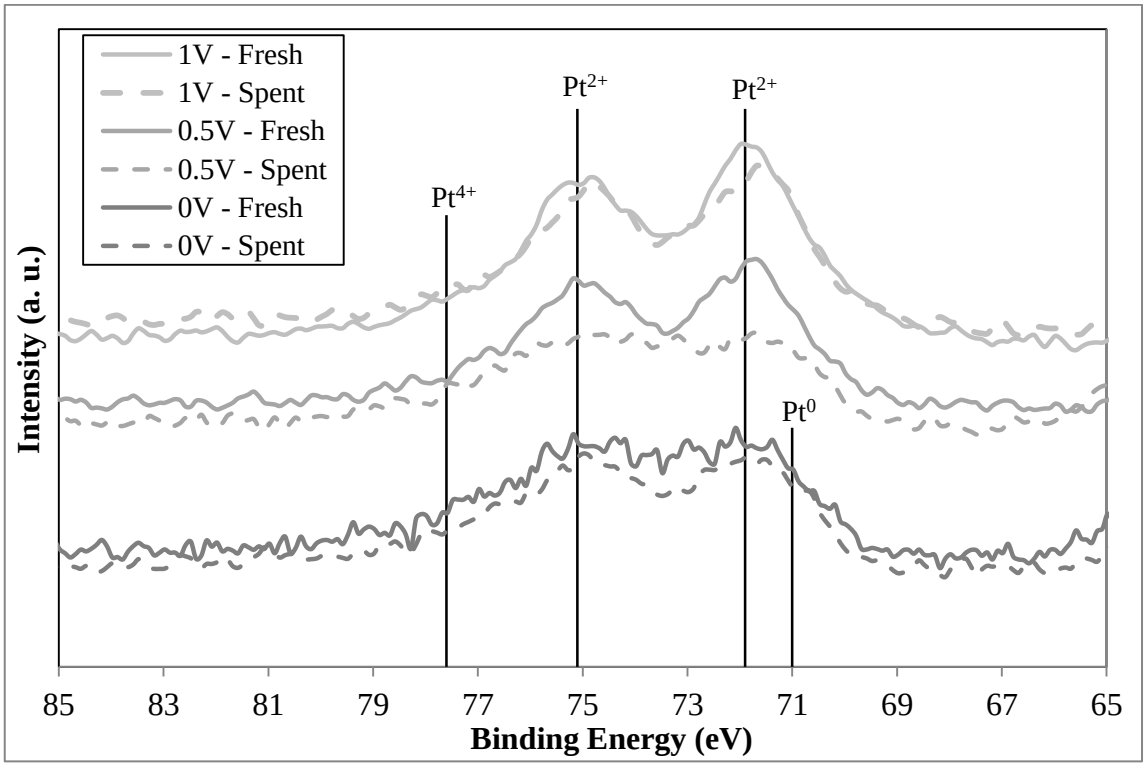

Figure 4.23. XP spectra showing the Pt 4f region of freshly reduced and spent (real feed #2, 350 °C) catalyst samples with different V loadings.

Further, XPS results of the Re 4f region (not shown) of all catalysts showed that Re exists as Re^{4+}, Re^{6+}, and Re^{7+} on all catalysts. Re was also reported to be in its oxide (ReO_x) form in the related literature (Iida *et al.*, 2006-Azzam *et al.*, 2008).

4.2.3. XRD

X-ray diffraction (XRD) patterns of the samples were recorded by using a Cu K_α radiation and continuous scan mode at 2° min^{-1}. Figure 4.24 shows the XRD spectra of the synthesized CeO_2 support, and freshly reduced 1Pt-1Re-3V/CeO_2, 1Pt-1Re-1V/CeO_2, 1Pt-1Re-0.5V/CeO_2 and 1Pt-1Re/CeO_2 catalysts.

The CeO_2 support used in this study exhibited the peak characteristics of cerianite structure. XRD profile of Pt-Re-V/CeO_2 catalysts were also similar to that of CeO_2 support. No detectable diffraction peaks of vanadium, rhenium or platinum were obtained in the analysis, suggesting high dispersion of the metals on the CeO_2 surface with small particle sizes. Another reason behind the similar XRD profiles could be the low loadings of the metals in the catalysts, since loadings below 2 wt.% are mostly invisible to XRD due to the resolution limit; Farias *et al.* observed V_2O_5 and $CeVO_4$ peaks in XRD analysis when V-loading was more than 8 wt.% (Duarte de Farias *et al.*, 2008).

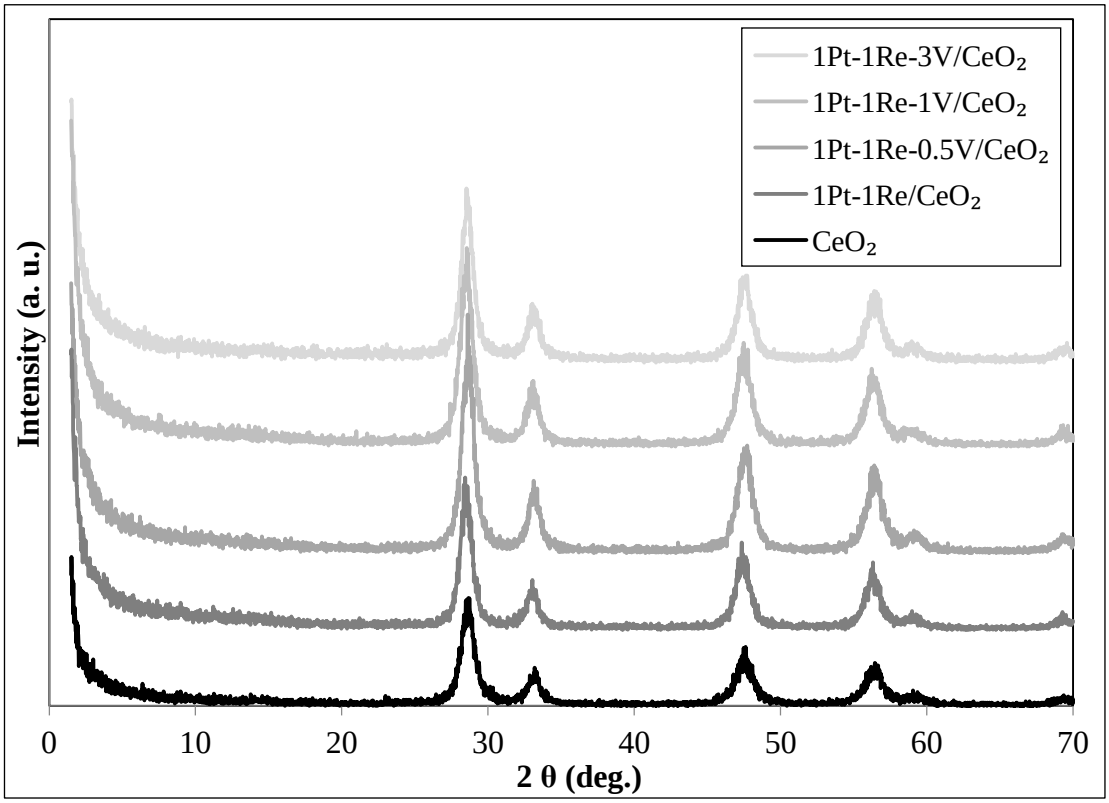

Figure 4.24. XRD patterns of the samples.

The lattice constant of the samples were calculated by applying Bragg's law using Equation 4.5 :

$$a = d\sqrt{h^2 + k^2 + l^2} \tag{4.5}$$

where d is the lattice spacing of the cubic crystal, and h, k and l are the Miller indices.

Scherrer Equation was used to calculate the mean crystallite sizes of the support and catalysts, as given in Equation 4.6:

$$\tau = \frac{K\,\lambda}{\beta \cos\theta} \tag{4.6}$$

where K is the shape factor (0.9), λ is the X-ray wavelength (0.15409 nm), β is the line broadening at half the maximum intensity (FWHM) in radians and θ is the Bragg angle in radians.

Lattice constants and crystallite sizes for CeO_2 and reduced catalysts are estimated using the diffraction peaks of the (111) plane and presented in Table 4.2 below.

Table 4.2. Ceria lattice constants and crystallite sizes of reduced samples.

Sample	**Lattice constant, a (nm)**	**Crystallite size, τ (nm)**
CeO_2	0.539	11.4
1Pt-1Re/CeO_2	0.540	12.0
1Pt-1Re-0.5V/CeO_2	0.538	13.3
1Pt-1Re-1V/CeO_2	0.541	12.8
1Pt-1Re-3V/CeO_2	0.539	11.7

Based on the results, V, Re and Pt addition to CeO_2 did not influence the CeO_2 lattice constant significantly. However, it is observerd that the crystallite sizes changed by metal addition. Addition of 1 wt.% Re and 1 wt.% Pt increased the CeO_2 crystallite size from 11.4 to 12 nm. Besides, 0.5 wt.% V addition increased the crystallite size to the highest value, 13.3 nm. Further increase in V addition to 1 wt.% led to a rather limited increase compared to that led by 0.5 wt.% addition. When the V loading was increased to 3 wt.%, approximately the same crystallite size as calculated for 1Pt-1Re/CeO_2 was observed. Eventually, increasing V content caused decrase in crystallite size. Therefore XRD results revealed that there might be an interaction between V and CeO_2 leading to changes in CeO_2 crystallite size. Furthermore, the catalysts with higher crystallite size, 1Pt-1Re-0.5V/CeO_2 and 1Pt-1Re-1V/CeO_2, were found having the highest activities in WGS performance tests.

4.2.4. Raman Spectroscopy

Raman spectroscopy is a method to observe vibrational, rotational, and other low frequency modes in a metal oxide system. Figure 4.25 shows the Raman spectra of the freshly reduced and spent Pt-Re-V samples having different V-loadings. The spent catalysts were tested in WGS during 6h TOS at 350 °C under the flow of real feed #2. As ceria was reported to be a perfect Raman scatterer overwhelming signal from surface vanadia species

(Wu *et al.*, 2011), and the catalysts used in this study are mostly composed of CeO_2 support; the spectra are dominated by CeO_2 bands. One sharp Raman main peak at around 460 cm^{-1} was observed for the bulk ceria in all freshly reduced and spent samples. Along with the main peak, the samples exhibited weak bands at around 265 cm^{-1} and 590 cm^{-1}, due to the presence of oxygen vacancies in the support (Hwang *et al.*, 2011-Yu *et al.*, 2011).

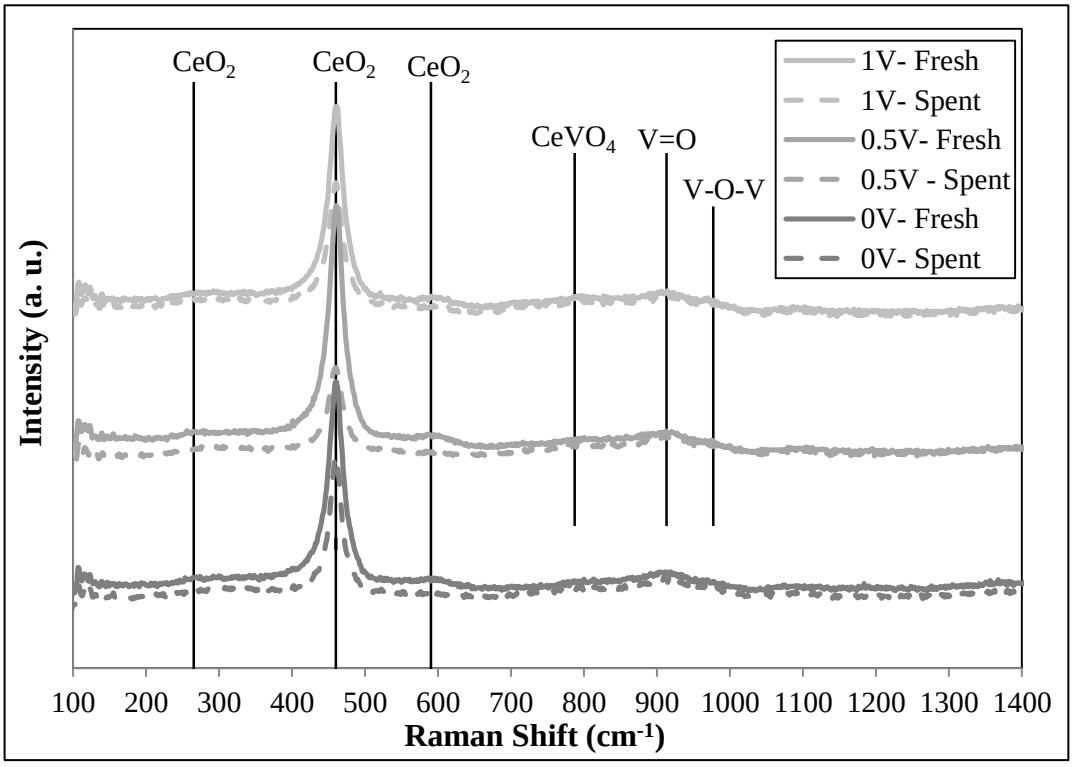

Figure 4.25. Raman spectra of the freshly reduced and spent (real feed #2, 350 °C) catalyst samples with different V-loadings.

V^{5+} ions were observed in XPS analysis; however it was not concluded whether those ions belonged to V_2O_5 or $CeVO_4$ species. In the Raman spectra of the fresh and spent V-loaded samples (Figure 4.25-4.26), a peak located at 787 cm^{-1} was observed, which is attributed to $CeVO_4$ species (Martinez-Huerta *et al.*, 2008-Wu *et al.*, 2011). Moreover, peaks appearing at 913 cm^{-1} and 977 cm^{-1} are ascribed to the stretching modes of V=O and V-O-V in polyvanadate surface species, respectively. On the other hand, bands corresponding to monovanadate surface species did not exist in the Raman studies of the samples (Wu *et al.*, 2011-Al-Ghamdi *et al.*, 2014). As an important point, no detectable

bands for bulk V_2O_5 crystals were observed in all samples. This might signify that vanadium is highly dispersed at the surface without bulk V_2O_5 formation (Al-Ghamdi *et al*., 2014-Zhu *et al*., 2015).

V^{4+} ions spotted in XPS were not observed in the Raman results. In addition, Re and Pt bonds did not appear in the Raman spectra, pointing to the incorporation of those atoms in the CeO_2 lattice (Rico-Frances *et al*., 2016). Moreover, no coke formation was observed on any of the spent samples at any reaction condition in Raman spectroscopy. This result was expected, since the catalysts were considerably stable with only little loss in activity.

Figure 4.26 displays the Raman spectra of the highly active freshly reduced 0.5V and 1V catalysts and their spent forms tested under two different real feed conditions. Tests under real feed #1 were conducted at 350 °C, as in the case of real feed #2. The explanations above are also valid for spent catalysts used under real feed #1. In addition, the CeO_2 mode at 460 cm^{-1} slightly shifted toward lower wavenumber values in spent 0.5V and 1V catalysts with respect to fresh samples. This suggests that part of cerium atoms are replaced by other atoms, indicating the active role of CeO_2 in WGS reaction (Rico-Frances *et al*., 2016).

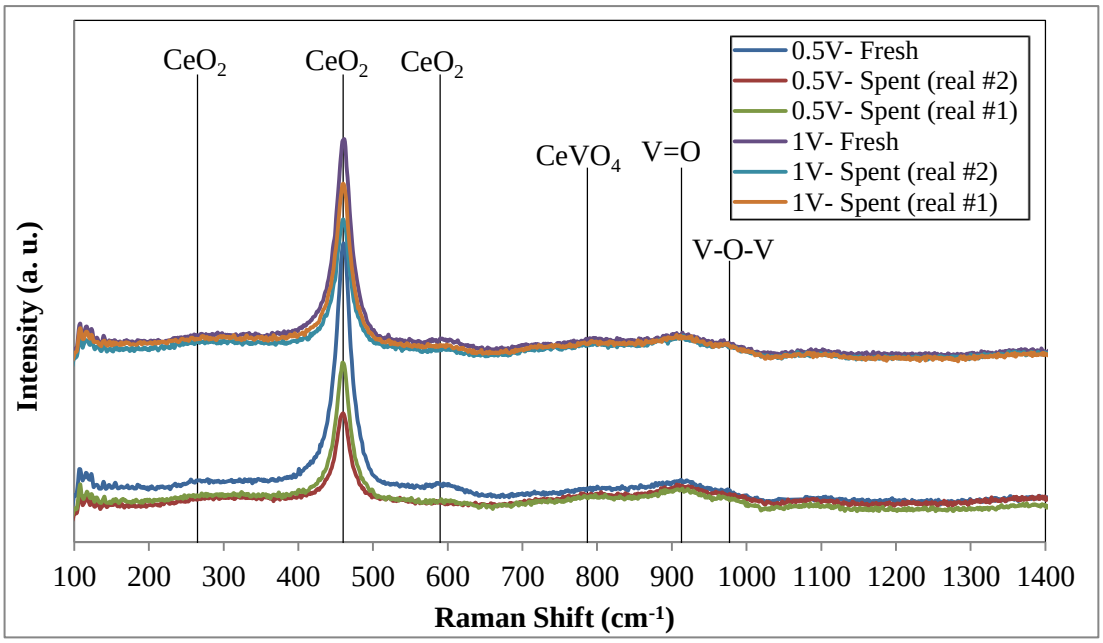

Figure 4.26. Raman spectra of the freshly reduced 0.5V and 1V catalysts and their spent forms tested under different real feed conditions.

5. CONCLUSION

5.1. Conclusions

The aim of this experimental study was to design and develop trimetallic Pt-Re-V/CeO_2 catalyst(s) having high WGS activity and stability with suppressed methanation activity under both ideal and real feed compositions in HTS-LTS transition temperatures, allowing the use of a single WGS reactor in a fuel processor. Pt- and Re-loadings were kept fixed as 1 wt.%, while V-loadings of 0, 0.5, 1, and 3 wt.% were used in the catalysts prepared. The major conclusions of this study can be summarized as follows:

All catalysts used in this study showed plausible WGS performance, ie. high CO conversion levels and positive net H_2 production values with no methanation activity, and between those 1Pt-1Re-0.5V/CeO_2 and 1Pt-1Re-1V/CeO_2 catalysts have superior performance, ie. high activity and selectivity with performance stability, indicating their quite high potential to be used in a practical fuel processor.

The results revealed that Pt-Re-V/CeO_2 system having optimized composition enables the use of a single WGS unit operating at HTS-LTS transition temperature region.

For ideal feed condition with high H_2O/CO ratio, CO conversion values close to equilibrium conversions were obtained at mid temperatures, as a consequence of high steam content of the feed leading suppressed RWGS.

The performance results obtained for two real feeds showed that higher CO conversion and net H_2 production values were achieved by real feed #1 having low H_2O/CO ratio for the temperature levels studied. On the other hand, all catalysts showed more stable performance when real feed #2 having high H_2O/CO ratio was used.

SEM-EDX analysis indicated that 1V catalyst has larger Pt particle size compared to that of V-free catalyst, which may have a positive effect on high catalytic activity for the V-

promoted sample. Besides, mapping images proved the uniform dispersion of the metals on CeO_2 surface.

XPS analysis of freshly reduced and spent samples showed that Ce^{3+} content, thus the extent of the electron transfer between the support and the metal sites, decreased during reaction as a consequence of high WGS activity. The decline of the oxygen in the ceria lattice indicated that CeO_2 plays an active role in the reaction, while the increase of hydroxyl groups after the reaction might point out to a reaction mechanism involving OH participation in rate determining step.

XRD results stated that V, Re, and Pt addition to CeO_2 did not change the CeO_2 lattice constant significantly. However, the results indicated that there is a change in crystallite size upon V addition, which points out that there might be an interaction between V and CeO_2 leading to changes in CeO_2 crystallite size.

XPS and Raman spectroscopy results showed that VO_2 and $CeVO_4$ formations were present on the surface. Raman results also revealed the existence of polyvanadate surface species. No bulk V_2O_5 crystals were observed in any sample, inferring that the vanadium was highly dispersed at the surface. Moreover, no coke formation was observed on any spent samples.

5.2. Recommendations

Considering the results of the present study, following recommendations are made for future studies on the optimization of Pt-Re-V/CeO_2 system:

- FTIR-DRIFTS studies can be performed to investigate reaction mechanism(s).

- Kinetic studies can be conducted to obtain a power-law type WGS rate expression.

- 1Pt-1Re-0.5V/CeO_2 or 1Pt-1Re-1V/CeO_2 catalysts can be used as WGS catalysts in tests conducted with serial OSR-WGS-PROX reactors.

- Cyclic stability of WGS catalysts can be studied during transient fuel processor operations involving exposure of catalyst to air and liquid water.

- Efficient start-up and shut-down strategies can be developed for transient fuel processor operations.

- Trimetallic Pt-Re-V/CeO_2 systems with 0.5 wt.% Pt-loading and/or 0.5 wt.% Re-loading and bimetallic Pt-V/CeO_2 systems can be studied.

REFERENCES

Al-Ghamdi, S. A. and H. I. de Lasa, 2014, "Propylene Production via Propane Oxidative Dehydrogenation over $Vo_x/ɤ$-Al_2O_3 Catalyst", *Fuel*, Vol. 128, pp. 120-140.

Azzam, K. G., I. V. Babich and S. L. Leffers, 2007a, "Bifunctional Catalysts for Single-Stage Water–Gas Shift Reaction in Fuel Cell Applications. Part 1. Effect of the Support on the Reaction Sequence", *Journal of Catalysis,* Vol. 251, pp. 153-162.

Azzam, K. G., I. V. Babich and S. L. Leffers, 2007b, "A Bifunctional Catalyst for the Single-Stage Water–Gas Shift Reaction in Fuel Cell Applications. Part 2. Roles of the Support and Promoter on Catalyst Activity and Stability", *Journal of Catalysis,* Vol. 251, pp. 163-171.

Azzam, K. G., I. V. Babich, K. Seshan and L. Lefferts, 2008, "Role of Re in Pt-Re/TiO_2 Catalyst for Water Gas Shift Reaction: A Mechanistic and Kinetic Study", *Applied Catalysis B: Environmental,* Vol. 80, pp. 129-140.

Azzam, K. G., I. V. Babich, K. Seshan, B. L. Mojet and L. Lefferts, 2013, "Stable and Efficient Pt-Re/TiO_2 Catalysts for Water-Gas-Shift: On the Effect of Rhenium", *ChemCatChem*, Vol. 5, pp. 557-564.

Ballarini, N., A. Battisti, F. Cavani, A. Cericola, C. Lucarelli, S. Racioppi and P. Arpentinier, 2006, "The Oxygen-Assisted Transformation of Propane to CO_x/H_2 through Combined Oxidation and WGS Reactions Catalyzed by Vanadium-Oxide Based Catalysts", *Catalysis Today,* Vol. 116, pp. 313-323.

Campbell, C. T. and C. H. F. Peden, 2005, "Oxygen Vacancies and Catalysis on Ceria Surfaces", *Science,* Vol. 309, pp. 713-714.

Castaño, M. G., T. R. Reine., S. Ivanova, M.A. Centeno and J. A. Odriozola, 2014, "Pt vs. Au in Water-Gas Shift Reaction", *Journal of Catalysis,* Vol. 314, pp. 1-9.

Colussi, S., L. Katta, F. Amoroso, R. Farrauto and A. Trovarelli, 2014, "Ceria-based Palladium Zinc Catalysts as Promising Materials for Water Gas Shift Reaction", *Catalysis Communications*, Vol. 47, pp. 63-66.

Çağlayan, B. S. and A. E. Aksoylu, 2009, "Water-Gas Shift Reaction over Bimetallic Pt-Ni/Al_2O_3 Catalysts", *Turkish Journal of Chemistry*, Vol. 33, pp. 249-256.

Çağlayan, B. S. and A. E. Aksoylu, 2011, "Water–Gas Shift Activity of Ceria Supported Au-Re Catalysts", *Catalysis Communications*, Vol. 12, pp. 1206-1211.

Çağlayan, B. S., 2011, *Design and Development of Catalysts & Adsorbents for CO_x Free H_2 Production*, Ph.D. Dissertation, Boğaziçi University.

Demeter, M., M. Neumann and W. Reichelt, 2000, "Mixed-Valence Vanadium Oxides Studied By XPS", *Surface Science*, Vol. 454-456, pp. 41-44.

Duarte de Farias, A. M., P. Bargiela, M. d. G. C. Rocha and M. A. Fraga, 2008, "Vanadium-Promoted Pt/CeO_2 Catalyst for Water-Gas Shift Reaction", *Journal of Catalysis*, Vol. 260, pp. 93-102.

Esch, F., S. Fabris, L. Zhou, T. Montini, C. Africh, P. Fornasiero, G. Comelli and R. Rosei, 2005, "Electron Localization Determines Defect Formation on Ceria Substrates", *Science*, Vol. 309, pp. 752-755.

Fiorot, S., C. Galletti, S. Specchia, G. Saracco and V. Specchia, 2007, "Development of Water Gas Shift Supported Catalysts for Fuel Processor Units", *International Journal of Chemical Reaction Engineering*, Vol. 5.

Gonzalez, I. D., R. M. Navarro, W. Wen, N. Marinkovic, J. A. Rodriguez, F. Rosa and J. L. G. Fierro, 2010, "A Comparative Study of the Water Gas Shift Reaction over Platinum Catalysts Supported on CeO_2, TiO_2 and Ce-modified TiO_2", *Catalysis Today*, Vol. 149, pp. 372-379.

Gradisher, L., B. Dutcher and M. Fan, 2015, "Catalytic Hydrogen Production from Fossil Fuels via the Water Gas Shift Reaction", *Applied Energy*, Vol. 139, pp. 335-349.

Gökaliler, F., 2012, *Characterization and Performance Analysis of Fuel Flexible OSR-WGS Catalysts*, Ph.D. Dissertation, Boğaziçi University.

Gökaliler, F., Z. İ. Önsan and A. E. Aksoylu, 2013, "Power-Law Type Rate Expression for WGS Reaction over Au–Re/CeO_2 Catalyst under Realistic Fuel Processor Conditions", *Catalysis Communication*s, Vol. 39, pp. 70-73.

Gradisher, L., B. Dutcher and M. Fan, 2015, "Catalytic Hydrogen Production from Fossil Fuels via the Water Gas Shift Reaction", *Applied Energy*, Vol. 139, pp. 335-349.

Guo, P., L. Chen, Q. Yang, M. Qiao, H. Li, H. Li, H. Xu and K. Fan, 2009, "Cu/ZnO/Al_2O_3 Water-Gas Shift Catalysts for Practical Fuel Cell Applications: The Performance in Shut-Down/Start-Up Operation", *International Journal of Hydrogen Energy*, Vol. 34, pp. 2361-2368.

Guo, P. J., L. F. Chen, G. B. Yu, Y. Zhu, M. H. Qiao, H. L. Xu and K. N. Fan, 2009b, "Cu/ZnO-based Water-Gas Shift Catalysts in Shut-Down/Start-Up Operation", *Catalysis Communications*, Vol. 10, pp. 1252-1256.

Hwang, K., J. Park and S. Ihm, 2011, "Si-Modified Pt/CeO_2 Catalyst for a Single-Stage Water-Gas Shift Reaction", *International Journal of Hydrogen Energy*, Vol. 36, pp. 9685-9693.

Iida, H. and A. Igarashi, 2006, "Structure Characterization of Pt-Re/TiO_2 (rutile) and Pt-Re/ZrO_2 Catalysts for Water Gas Shift Reaction at Low Temperature", *Applied Catalysis A: General*, Vol. 303, pp.192-198.

Ilinich, O., W. Ruettinger, X. Liu and R. Farrauto, 2007, "Cu-Al_2O_3-$CuAl_2O_4$ Water-Gas Shift Catalyst for Hydrogen Production Infuel Cell Applications: Mechanism of

Deactivation under Start-Stop Operating Conditions", *Journal of Catalysis*, Vol. 247, pp. 112-118.

Iulianelli, A., C. Pirola, A. Comazzi, F. Galli, F. Manenti and A. Basile, 2015, "Water Gas Shift Membrane Reactors", *Membrane Reactors For Energy Applications And Basic Chemical Production*, Elsevier, United Kingdom.

Jeong, D. W., W. J. Jang, J. O. Shim, W. B. Han, H. S. Roh, U. H. Jung and L. W. Yoon, 2014, "Low-Temperature Water-Gas Shift Reaction over Supported Cu Catalysts", *Renewable Energy*, Vol. 65, pp. 102-107.

Junior, I. L., J. M. Millet, M. Aouine and M. C. Rangel, 2005, "The Role of Vanadium on the Properties of Iron Based Catalysts for the Water Gas Shift Reaction", *Applied Catalysis A: General*, Vol. 283, pp. 91-98.

Kalamaras, C. M., S. Americanou and A. M. Efstathiou, 2011, "Redox vs Associative Formate with –OH Group Regeneration WGS Reaction Mechanism on Pt/CeO_2: Effect of Platinum Particle Size", *Journal of Catalysis*, Vol. 279, pp. 287-300.

Kalmula, B. and V. R. Kondapuram, 2015, "Fuel Processor-Fuel Cell Integration: Systematic Issues and Challenges", *Renewable and Sustainable Energy Reviews*, Vol. 45, pp. 409-418.

Kam, R., J. Scott, R. Amal and C. Selomulya, 2010, "Pyrophoricity and Stability of Copper and Platinum Based Water-Gas Shift Catalysts during Oxidative Shut-down/Start-up Operation", *Chemical Engineering Science*, Vol. 65, pp. 6461-6470.

Lee, D., M. S. Lee, J. Y. Lee, S. Kim, H. Eom, D. J. Moon and K. Lee, 2013, "The Review of Cr-free Fe-based Catalysts for High-Temperature Water-Gas Shift Reactions", *Catalysis Today*, Vol. 210, pp. 2-9.

Lenite, B. A., C. Galletti and S. Specchia, 2011, "Studies on Au Catalysts for Water Gas Shift Reaction", *International Journal of Hydrogen Energy*, Vol. 26, pp. 7750-7758.

Leppelt, R., B. Schumacher, V. Plzak, M. Kinne and R. J. Behm, 2006, "Kinetics and Mechanism of the Low-Temperature Water-Gas Shift Reaction on Au/CeO_2 Catalysts in an Idealized Reaction Atmosphere", *Journal of Catalysis*, Vol. 244, pp. 137-152.

LeValley, T. L., A. R. Richard and M. Fan, 2014, "The Progress in Water Gas Shift and Steam Reforming Hydrogen Production Technologies-A Review", *International Journal of Hydrogen Energy*, Vol. 39, pp. 16983-17000.

Li, L., L. Song, H. Wang, C. Chen, Y. She, Y. Zhan, X. Lin and Q. Zheng, 2011, "Water-Gas Shift Reaction over CuO/CeO_2 Catalysts: Effect of CeO_2 Supports Previously Prepared by Precipitation with Different Precipitants", *International Journal of Hydrogen Energy*, Vol. 36, pp. 8839-8849.

Liu, Q., W. Ma, R. He and Z. Mu, 2005, "Reaction and Characterization Studies of an Industrial Cr-Free Iron-Based Catalyst for High-Temperature Water Gas Shift Reaction", *Catalysis Today*, Vol. 106, pp. 52-56.

Liu, X., P. Guo, S. Xie, Y. Pei, M. Qiao and K. Fan, 2012, "Effect of Cu Loading on Cu/ZnO Water-Gas Shift Catalysts for Shut-down/Start-up Operation", *International Journal of Hydrogen Energy*, Vol. 37, pp. 6381-6388.

Liu, X., P. Guo, B. Wang, Z. Jiang, Y. Pei, K. Fan and M. Qiao, 2013, "A Comparative Study of the Deactivation Mechanisms of the Au/CeO_2 Catalyst for Water-Gas Shift under Steady-State and Shutdown/Start-Up Conditions in Realistic Reformate", *Journal of Catalysis*, Vol. 300, pp. 152-162.

Martinez-Huerta, M. V., G. Deo, J. L. G. Fiberro and M. A. Bañares, 2008, "Operando Raman-GC Study on the Structure-Activity Relationships in V^{5+}/CeO_2 for Catalyst Ethane Oxidative Dehydrogenation: The Formation of $CeVO_4$", *The Journal of Physical Chemistry C*, Vol. 112, pp. 11441-11447.

Mishra, A. and R. Prasad, 2011, "A Review of Preferential Oxidation of Carbon Monoxide in Hydrogen Rich Gases", *Bulletin of Chemical Reaction Engineering & Catalysis*, Vol. 6, No.1, pp. 1-14.

Marono, M., E. Ruiz, J. M. Sanchez, C. Martos, J. Dufour, and A. Ruiz, 2009, "Performance of Fe-Cr Based WGS Catalysts Prepared by Co-Precipitation and Oxi-Precipitation Methods", *International Journal of Hydrogen Energy*, Vol. 34, pp. 8921-8928.

Meshkani, F. and M. Rezaei, 2014, "A Facile Method for Preparation of Iron Based Catalysts for High Temperature Water Gas Shift Reaction", *Journal of Industrial and Engineering Chemistry*, Vol. 20, pp. 3297-3302.

Meshkani, F. and M. Rezaei, 2015, "Mesoporous Ba-Promoted Chromium Free Fe_2O_3-Al_2O_3-NiO Catalyst with Low Methanation Activity for High Temperature Water Gas Shift Reaction", *Catalysis Communications*, Vol. 58, pp. 26-29.

Natesakhawat, S., X. Wang, L. Zhang and U. S. Ozkan, 2006, "Development of Chromium-Free Iron-Based Catalysts for High-Temperature Water-Gas Shift Reaction", *Journal of Molecular Catalysis A: Chemical*, Vol. 260, pp. 82-94.

Nguyen-Thanh, D., A. M. Duarte de Farias and M. A. Fraga, 2008, "Characterization and Activity of Vanadia-Promoted Pt/ZrO_2 Catalysts for the Water-Gas Shift Reaction", *Catalysis Today*, Vol. 138, pp. 235-238.

Nishimura, S., T. Shishido, K. Ebitani, K. Teramura and T. Tanaka, 2010, "Novel Catalytic Behavior of Cu/Al_2O_3 Catalyst against Daily Start-Up and Shut-Down (DSS)-like Operation in the Water Gas Shift Reaction", *Applied Catalyst A: General*, Vol.387, pp. 185-194.

Pierre, D., W. Deng and M. F. Stephanopoulos, 2007, "The Importance of Strongly Bound Pt-CeO_x Species for the Water-gas Shift Reaction: Catalyst Activity and Stability Evaluation", *Topics in Catalysis*, Vol. 46, pp. 363-373.

Pradhan, S., A. S. Reddy, R. N. Devi and S. Chilukuri, 2009, "Copper-Based Catalysts for Water Gas Shift Reaction: Influence of Support on Their Catalytic Activity", *Catalysis Today*, Vol. 141, pp. 72-76.

Ratnasamy, C., J. P. Wagner and S. Chemie, 2009, "Water Gas Shift Catalysis", *Catalysis Reviews: Science and Engineering*, Vol. 51, No. 3, pp. 325-440.

Rebrov, E. V., 2011, "*Advances in Water Gas Shift Technology: Modern Catalysts and Improved Reactor Concepts*", Woodhead Publishing, UK.

Rico-Frances, S., E. O. Jardim, T. A. Wezendonk, F. Kapteijn, J. Gascon, A. S. Escribano and E. V. Ramos-Fernandez, 2016, "Highly Dispersed $Pt^{\delta+}$ on $Ti_xCe_{(1-x)}O_2$ as an Active Phase in Preferential Oxidation of CO", *Applied Catalyst B: Environmental*, Vol. 180, pp. 169-178.

Roh, H. S., H. S. Potdar, D. W. Jeong, K. S. Kim, J. O. Shim, W. J. Jang, K. Y. Koo, W. L. Yoon, 2012, "Synthesis of Highly Active Nano-sized (1 wt.% Pt/CeO_2) Catalyst for Water Gas Shift Reaction in Medium Temperature Application", *Catalysis Today*, Vol. 185, pp. 113-118.

Shekhawat, D., J. J. Spivey and D. A. Berry, 2011, "Fuel Cells: Technologies for Fuel Processing", Elsevier.

Silva, A. M., A. M. Duarte de Farias, L. O. O. Costa, A. P. M. G. Brandas, L. V. Mattos, M. A. Fraga and F. B. Noronha, 2008, "Partial Oxidation and Water Gas Shift Reaction in an Integrated System for Hydrogen Production from Ethanol", *Applied Catalysis A: General*, Vol. 334, pp. 179-186.

Silversmit, G., D. Depla, H. Poelman, G. B. Marin and R. D. Gryse, 2004, "Determination of the V2p XPS Binging Energies for Different Vanadium Oxidation States (V^{5+} to V^{0+})", *Journal of Electron Spectroscopy and Related Phenomena*, Vol. 135, pp. 167-175.

Sharma, S. and S. K. Ghoshal, 2015, “Hydrogen for Future Transportation Fuel: From Production to Applications”, *Renewable and Sustainable Energy Reviews*, Vol. 43, pp. 1151-1158.

Suchorski, Y., L. R. Struckmann, F. Klose, Y. Ye, M. Alandjiyska, K. Sundmacher and H. Weiss, 2005, “Evolution of Oxidation States in Vanadium-based Catalysts under Conventional XPS Conditions”, *Applied Surface Science*, Vol. 249, pp. 231-237.

Tabakova, T., F. Boccuzzi, M. Manzoli and D. Andreeva, 2003, “FTIR Study of Low-Temperature Water-Gas Shift Reaction on Gold/Ceria Catalyst”, *Applied Catalyst A: General*, Vol.252, pp. 385-397.

Vignatti, C. I., M. S. Avila, C.R. Apesteguia and T. F. Garetto, 2011, “Study of the Water Gas Shift Reaction over Pt Supported on CeO_2-ZrO_2 Mixed Oxides”, *Catalysis Today*, Vol. 171, pp. 297-303.

Vindigni, F., M. Manzoli, T. Tabakova, V. Idakiev, F. Boccuzzi, and A. Chiorino, 2012, “Gold Catalysts for Low Temperature Water-Gas Shift Reaction: Effect of ZrO_2 Addition to CeO_2 Support”, *Applied Catalysis B: Environmental*, Vol. 125, pp. 507-515.

Wang, T., M. D. Porosoff and J. G. Chen, 2014, “Effects of Oxide Supports on the Water-Gas Shift Reaction over Pt-Ni Bimetallic Catalysts: Activity and Methanation Inhibition”, *Catalysis Today*, Vol. 233, pp. 61-69.

Wu Z., A. J. Rondinone, I. N. Ivanov and S. H. Overbury, 2011, “Structure of Vanadium Oxide Supported on Ceria by Multiwavelength Raman Spectroscopy”, *The Journal of Physical Chemistry C*, Vol. 115, pp. 25368-25378.

Yu, Q., W. Chen, Y. Li, M. Jin and Z. Suo, 2010, “The Action of Pt in Bimetallic Au-Pt/CeO_2 Catalyst for Water-Gas Shift Reaction”, *Catalysis Today*, Vol. 158, pp. 324-328.

Yu, Q., X. Wu, C. Tang, L. Qi, B. Liu, F. Gao, K. Sun, L. Dong and Y. Chen, 2011, "Textural, Structural, and Morphological Characterizations and Catalytic Activity of Nanosized CeO_2-MO_x ($M=Mg^{2+}$, Al^{3+}, Si^{4+}) Mixed Oxides for CO Oxidation", *Journal of Colloid and Interface Science*, Vol. 354, pp. 341-352.

Zhu, X., M. Shen, L. L. Lobban and R. G. Mallinson, 2011, "Structural Effects of Na Promotion for High Water Gas Shift Activity on Pt-Na/TiO_2", *Journal of Catalysis*, Vol. 278, pp. 123-132.

Zhu, X., M. Shen, L. L. Lobban and R. G. Mallinson, 2011, "Structural Effects of Na Promotion for High Water Gas Shift Activity on Pt-Na/TiO_2", *Journal of Catalysis*, Vol. 278, pp. 123-132.

Zhu, H., S. Ould-Chikh, H. Dong, I. Llorens, Y. Saih, D. H. Anjum, J. L. Hazemann and J. M. Basset, 2015, "VO_x/SiO_2 Catalyst Prepared by Grafting $VOCl_3$ on Silica for Oxidative Dehydrogenation of Propane", *ChemCatChem*, Vol. 7, pp. 3332-3339.

APPENDIX A: TIME-ON-STREAM ACTIVITY DATA

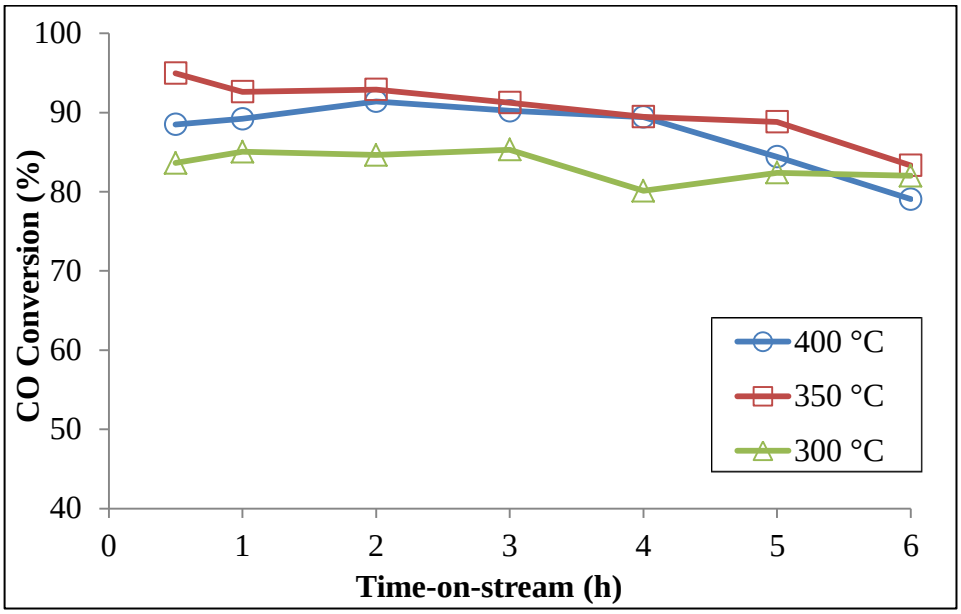

Figure A.1. Temperature dependence of time-on-stream activity data of 1Pt-1Re-3V/CeO_2 for ideal feed #1.

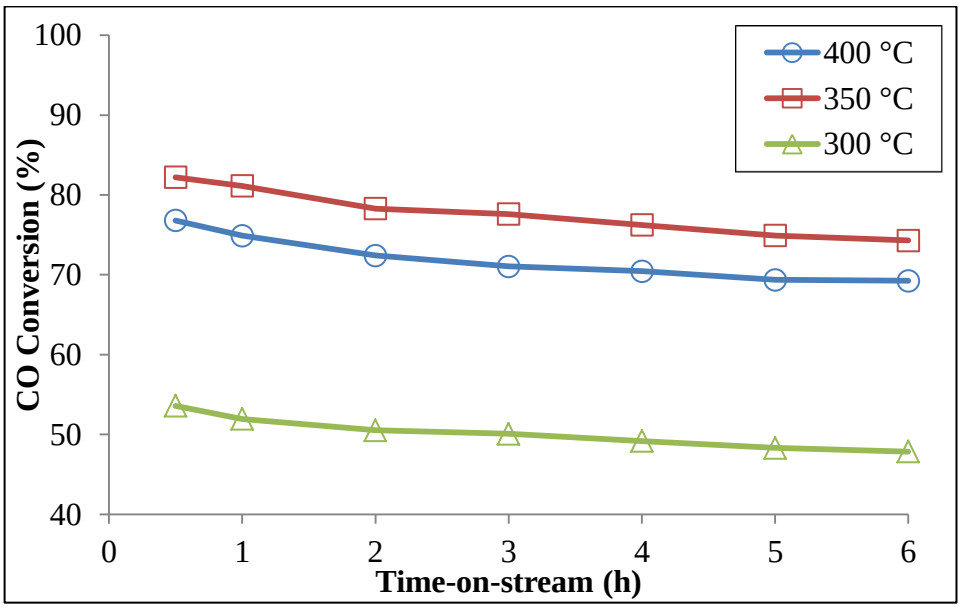

Figure A.2. Temperature dependence of time-on-stream activity data of 1Pt-1Re-3V/CeO_2 for ideal feed #2.

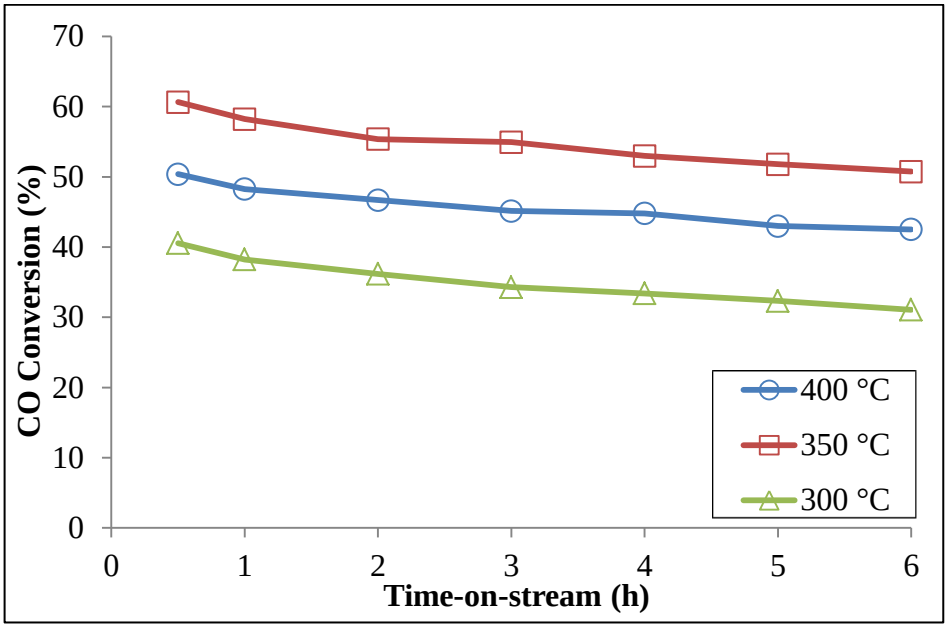

Figure A.3. Temperature dependence of time-on-stream activity data of 1Pt-1Re-3V/CeO_2 for real feed #1.

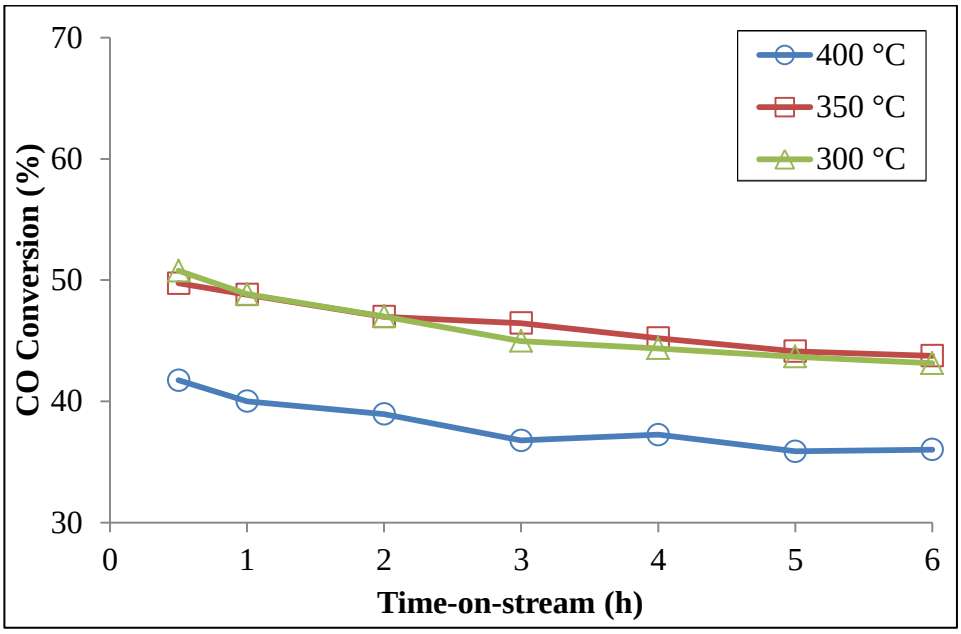

Figure A.4. Temperature dependence of time-on-stream activity data of 1Pt-1Re-3V/CeO_2 for real feed #2.

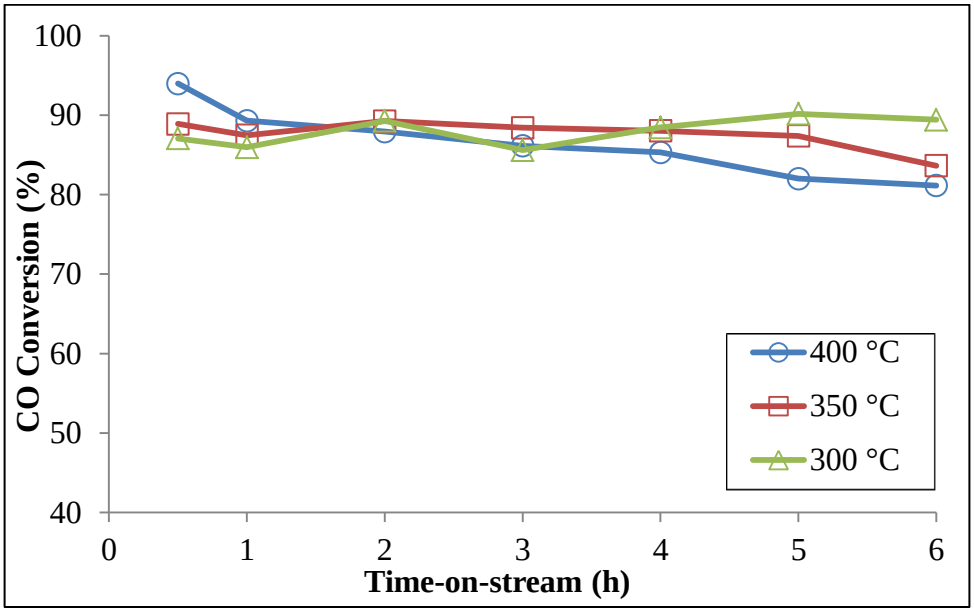

Figure A.5. Temperature dependence of time-on-stream activity data of 1Pt-1Re-1V/CeO_2 for ideal feed #1.

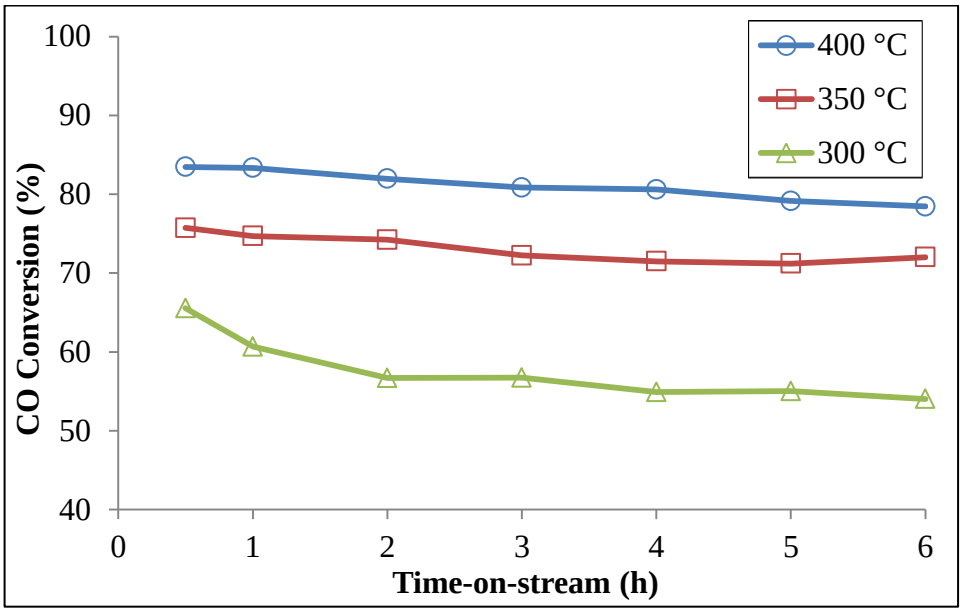

Figure A.6. Temperature dependence of time-on-stream activity data of 1Pt-1Re-1V/CeO_2 for ideal feed #2.

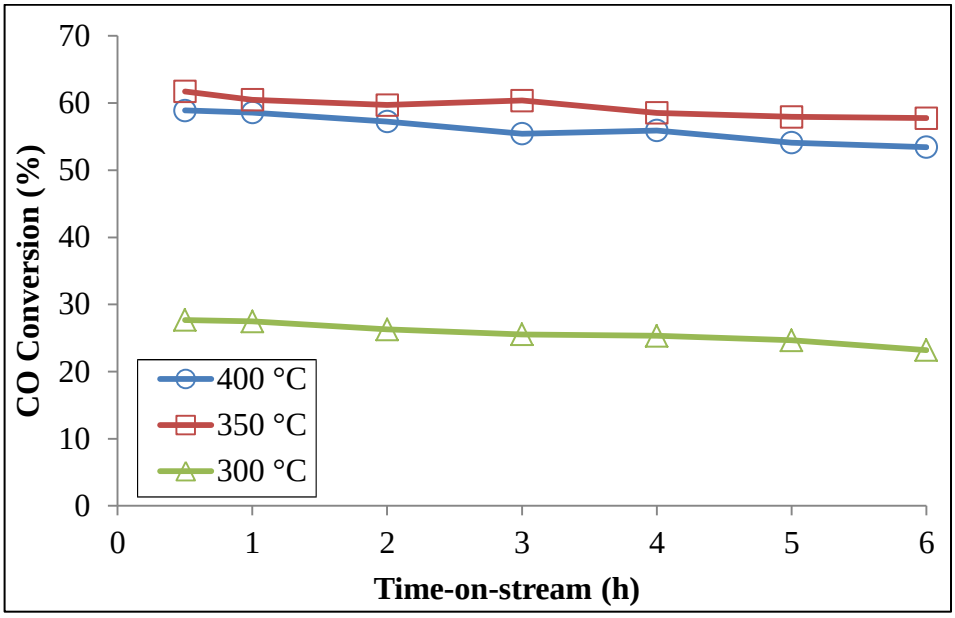

Figure A.7. Temperature dependence of time-on-stream activity data of 1Pt-1Re-1V/CeO_2 for real feed #1.

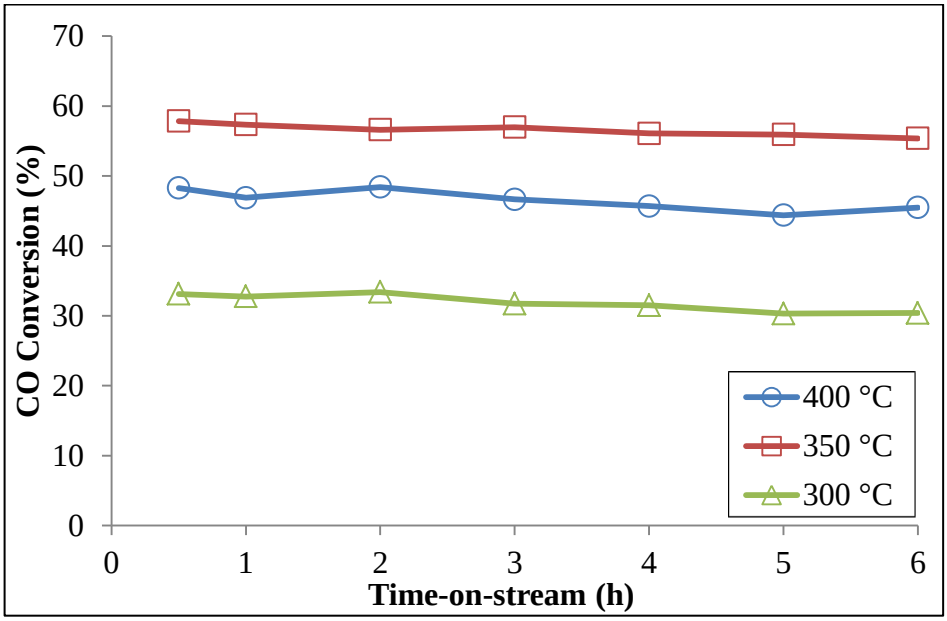

Figure A.8. Temperature dependence of time-on-stream activity data of 1Pt-1Re-1V/CeO_2 for real feed #2.

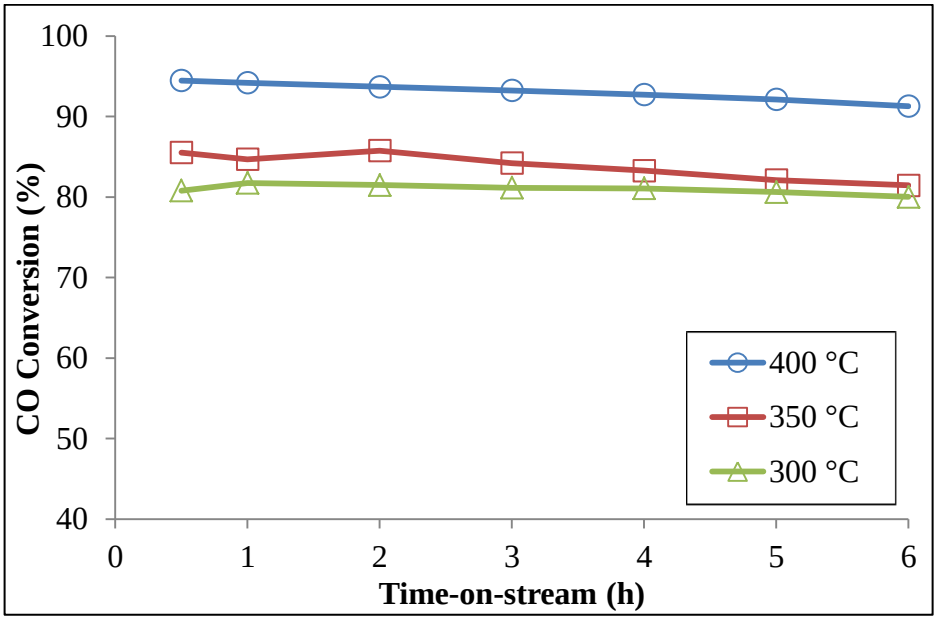

Figure A.9. Temperature dependence of time-on-stream activity data of 1Pt-1Re-0.5V/CeO_2 for ideal feed #1.

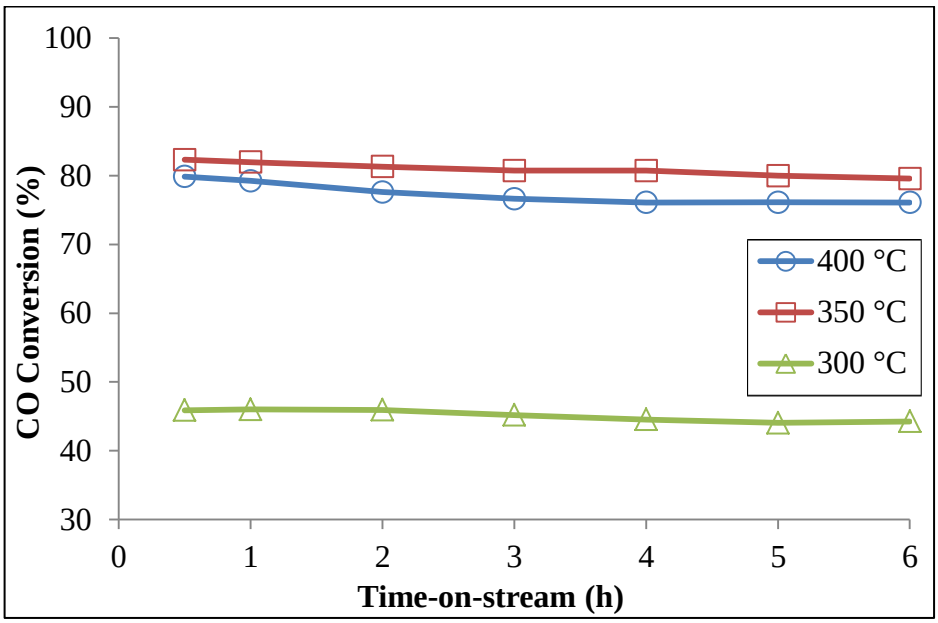

Figure A.10. Temperature dependence of time-on-stream activity data of 1Pt-1Re-0.5V/CeO_2 for ideal feed #2.

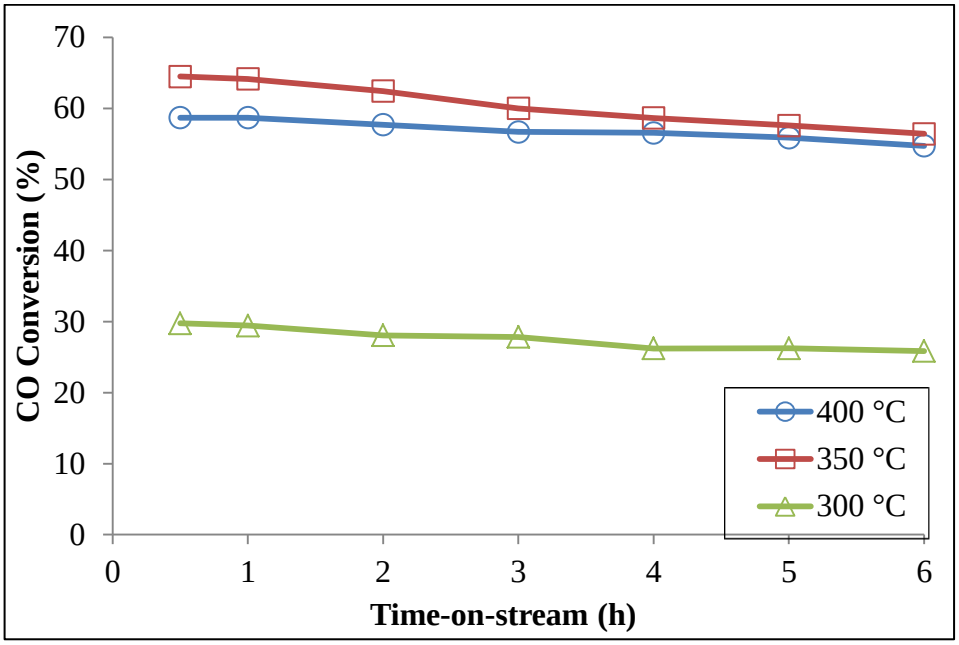

Figure A.11. Temperature dependence of time-on-stream activity data of 1Pt-1Re-0.5V/CeO_2 for real feed #1.

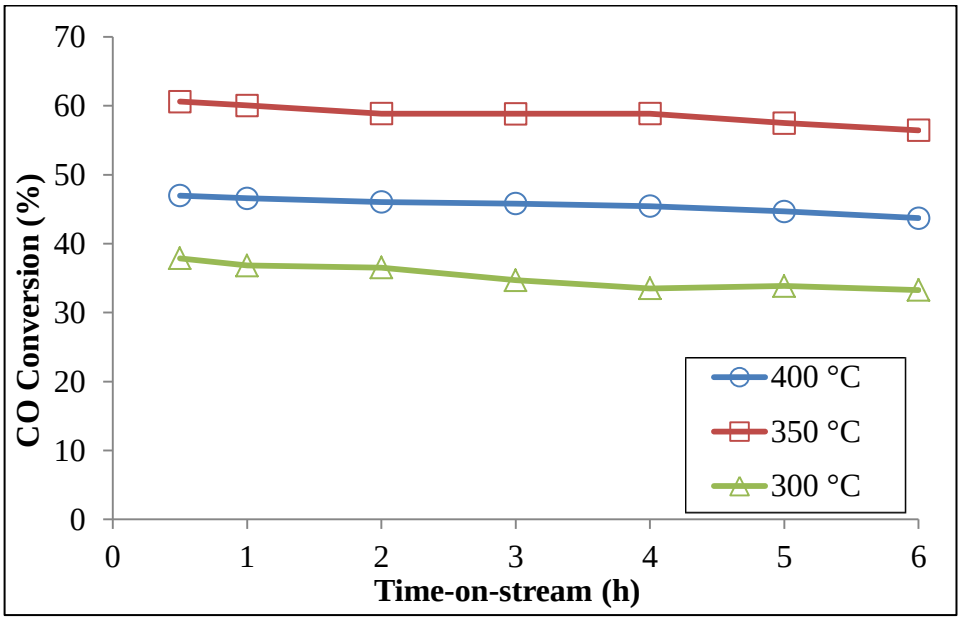

Figure A.12. Temperature dependence of time-on-stream activity data of 1Pt-1Re-0.5V/CeO_2 for real feed #2.

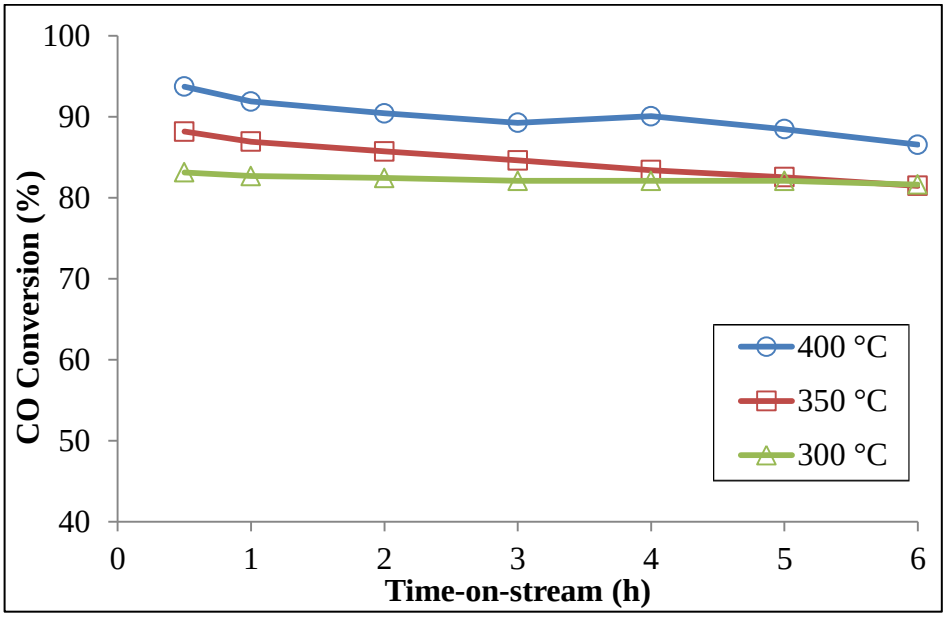

Figure A.13. Temperature dependence of time-on-stream activity data of 1Pt-1Re/CeO_2 for ideal feed #1.

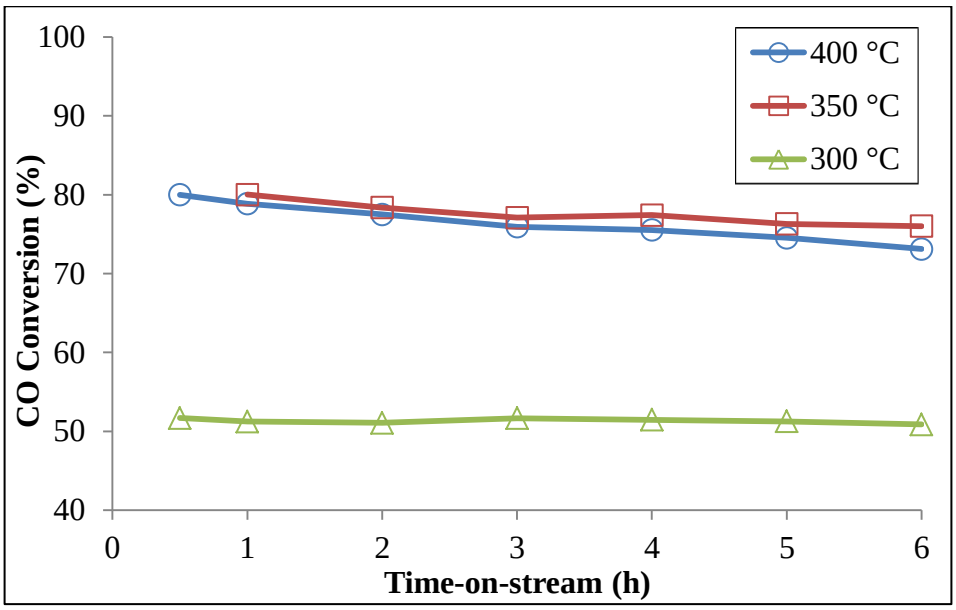

Figure A.14. Temperature dependence of time-on-stream activity data of 1Pt-1Re/CeO_2 for ideal feed #2.

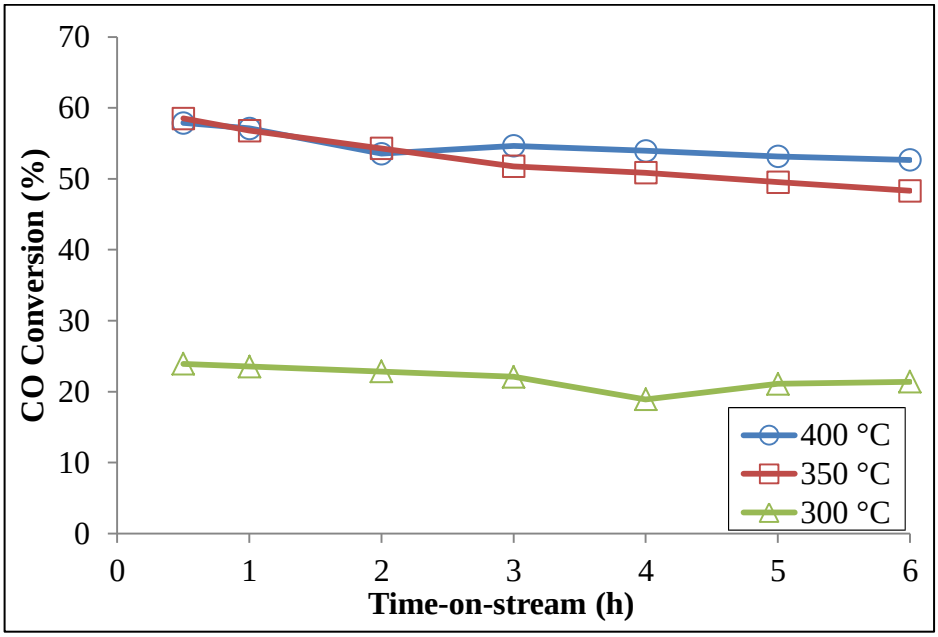

Figure A.15. Temperature dependence of time-on-stream activity data of 1Pt-1Re/CeO_2 for real feed #1.

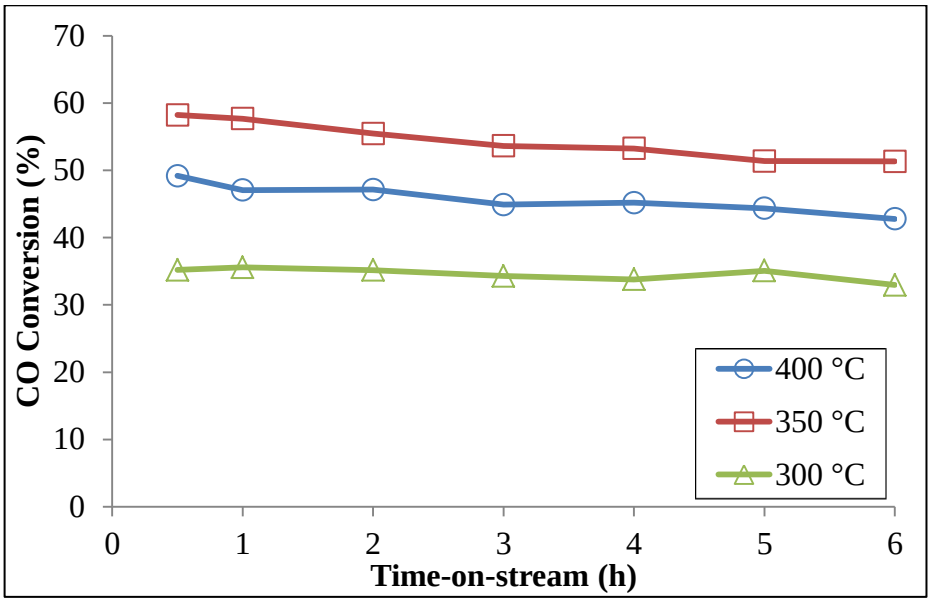

Figure A.16. Temperature dependence of time-on-stream activity data of 1Pt-1Re/CeO_2 for real feed #2.